

Department of Electrical and Computer Engineering

**A New Cost Effective Approach to Suppress Very Fast Transients on
Power Transformers Connected to Gas Insulated Substations**

Mehdi Babaeilaktarashani

**This thesis is presented for the Degree of
Master of Philosophy
of
Curtin University**

December 2016

Declaration

To the best of my knowledge and belief this thesis contains no material previously published by any other person except where due acknowledgment has been made.

This thesis contains no material which has been accepted for the award of any other degree or diploma in any university.

Signature: Mehdi Babaeilaktarashani

Date: 05/12/2016

Publication

1. **Mehdi Babaei**, Ahmed Abu-Siada, Maziar Babaei, “Suppressing Resonance Overvoltages in Transformer Winding under Very Fast Transient”, presented in IEEE ISGT Asia 2016 Conference, 29 Nov-1 Dec 2016, Melbourne, Victoria.
2. **Mehdi Babaei**, Ahmed Abu-Siada, “Preventing Transformer Internal Resonance under Very Fast Transient Overvoltage Using RC Surge Suppressor”, Accepted to be published in IEEE Transactions on Dielectrics and Electrical Insulation, In Press.

Abstract

This thesis investigates the feasibility of a new method to prevent internal resonance in power transformers connected to gas insulated substation (GIS) due to very fast transient overvoltage (VFTO) emanating from the GIS. Internal resonance within the transformer windings will take place if one of the VFTO frequencies matches the power transformer natural frequency. In this context, the effect of VFTO originating from a GIS on the transformer connected to the GIS terminals is firstly investigated. The possibility of utilizing a cost effective RC surge suppressor to prevent internal transformer resonance is then analyzed using a simulation of a 400kV GIS connected to a 250MVA, three phase, power transformer. For this purpose, several topologies of RC circuits are introduced and analyzed. The optimum suppressor, in terms of capability to suppress high risk frequencies of VFTO, is defined by various critical indices such as VFTO peak value and steepness considering magnification of very fast transient current (VFTC) is proposed. Presented procedure for selecting the best suppressor shows that a first order surge suppressor can be an acceptable choice to suppress the severity of a VFTO surge. In contrary with existing resonance suppressing approaches that call for modifications in the GIS structure, the proposed method given in this thesis is a cost effective method which can be employed with any existing GIS without any change to its structure.

Acknowledgments

I would like to express my most sincere gratitude to my supervisor, A/Professor Ahmed Abu-Siada for his kind support and guidance throughout my MPhil study.

My special thanks to my beloved wife, Sara, for her support, patience, and unconditional love during my study. She gave me the encouragement to follow my education and stood beside me throughout the completion of my MPhil studies.

Table of Contents

1	Introduction.....	1
1.1	Scope of Work	2
1.2	Thesis Outline	2
2	Background.....	3
2.1	Gas Insulated Substation (GIS).....	3
2.2	Definition of transient voltages.....	5
2.3	Origin of VFTO in GIS.....	7
2.3.1	Voltage collapse during SF ₆ breakdown.....	7
2.3.2	Disconnecting Switch operation	8
2.3.3	Frequent restrikes.....	9
2.4	Propagation of VFTO in GIS	10
2.4.1	Internal and External modes	14
2.5	Calculation of VFTO at transformer terminals	15
2.6	Effective Factors in VFTO magnitude.....	19
2.6.1	Trapped Charge.....	19
2.6.2	DS operation speed	19
2.6.3	GIS Layout.....	19
2.6.4	Capacitance at Transformer terminal	20
2.7	VFTO in Transformer Winding.....	20
2.7.1	Initial distribution of transient in winding	20
2.7.2	Internal resonance	22
3	Power System Modelling.....	27
3.1	GIS Modelling	29
3.1.1	Components of GIS model.....	34
3.1.2	Improved model of GIS by Maxwell 3D	42
3.1.3	GIS Overall Model.....	48
3.1.4	Effect of SF ₆ degradation on VFTO.....	50
3.2	Transformer Modelling.....	53
3.2.1	High Frequency Transformer Models.....	53
3.2.2	Determination of Parameters	59
3.2.3	Resulted transformer model	64
4	VFTO Surge Suppression	67
4.1	RC Surge Suppressor	67
4.1.1	First Order Surge Suppressor	68
4.1.2	Second Order Surge Suppressor	69
4.1.3	Third Order Surge Suppressor	71

4.2	Indices to Assess Suppressing Performance	76
4.3	Investigation Procedure for Selection of Surge Suppressor.....	78
4.4	Procedure Results.....	82
4.5	Cost analysis	91
4.6	Loss analysis	92
5	Comparison and Conclusion.....	93
5.1	Comparison with Existing Suppressing Methods	93
5.2	Conclusion	94
5.3	Future Work.....	94

1 Introduction

Within recent decades there has been a growing demand for installing high voltage gas insulated substations (GIS), particularly in heavily industrial areas due to several advantages in comparison with conventional air insulated substations, such as less required space, higher personal and operational safety level, easy installation, maintenance and commissioning. Despite the advantages of GIS over conventional air insulated substations, very fast transients (VFT) emerged in GIS necessitates careful attention to design gas insulated substation and protect all high voltage equipment against these severe over voltages. Until 70s, all power system transients investigated and addressed were limited to fast transient with frequencies less than few megahertz. Significant increases in GIS manufacturing and operation at extra high voltage (EHV) and ultra-high voltage (UHV) voltage levels called for further research and study in power transients because the transients originated from GIS may reach to a few hundred megahertz due to dimensions of new gas insulated substations. Therefore newly emerged phenomenon of Very Fast Transient Overvoltage (VFTO) has been under investigation within recent years and several mitigation methods have been introduced.

The main source of very fast transients in GIS is switching operation. Due to physical characteristics of SF₆ as the insulation medium used in GIS, any insulation breakdown in GIS will result in very short rise time voltage collapse which propagates inside the GIS. Reflection and refraction of these travelling waves can produce high amplitude overvoltages. Insulation breakdown within GIS caused by disconnecting switch (DS) operation or ground faults during tests results in VFTO [1]. Although there is no standard for neither VFTO waveshapes nor its amplitude, according to IEC standard [2] VFTO belongs to the category of highest range of frequencies (30kHz to 100MHz).

VFTO has detrimental impacts on equipment in substation and probably causes undesired effects on high voltage apparatuses including power transformer as the most important asset within the GIS. As dominant frequencies of VFTO are in the range of few megahertz, they may coincide with the natural frequencies of power transformer connected to a GIS, and consequently internal resonance may take place within the transformer winding resulting in possible catastrophic damage to the power transformer. Mitigating internal resonance involves changing of the transformer parameters. However, since the natural frequency of the transformer is strongly dependent on core, winding construction and insulation system, this option is not a possible solution. The other viable solution is by suppressing the high frequency contents of VFTO.

Several VFTO mitigation methods have been suggested in the literatures as will be detailed in this thesis. All these methods are designed and applied to mitigate VFTO at the origin of the transient that will require changes to the design and construction of

the GIS. Moreover, these techniques are very expensive in comparison with the proposed method in this study.

1.1 Scope of Work

This research is aimed at producing a simple cost effective method for mitigating internal resonance of a power transformer connected to GIS that is not equipped with any predesigned special measures to suppress VFTO. In order to achieve this, the following objectives are considered within this study:

- Investigating the main influential factors affecting the VFTO magnitude.
- Investigating the impacts of VFTO on equipment connected to GIS.
- Developing a suitable high frequency model for GIS and power transformer for VFTO studies.
- Investigating various mitigation techniques for VFT waves in GIS
- Investigating the feasibility of using RC circuits as surge suppressors at the terminal of the power transformer.
- Comparing the new proposed method with other existing methods.

1.2 Thesis Outline

Chapter 2 begins by introducing different power system transients categorized based on their waveshape, duration and frequency content. Then, the background theory of the mechanism is presented which usually results in generation of VFTO in gas insulated substation. This is followed by a comprehensive literature review of the parameters affecting VFTO magnitude and side effects of VFTO.

In chapter 3, the modelling of GIS according to IEC standard and IEEE guidelines is presented. Then methods of modelling winding of transformer are discussed according to available guidelines. These models are used to simulate both GIS and transformer using EMTP-RV (Electromagnetic Transient Program Reconstructed Version), a specialized software for simulation and analysis of power system transients. Required data for simulation are obtained from a real 400kV GIS connected to 400/18kV, 250MVA three phase transformer [3].

In chapter 4, different VFTO suppressing topologies are presented. The performances of all possible RC topologies are compared according to an optimum algorithm for selecting the most optimum topology resulting in the most acceptable suppression. The comparison procedure is performed based on some predefined performance indices which are employed to quantify VFTO severity such as magnitude, steepness and amplitude of high risk frequency. Cost study is also performed to select the most economic topology.

Chapter 5 compares the proposed method with other existing mitigation methods. Finally, the conclusion of the thesis is included in Chapter 5.

2 Background

2.1 Gas Insulated Substation (GIS)

A Gas Insulated Substation (GIS) is a compact multicomponent assembly enclosed in grounded metallic housing, in which the primary insulating medium is a compressed gas, and that normally consists of buses, switchgear and associated equipment. GIS substations have become a major component of the power network worldwide and they have been used with considerable success over the past fifty years [4]. In conventional Air Insulated Substations (AIS), air is used as the main insulating medium between phases, while in GIS, air is replaced by sulphur hexafluoride (SF_6) gas. SF_6 is employed as insulation in all parts of the installation and in the circuit-breaker for arc-quenching. SF_6 is an electronegative gas, which has a dielectric strength at atmospheric pressure approximately three times that of the air. This gas is incombustible, non-toxic, odourless, chemically inert with arc-quenching properties 3 to 4 times better than air at the same pressure [5]. GIS is extensively used at ratings of 72.5 up to 1200 kV with breaking currents of up to 63 kA, and in special cases up to 80 kA [5]. Fig. 2. 1 and Fig. 2. 2 show the arrangement of high voltage equipment within typical GIS; transformer and line feeders respectively.

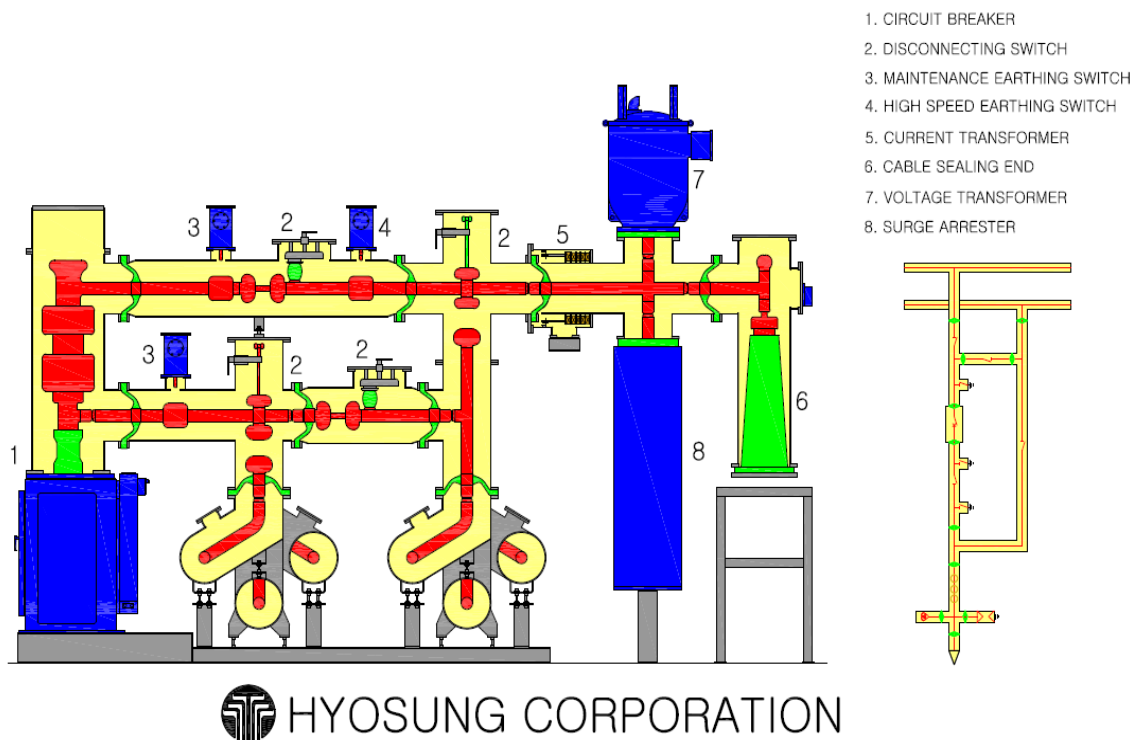


Fig. 2. 1 Arrangement of components in 420kV, 50kA GIS (Transformer feeder) [6]

Initially GIS was used as an alternative to AIS to be installed in places with space restriction or places where land cost is too expensive, but rapid development in GIS technology reduced the price gap between AIS and GIS that enabled GIS become the most economical solution for feeding industrial loads [7]. Although the primary cost

of GIS is greater than AIS, the advantages provided by modern gas insulated substations that are listed below, make it more superior than AIS [7, 8]:

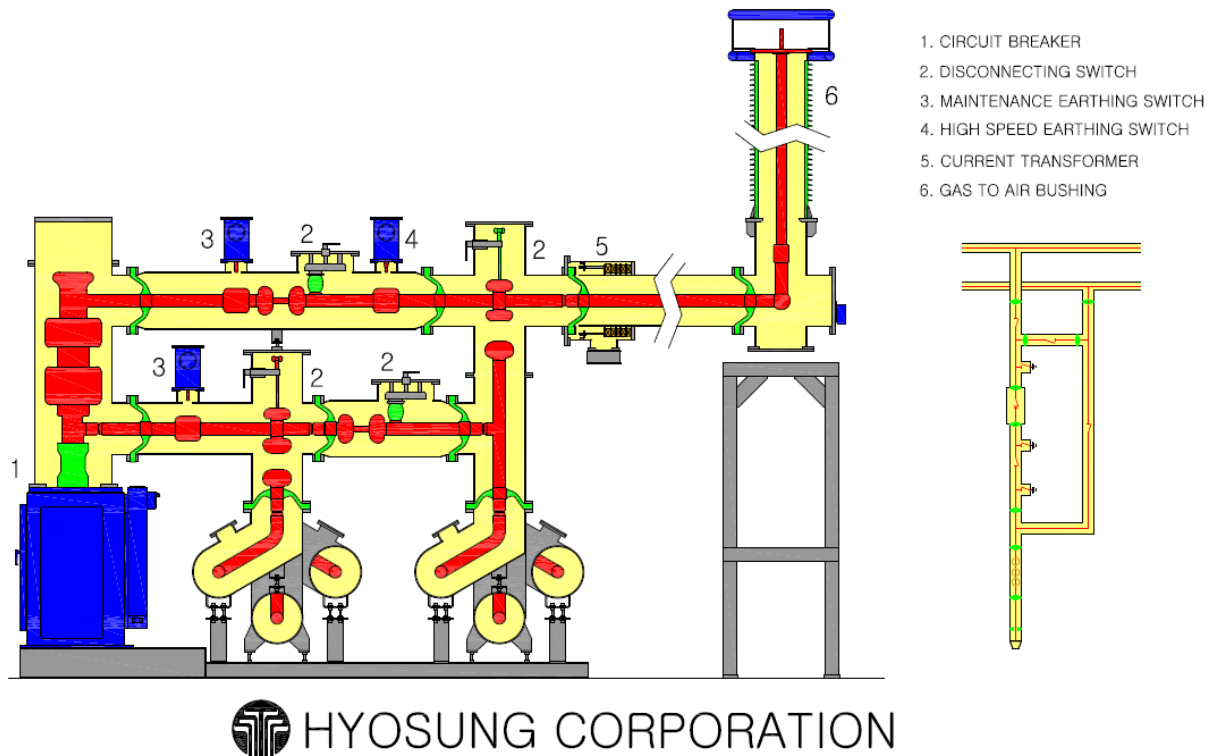


Fig. 2. 2 Arrangement of components in 420kV, 50kA GIS (Line feeder) [6]

Minimal space requirements:

The most important factor which is effective in specifying the type of switchgear to be used is the availability and price of land. In cases with space restrictions such as dense cities with large population, industrial areas, mountainous regions with narrow valleys and underground power stations, GIS is replacing conventional switchgear because of its very small space requirement and low weight. Total area required for GIS to be installed is almost 10% of the area required by AIS.

Personal and operational safety:

Since all high voltage components of GIS are enclosed by a metal enclosure (usually steel or aluminum), it provides full protection against contact with live parts under all operating and fault conditions.

Pollution Effect:

GIS is surrounded by a metal enclosure, all components are fully protected against some environmental effects that may have negative effects on air insulated substation such as salt deposits in coastal regions and industrial vapour. Also, GIS can be installed in building known as GIS hall which protects the substation against variations in weather condition.

Free choice of installation site:

Conventional extra high voltage substations need sites with a large area which usually needs a large amount of earthwork to level the ground. GIS with small site area saves costs required for construction of high voltage substations including earthworks and grading, foundation construction and all land preparation costs. Also short time is required for erecting a GIS substation when compared to AIS.

Compatibility with environment:

Finding a location for the building containing GIS is easier than locating a large area for constructing an AIS substation. GIS is, due to the modular system, very flexible and can meet all requirements of configuration given by network design and operating conditions.

Easy Maintenance

Gas Insulated Substations needs less maintenance and have longer life rather than air insulated substations. Maintenance and repair costs are lower compared to conventional AIS and also maintenance intervals are prolonged.

Simple Commissioning

Extensive in-plant preassembly and testing of large units and complete bays reduce assembly and commissioning time on the construction site.

Beside its unquestionable advantages, GIS also has its disadvantages. This study aims to investigate an undesired phenomenon that may affect the power transformer connected to a GIS as a result of using SF₆ insulation. Occurrence of very fast transients (VFT) is a consequence of insulation breakdown in SF₆ which is accompanied with extreme steep arcing voltages in GIS.

2.2 Definition of transient voltages

According to IEC standard [2, 9, 10] transient overvoltage is a short-duration overvoltage of few milliseconds or less, oscillatory or non-oscillatory which is usually highly damped. Transient overvoltages are divided into:

- Temporary overvoltage: is a power frequency overvoltage of relatively long duration with oscillations time to peak $0.02 \text{ s} < T_t \leq 3600 \text{ s}$, at frequency range $10 \text{ Hz} < f < 500 \text{ Hz}$. Load rejection, Transformer energization, Line energization, Line re-energization, switching of inductive and capacitive currents are the main origins of temporary overvoltage.
- Slow-front overvoltage: is a transient overvoltage, usually unidirectional, with time to peak $20 \mu\text{s} < T_p \leq 5000 \mu\text{s}$, and tail duration $T_2 \leq 20 \text{ ms}$. Transformer energization, Fault clearing and switching of inductive and capacitive currents are the main origins of slow front overvoltage.

- Fast-front overvoltage: is a transient overvoltage, usually unidirectional, with time to peak $0.1 \mu\text{s} < T_1 \leq 20 \mu\text{s}$, and tail duration $T_2 < 300 \mu\text{s}$. Direct lightning stroke and back flashover on the transmission line are the main origins of fast front overvoltages [9].
- Very-fast-front overvoltage (known as very fast transient voltage by IEEE): is a transient overvoltage, usually unidirectional with time to peak $T_f \leq 0,1 \mu\text{s}$, and with or without superimposed oscillations at frequency range $30 \text{ kHz} < f < 100 \text{ MHz}$. VFTO appears under switching conditions inside GIS substation, flashover in GIS substation and vacuum circuit-breaker switching in medium voltage switchgears [9].

Table 1. 1 shows classes and shapes of overvoltages, standard voltage shapes and standard withstand tests. According to the IEEE standards, these transients generally have a very short rise time, in the range of 4 to 100ns, and are normally followed by oscillations having frequencies in the range of 1 to 50 MHz [11].

Table 1. 1 Categories of different overvoltages defined by IEC [10]

Class	Low frequency		Transient		
	Continuous	Temporary	Slow-front	Fast-front	Very-fast-front
Voltage or over-voltage shapes					
Range of voltage or over-voltage shapes	$f = 50 \text{ Hz or } 60 \text{ Hz}$ $T_t \geq 3 \text{ 600 s}$	$10 \text{ Hz} < f < 500 \text{ Hz}$ $0,03 \text{ s} \leq T_t \leq 3 \text{ 600 s}$	$20 \mu\text{s} < T_p \leq 5 \text{ 000 } \mu\text{s}$ $T_2 \leq 20 \text{ ms}$	$0,1 \mu\text{s} < T_1 \leq 20 \mu\text{s}$ $T_2 \leq 300 \mu\text{s}$	$3 \text{ ns} < T_f \leq 100 \text{ ns}$ $0,3 \text{ MHz} < f_1 < 100 \text{ MHz}$ $30 \text{ kHz} < f_2 < 300 \text{ kHz}$
Standard voltage shapes	 $f = 50 \text{ Hz or } 60 \text{ Hz}$ T_t ¹⁾	 $48 \text{ Hz} \leq f \leq 62 \text{ Hz}$ $T_t = 60 \text{ s}$	 $T_p = 250 \mu\text{s}$ $T_2 = 2 \text{ 500 } \mu\text{s}$	 $T_1 = 1,2 \mu\text{s}$ $T_2 = 50 \mu\text{s}$	1)
Standard withstand test	1)	Short-duration power frequency test	Switching impulse test	Lightning impulse test	1)
1) To be specified by the relevant apparatus committees.					

VFTO is a switching overvoltage which is usually in the range of 1.5-2 p.u. and it can reach 2.5 p.u. [11]. For normal disconnector operation, the worst-case transient wavefront generation occurs for a breakdown from 1 p.u. on one side of the disconnector to -1 p.u. on the other side. The resulting 1 p.u. travelling wavefronts that propagate away from the disconnector can result in peak waveform amplitudes of 3 p.u.. Numerous studies indicate that theoretical worst-case conditions result in actual worst-case transient induced voltages in the range of 2.8 p.u. while in most GIS, a worst case transient magnitude of a little over 2 p.u. is more typical [12]. Fig. 2. 3 shows the magnitude of different transient types [9]. According to this figure, VFTO is less than 2.5 p.u. while lightning overvoltage is about 6.5 p.u.. Insulation in power systems are designed to withstand Basic Insulation Level (BIL) of each voltage level or Lightning Impulse Withstand Level (LIWL). As seen in Fig. 2. 3 VFTO maximum values introduced by IEC and IEEE standards are below the BIL of typical high voltage equipment. Therefore normally it shouldn't be a major concern, but the problem is that BIL at extra high voltage levels is less than 6.5 p.u. and BIL decreases with increasing system voltage level. Therefore, the maximum VFTO value becomes closer to the BIL at highest voltage. It means the severity of vary fast transients, relative to withstand of the GIS, increases with increasing voltage class, and the transient voltage levels are a function of the system voltage, and, therefore need special consideration at EHV levels (345 kV and above) [12]. Although VFTO magnitude in these EHV level is lower than BIL of the system, they contribute to the aging on the insulation of the system due to their frequent occurrences.

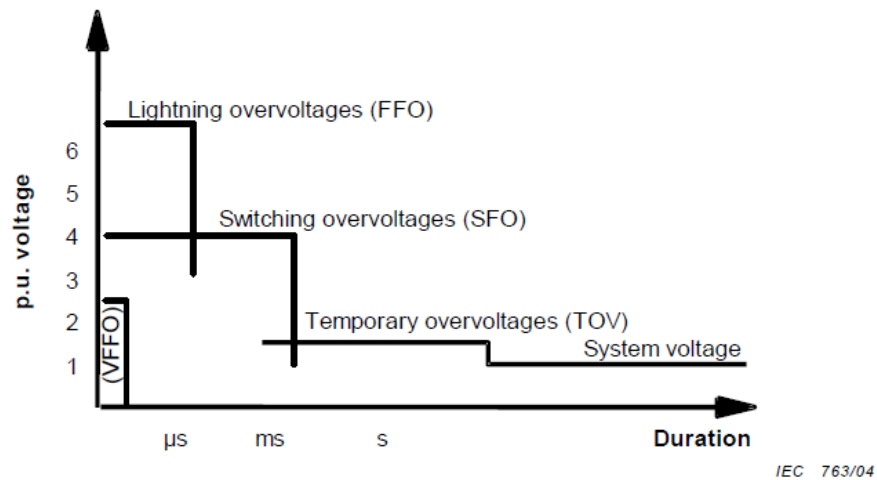


Fig. 2. 3 Types and magnitude of overvoltages [9]

2.3 Origin of VFTO in GIS

2.3.1 Voltage collapse during SF₆ breakdown

According to the Toepler spark model [1, 13], after a breakdown channel has bridged to the electrodes, a spark channel is formed with a few nano-seconds time lag.

During this time T_z , the spark resistance changes from a very high value ($\gg 10^6 \Omega$) to a very low value (5Ω).

$$T_z = 13.3 \frac{k_t}{E} \quad (2.1)$$

K_t : Toepler Spark Constant = 0.5×10^{-2} V.s/m for air or SF₆

E : Breakdown Field Strength at gas pressure $P = E_0 \cdot P \cdot \eta$

(E increases in proportion to the pressure of insulating gas.)

$$E_0: \text{ Breakdown Field Strength in 100 kPa} = \begin{cases} 8.6 \times 10^6 \frac{\text{V}}{\text{m}} \text{ for SF}_6 \\ 3.2 \times 10^6 \frac{\text{V}}{\text{m}} \text{ for air} \end{cases}$$

η : field utilization factor = $E_{mean}/E_{max} = 0.5 - 0.8$ for a normal GIS design

Therefore, it can be concluded that the transients originating from GIS have rise times much less than transients from AIS. The maximum rate of voltage change along a spark fed by a transmission line is given by:

$$\left(\frac{du}{dt}\right)_{max} = -0.15 \frac{l \cdot E_0^2}{k_t} \quad (2.2)$$

l : Spark length

Maximum $du/dt = 0.6$ MV/ns for 3 cm spark

According to Toepler [1, 13], the instantaneous value of the spark resistance R , is inversely proportional to the charge conducted through the spark channel. The spark resistance can be calculated from Toepler formula:

$$R_s = k_t \frac{l}{\int_0^t i dt} \quad (2.3)$$

$\int_0^t i dt$ is the amount of charge transmitted by a spark.

Protrusions, excessive roughness and particles lead to longer rise times [1].

2.3.2 Disconnecting Switch operation

VFTOs in GIS are usually generated during the operation of switching devices, such as Disconnecter Switch (DS) or Circuit Breaker (CB), which is a frequent event in high voltage substations as a result of voltage collapse in the GIS. VFTO sometimes occurs after phase to ground insulation breakdown which is not usual event in GIS. In any case, a travelling wave transient propagates in both directions away from the source. Assuming that the load side of a disconnecter has a trapped charge, V_L , and a characteristic (surge) impedance, Z_L , and that the source side of the disconnecter has a characteristic impedance, Z_S , and at a voltage, V_S . At the time of the inter-contact breakdown, the voltage on the load side of the disconnecter changes from V_L to $V_L + \{(V_S - V_L)/(Z_S + Z_L)\} \times Z_L$ while the source side changes from V_S to $V_S - \{(V_S - V_L)/(Z_S + Z_L)\} \times Z_S$. It is seen that the initial amplitude of these steps

depends on the voltage Δu across the DS at the instant of restrike or on the line to ground voltage before the fault. In a simple case that is $Z_S=Z_L$, $V_S=1$ p.u., and $V_L=0$ (i.e., a previously grounded load and a DS closing slowly enough that the first pre-strike will occur at the peak of the ac waveform), V_S will change from 1.0 p.u. to 0.5 p.u. in 3-5 ns, while V_L changes from 0 to 0.5 p.u. in about the same time. For a 400 kV GIS, this means a change of about 170kV in 4 ns, or a rate of change of about 43 MV/ μ s that is corresponding to voltage change of 170kV over a distance of about 130 cm (1.3 kV/cm). Fig. 2. 4 shows the voltage changes in either cases of switch operation or insulation breakdown at the origin of VFTO.

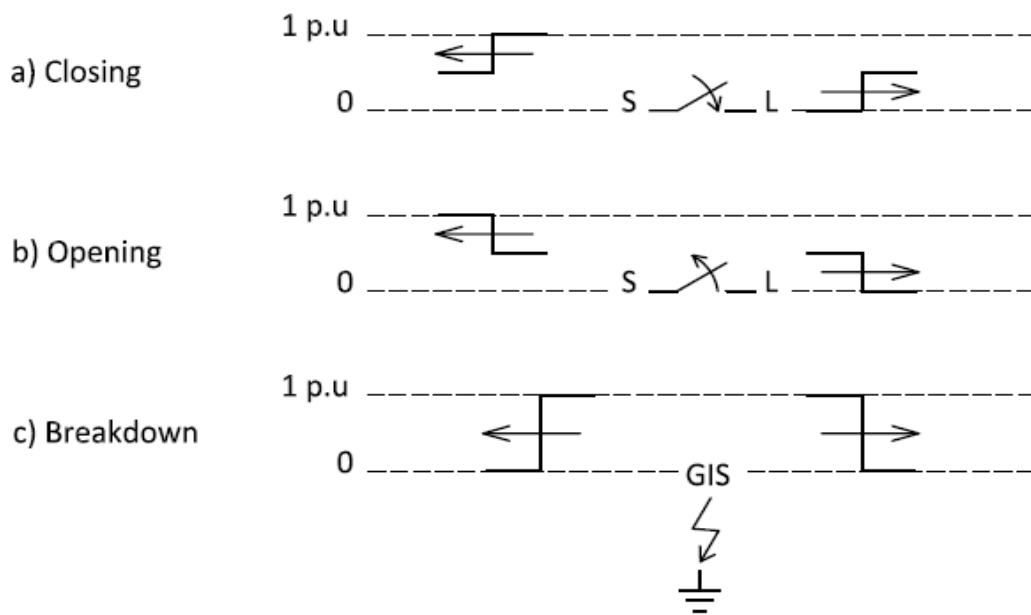


Fig. 2. 4 Voltage change at DS during a switching operation

2.3.3 Frequent restrikes

The reason for formation of such high frequency complicated VFTO waveform in GIS will be understood by explaining what happens during a switching operation. The occurrence of sequence of re-strikes during switching operation including opening and closing operations is illustrated in Fig. 2. 5. During an opening operation, at the instant of separation, both sides of DS contacts will have the same value. When the separation starts, V_S will have its power frequency value while V_L keeps its previous value. At the time (V_S-V_L) reaches the dielectric strength of the gap between contacts, a breakdown happens and the first prestrike generates a spark that connects the two contacts electrically and the load side voltage will change to a value of V_S abruptly and the spark extinguishes. As opening operation is continuing and distance between gaps is increasing, new dielectric strength level will be greater than the previous one. The next restrike occurs when voltage difference reaches to this new dielectric strength level. This process continues until the gap no longer can be broken down [14]. As shown in the figure, there may be a charge left on the load side due to DS contact design which has a considerable effect on VFT magnitude [15]. The

behaviour during closing operation is similar to opening operation but in reverse direction.

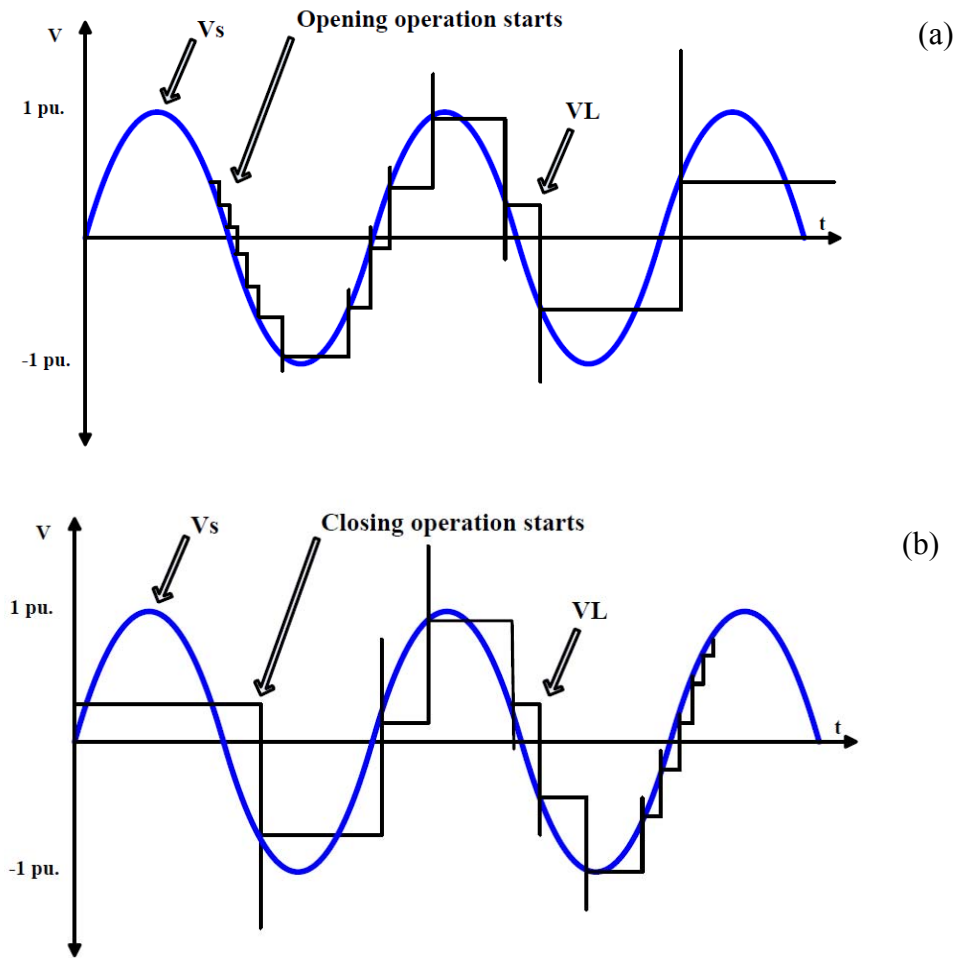


Fig. 2. 5 Generation of VFTO waveform during DS multiple restrikes a) DS opening b) DS closing

Since the operational speed of contacts in DS is very slow in comparison with CB, prestriking or restriking occurs many times before the switching operation is completed [15]. As the initial travelling wave encounters GIS discontinuities such as open DS, Bushing and other connections, the travelling waves are reflected and transmitted according to basic transmission line theory. The superposition of all travelling waves (reflected and refracted) generated in GIS network results in high voltage amplitude that is proportional to the amplitude of the initial voltage step and the arrangement of GIS equipment. Also it was observed that larger disconnector-induced transients occur during opening as a result of the statistical variation in the generally systematic nature of disconnector operation [12].

2.4 Propagation of VFTO in GIS

According to Fig. 2. 4, DS operation induces travelling wave transients at both sides of the switch with opposite polarity and insulation breakdown causes travelling wave transients to propagate away from the fault location at both sides with

magnitude equal to the voltage at the instant of fault [12]. VFTs propagate away from their source at approximately the speed of light (30cm/ns) reflecting and refracting at impedance mismatches according to the standard transmission line theory. This results in a complex pattern of travelling waves within the substation that superimpose to generate greater voltages at some locations than at others. Thus the voltage stress to which the substation is subjected to as a result of switching induced (or breakdown-induced) transients is a function of the station configuration, the position of the operated switch, switch characteristics (which affect trapped charge during switching), and the position at which the voltage is measured.

Figs 2.6 to 2.9 show the basic mechanism of generating and propagation of a high frequency VFTO surge in a simplified gas insulated substation structure. In this example, only the first restriking is considered to travel in the GIS for simplicity. Fig. 2. 6 shows a very simplified structure of DS connection to GIS busducts. Generally, the main function of DS in high voltage substations is to isolate CB from the rest of the network [16]. Therefore, DS necessarily operates after CB operation and is designed to switch a line which is unloaded after CB operation. Then for illustration of VFTO generating from DS operation, the load side of DS is considered to be open circuit with initial voltage of -1 p.u. and DS is considered to be closed at $t=0$. L represents the source inductance, including the impedance of the power transformer. GIS bus bars are assumed to have 10m and 100m length with $z=70 \Omega$ according to typical busbar lengths in GIS substations with double busbar arrangement [16] and the surge travelling time is 300 m/ μ s. The voltage waveform at nodes “T” & “Q” within the first 3 μ s shows a high frequency oscillation without overvoltage. Stray capacitances of some high voltage equipment in the GIS such as capacitive voltage transformer, surge arrester and spacer are added to the GIS model in Fig. 2. 7. As a consequence of this capacitive branch, overvoltages with an amplitude of about 2.8 p.u. appears at the open end terminal. Fig. 2. 8 shows the connection of several branches at the load side of the DS without considering stray capacitance of equipment. By calculating the waveforms at the transformer terminals and open end of busbar, overvoltages of about 1.8 p.u. and 2.3 p.u. are respectively developed. By considering stray capacitance (as shown in Fig. 2. 9), an overvoltage up to 3.5 p.u. emerges at the open end of GIS bus bar is developed. Fig. 2. 9 shows that multiple reflections at the open end terminal of the GIS can generate overvoltage with very high frequencies in the range of MHz with remarkable amplitude of about 3.5 p.u.. This case is the most similar case to the real GIS with several branches and many capacitors representing all equipment and discontinuities in GIS such as spacers, elbows and connectors. In all cases considered capacitive components, an overvoltage across the GIS terminals after switching operation can be easily observed. Also it is concluded from these calculation that two factors are very important in determining the severity of VFTO: GIS layout and details of GIS modelling.

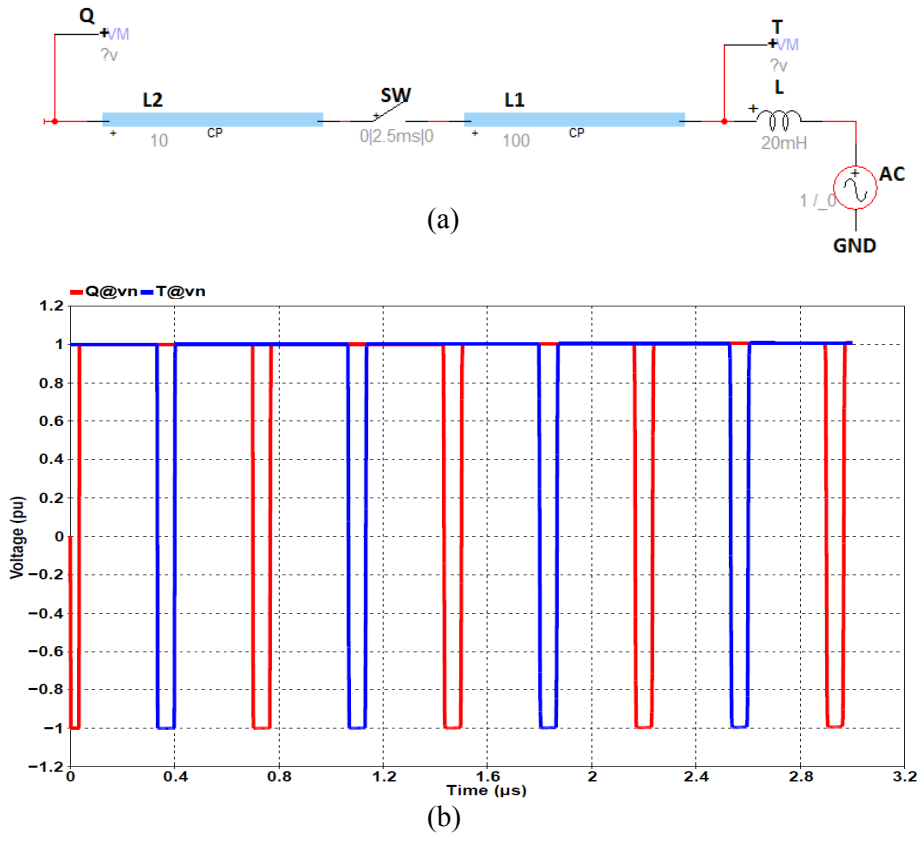


Fig. 2. 6 Connection without any branches a) Model circuit b) Voltage waveform at T & Q

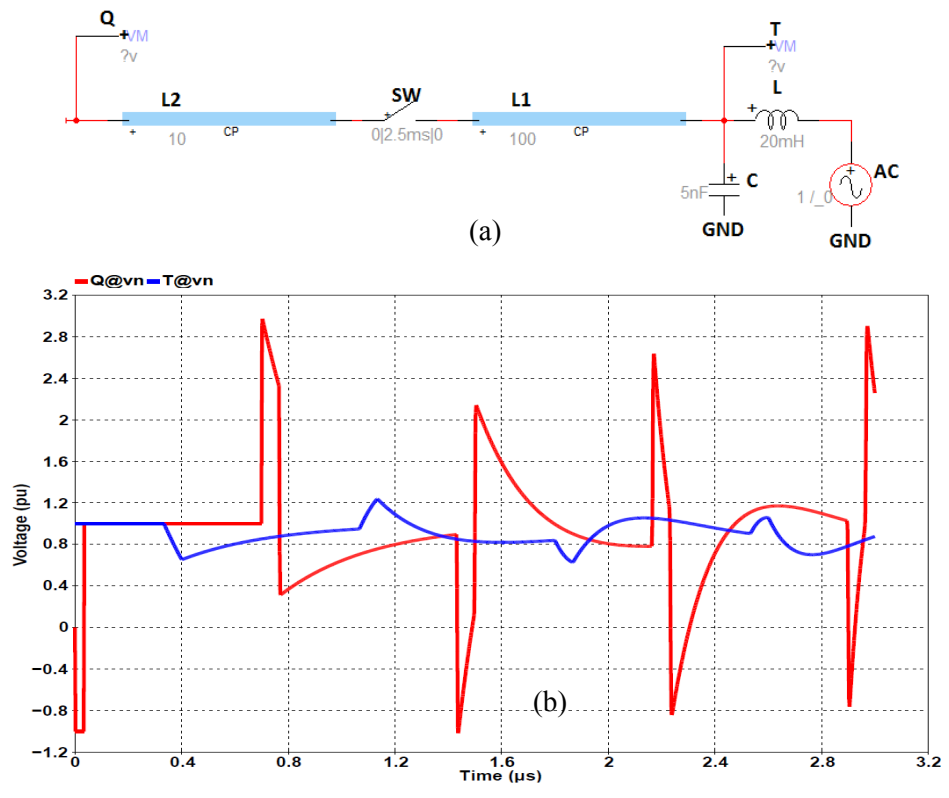
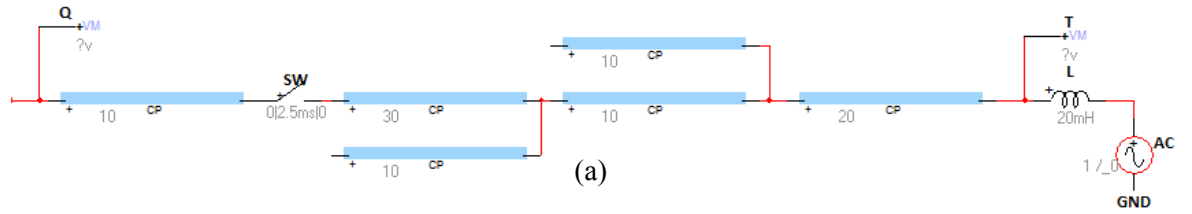
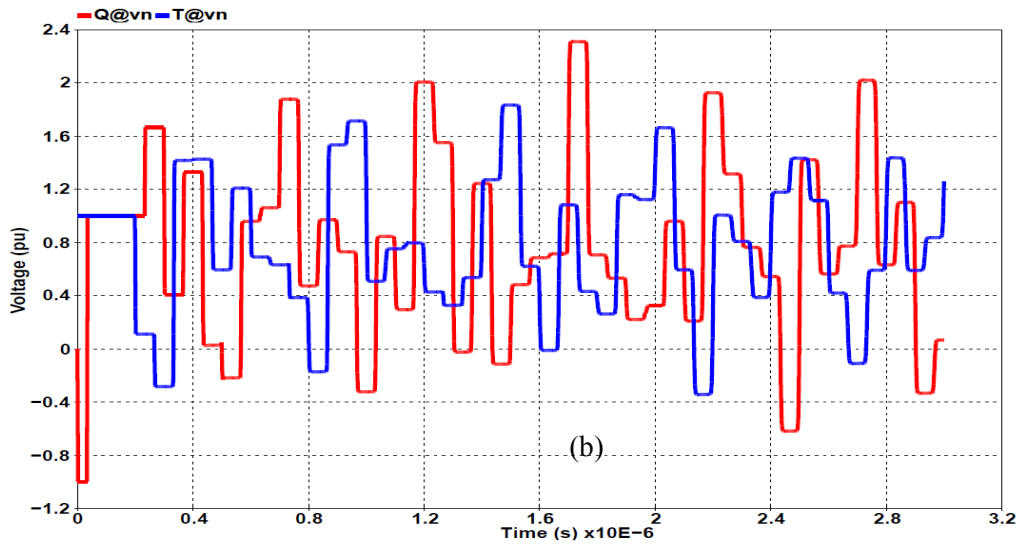


Fig. 2. 7 Connection with stray capacitance of equipment a) Model circuit b) Voltage waveform at T & Q

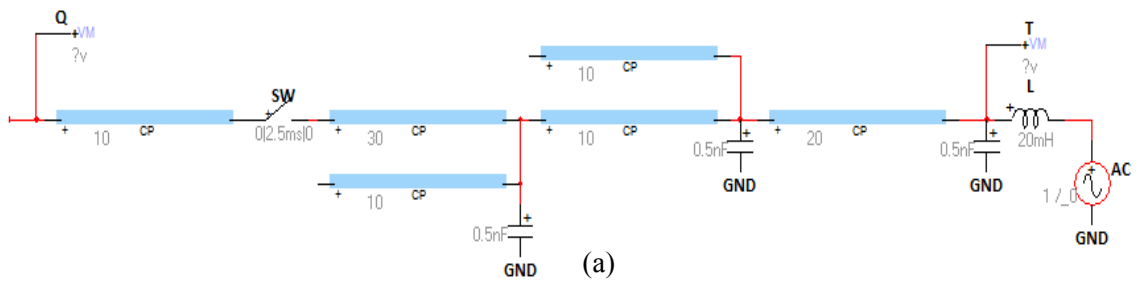


(a)

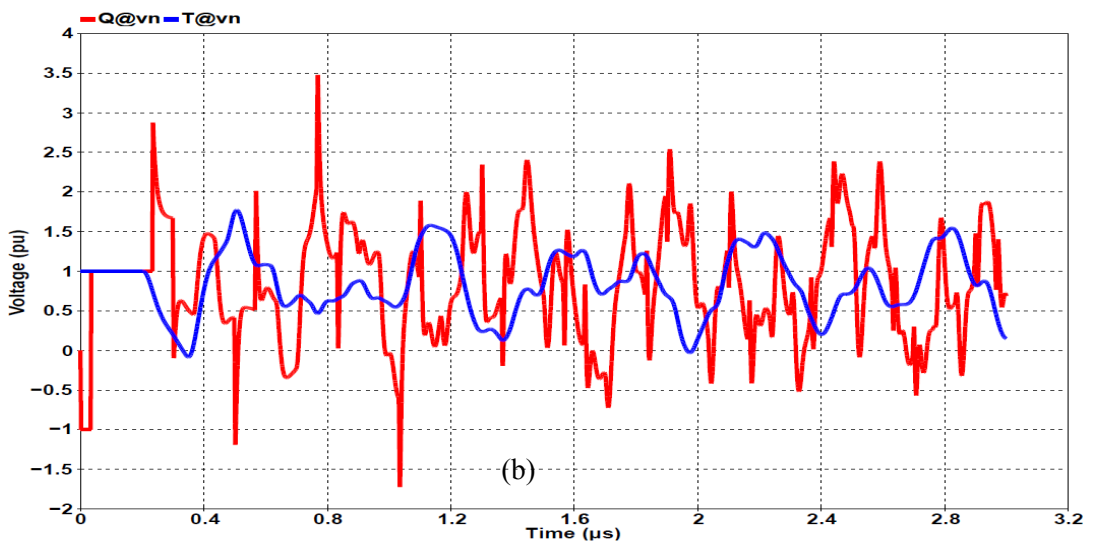


(b)

Fig. 2. 8 Connection with branches at load side a) Model circuit b) Voltage waveform at T



(a)



(b)

Fig. 2. 9 Connection with branch and stray capacitances a) Model circuit b) Voltage waveform at T & Q

2.4.1 Internal and External modes

VFT has both internal and external effects [11]. Transients which occur between the GIS main conductor and the enclosure are called internal transients, which are investigated in this thesis. The transients appearing on the enclosure, secondary and adjacent equipment outside the GIS are called external transients. After the generation of step voltage at the operating switch, whenever this travelling wave encounters a discontinuity in its propagation i.e. nodes that characteristic impedance changes, reflection and refraction happens. Finally, the VFTO wave will be formed by superposition of all these waves with remarkable magnitude on the internal conductor of the GIS. This internal effect has a different severity at different locations in the GIS. Fig. 2. 10 shows the propagation path of VFTO surge at SF₆-air bushing. In this figure, the impedance between GIS main conductor and enclosure is represented by Z_1 , the impedance between overhead line conductor and earth is represented by Z_2 , and the impedance between enclosure and earth is represented by Z_3 [17]. As a VFTO wave or internal transient arrives at the interface of GIS and air, it is partly transmitted to the enclosure (through Z_3), partly transmitted to overhead line conductor (through Z_2) and partly reflected in the GIS.

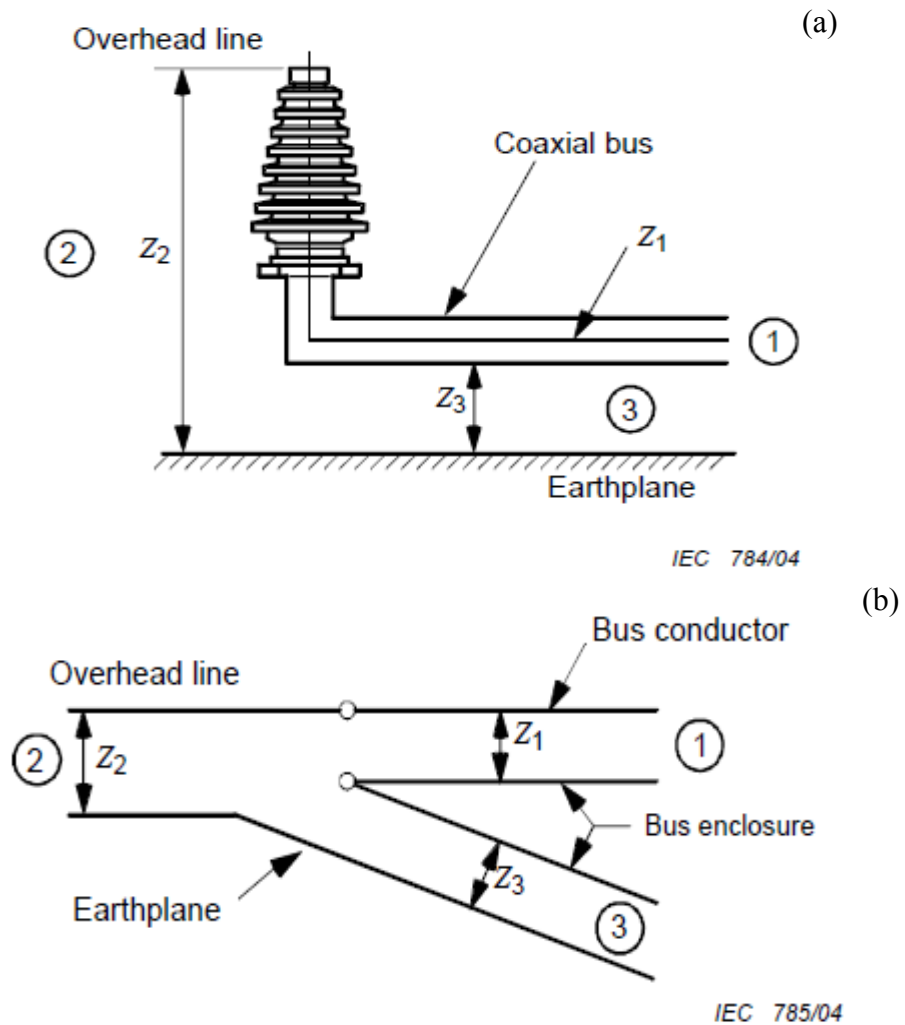


Fig. 2. 10 At the GIS-air bushing a) Actual configuration b) Schematic configuration

External transients may have dangerous consequences regarding reliability of high voltage equipment (such as protective instruments, transformer and insulators) and also safety of personnel. The outgoing travelling wave from GIS termination can accelerate the aging process of power transformer insulation system. Moreover, travelling waves are accompanied by Very Fast Transient Current (VFTC), which is the sources of electromagnetic fields radiating from main the GIS conductor, and cause malfunctioning to the secondary equipment [18]. External transients include:

Transient Enclosure Voltages (TEV):

Also known as Transient Ground Potential Rise (TGPR) these are high frequency and voltage transients with very short duration appearing on GIS enclosure as a consequence of coupling between internal transients and enclosure at the points of impedance changes, such as SF₆ to air bushing, CT, cable termination and flanges. The amplitude of TEV can be within 10-30% of DS operating voltage with high frequencies in the range of 10-20 MHz [19].

Transients on Overhead Line connections:

Part of the VFT wave travelling inside the GIS is transferred onto the overhead connection when arrives to SF₆-air bushing and propagates to other components outside the GIS. These VFTs will be damped because of the loss in propagation then the rise time will increase consequently. Generally, external transients have two characteristics: the overall wave, with rise time in the range of few hundred ns, has a typical significant frequency component at about 10 MHz which is determined by lumped circuit parameters like capacitor of VTs or inductance of the transmission line and the second is that there is a faster portion in the wave with rise time in the range of 20 ns, which is determined by transmission line effects, and is usually damped passing the line [9, 11].

Transient Electromagnetic Fields:

The electromagnetic fields radiated from the enclosure usually stress the secondary equipment, especially the electronic controls and computer equipment. Their frequency are determined by the arrangement of equipment in the GIS, and is typically in the range of 10-20 MHz [11]. The electromagnetic radiation is associated with VFTC in GIS [20], which can reach to 5kA for a 400kV GIS, and has frequencies more than 100MHz. While the electrical field strength rapidly reduces with distance, its frequency increases [21]. The mechanism that generates the external transients from the internal transients can be analysed by the interface shown in Fig. 2. 10.

2.5 Calculation of VFTO at transformer terminals

Based on Telegraph equations for π equivalent circuit of transmission lines, propagation of travelling waves in a line can be described by equivalent series impedance and shunt admittance [22]. Here as shown in Fig. 2. 11, for simplicity of calculation, series impedance is replaced by equivalent admittance:

$$Y_1 = \frac{1}{z} \tanh\left(\frac{sT}{2}\right) \quad (2.4)$$

$$Y_2 = \frac{1}{z \sinh(sT)} \quad (2.5)$$

T and z are the transit time and surge impedance of the line, respectively and E_0 is the initial voltage due to the trapped charge of the line. Now, if a terminal resistance R is considered to be open, Y_1 and Y_2 will be connected in series while connected with input admittance Y_1 in parallel. Thus, the Thevenin impedance looking from the source (S) side is:

$$Z_s = \frac{z}{\tanh(sT)} \quad (2.6)$$

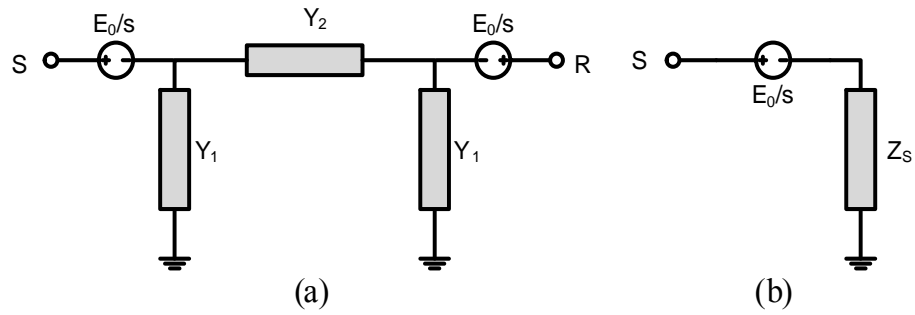


Fig. 2. 11 Equivalent circuit of transmission line a) π equivalent circuit b) Terminal equivalent circuit

Assume that two GIS busbars BUS_1 & BUS_2 are connected to DS at both sides such as shown in Fig. 2. 12, and BUS_1 is considered to be open end (representing open CB), the Thevenin voltage and impedance from point P can be obtained:

$$(2.6) \Rightarrow Z_1 = \frac{z}{\tanh(sT_1)} \quad (2.7)$$

$$(2.4) \Rightarrow Z_{21} = \frac{z}{\tanh\left(\frac{sT_2}{2}\right)} \quad (2.8)$$

$$(2.5) \Rightarrow Z_{22} = z \sinh(sT_2) \quad (2.9)$$

$$E_{th} = \frac{E_2}{s} + \left(\frac{E_1 - E_2}{s}\right) \cdot \frac{\sinh(sT_1)}{\sinh(s(T_1 + T_2))} \quad (2.10)$$

$$Z_{th} = \frac{z}{\tanh(s(T_1 + T_2))} \quad (2.11)$$

In the above equations T_1 and T_2 are the surge travelling time in BUS_1 and BUS_2 respectively.

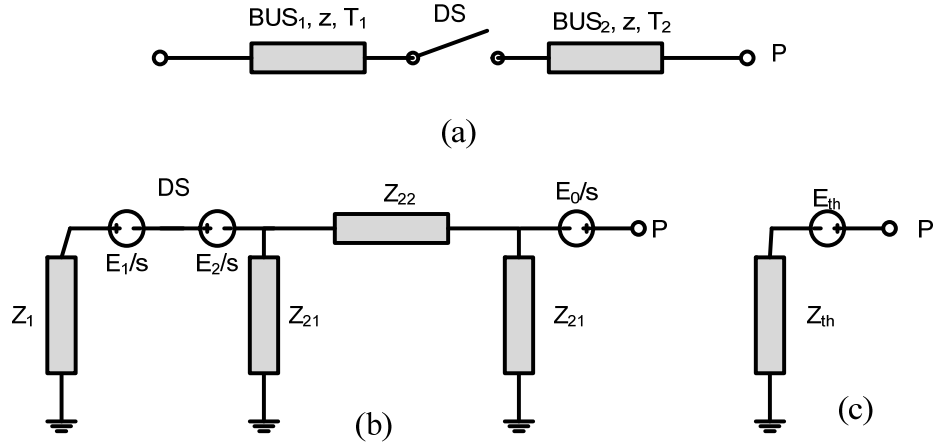


Fig. 2. 12 GIS busbars connected to operating DS a) GIS busbars 1 &2 b) connection of equivalent circuits c) Thevenin equivalent circuit

Fig. 2. 13 illustrates a simplified structure of GIS system connected to a transformer during DS operation. BUS₁ and BUS₂ represent the GIS busducts connecting the DS to the source and load sides. Since the DS in substation operates after the operation of circuit breaker, BUS₁ side of the circuit is considered to be open circuit. DS closes at $t=0$. E_1 is trapped voltage at the open terminal and E_2 is the initial voltage of the transformer terminals at $t=0$.

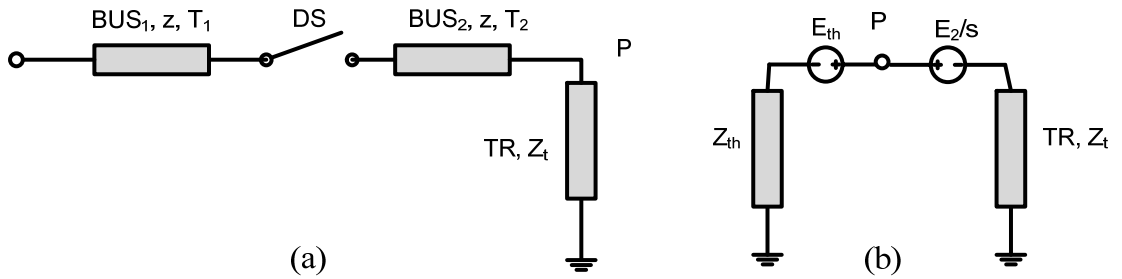


Fig. 2. 13 Connection GIS to Transformer a) Simplified GIS structure b) Equivalent circuit

Since VFTO comprises very high frequencies, the transformer can be modelled as a capacitance C_t . Then the voltage at the terminal of the transformer can be calculated as below [23]:

$$V_t = \frac{E_2}{s} + \frac{E_1 - E_2}{s} \cdot \frac{\sinh(sT_1)}{\sinh(sT) + sC_t z \cosh(sT)} \quad (2.12)$$

In which $T = T_1 + T_2$

Frequencies that lead to maximum voltage at power transformer terminals can be obtained by solving the below equation:

$$sC_t + \frac{\tanh(sT)}{z} = 0 \quad (2.13)$$

Generally, Laplace equations have roots at $s=\alpha\pm j\omega_k$. Ignoring the resistive loss, Equation (2.13) will have only imaginary roots at $s=\pm j\omega_k$ which means that V_t can be expressed as:

$$V_t = E_0 + \sum_{k=1}^{\infty} G_k \cos(\omega_k t)$$

$$\omega_k C_t z = -\tan(\omega_k T); \quad k = 1, 2, \dots \quad (2.14)$$

Equation (2.14) can be solved using geometrical method to obtain all frequencies at which V_t is maximum [24]. According to Fig. 2. 14, all ω_k can be obtained by finding the intersections of graphs: $\omega_k C_t z$ and $-\tanh(\omega_k t)$. It is concluded that:

$$(k - \frac{1}{2}) \frac{\pi}{T} < \omega_k < k \frac{\pi}{T} \quad (2.15)$$

As a result, the amplitude of the k_{th} harmonic and the DC component are obtained as [23]:

$$G_k = \frac{\sin(\omega_k T_1) \cos(\omega_k T)}{\omega_k T - \sin(\omega_k T) \cos(\omega_k T)} (E_1 - E_2) \quad (2.16)$$

$$E_0 = \frac{T_1}{T + z C_t} (E_1 - E_2) + E_2 \quad (2.17)$$

By substituting (14) into (15):

$$|G_k| = \frac{1}{\omega_k} \left| \frac{\sin(\omega_k T_1) \cos(\omega_k T)}{T + C_t z \cos^2(\omega_k T)} (E_1 - E_2) \right| \quad (2.18)$$

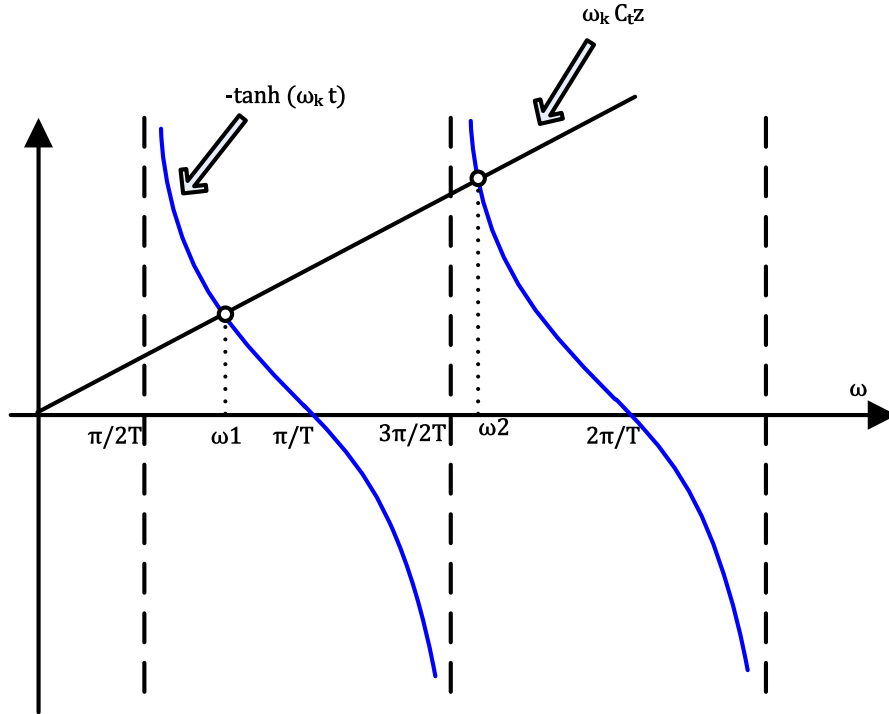


Fig. 2. 14 Determination of ω_k

According to (2.17) and (2.18), it is clear that by increasing the value of C_t , amplitude of both DC and high frequency components of V_t are decreasing. In other words, the high frequency components of VFTO can be suppressed by installing a capacitor in parallel with the power transformer.

2.6 Effective Factors in VFTO magnitude

2.6.1 Trapped Charge

It is clear from equation 2.18 that magnitude of VFTO high frequency components strongly depends on E_1 and E_2 . E_2 represents the voltage at the transformer side of the DS at switching instant, while E_1 is the initial voltage of the other side of DS resulted from trapped charge. As shown in Fig. 2. 5b, during closing operation of DS, there is a trapped charge on the CB side of DS remained on the floating section between CB and DS. The potential cause by trapped charge may last for several hours to days and usually leaks through the spacers [15]. The amount of trapped charge is dependent on the design of DS contact system, and the asymmetrical breakdown voltage is the main reason for formation of trapped charge during switching operation because the negative breakdown during the switch operation occurs at about 15% greater potential difference than positive breakdown [15]. Since this relation between the geometry of DS and VFTO magnitude was found, several studies has been performed to improve the design of DS contact system to mitigate VFTO effects [25]. Also several studies and experiments addressed the amount of trapped charge from a small percentage to relatively large values [15]. Analyzed results of measurements on a 500kV GIS concluded that trapped charge value rarely exceeds 0.3 p.u., while according to [26] the potential can reach up to 1 p.u.. IEC standard suggests the maximum trapped charge value to reach 0.5 p.u. [9].

2.6.2 DS operation speed

Generally, there is a correlation between trapped charge and DS operation speed. If DS operates faster, the number of strikes during one operation decreases but, the probability of large transients and large trapped charge after an opening operation will increase, and it needs a careful switch design to avoid this phenomenon. More slowly operating DS can be designed so as to limit inter-contact breakdowns to about 1.4 p.u. and to leave a trapped charge during opening of less than 0.4 p.u.. [12] Rapid disconnecting switch operation could have other effects. The increased mechanical stresses on the operating mechanism could reduce the overall system reliability. Therefore there should be a balance between number of strikes and the value of trapped charge.

2.6.3 GIS Layout

It was shown in section 2.4 that branching in GIS arrangement has a remarkable effect on the magnitude of VFTO. Also according to (2.17), DC component of VFTO change with T , T_l and z . Equation (2.17) reveals that by increasing T while T_l doesn't

change, deviation of voltage at transformer terminal from its original value (E_2) is reducing. In other words, if the length of BUS₁ is constant, the magnitude of VFTO is reduced by increasing the length of BUS₂, or if length of BUS₁ is reduced while the length of BUS₂ is increased in such a way the total length doesn't change, amplitude of E_0 decreases and therefore the magnitude of VFTO decreases. One important result of VFTO calculation in section 2.5 is that from (2.14), dominant frequencies of VFTO depend only on total GIS length. Therefore changing the GIS busbars at either sides of DS while the total length is fixed, doesn't have any effect on VFTO magnitude. It means that the location of DS doesn't have influence on the magnitude of VFTO at the transformer terminals, and dominant frequencies of VFTO resulting from DS operations are the same for all switches within the substation. VFTO magnitude experiences significant changes due to changes in length of GIS busbars.

2.6.4 Capacitance at Transformer terminal

Similar to the effect of T in (2.17), increasing C_t can have suppressing effect on the magnitude of VFTO. Calculation results show that by increasing the capacitor value at the transformer terminal, high frequency components will be more attenuated. It can be shown that among different alternatives available to connect the GIS to power transformer such as overhead conductor, Gas Insulated Line (GIL) and cable, the latter has the best performance in attenuating the VFTO high frequency due to its better capacitive characteristics [27].

2.7 VFTO in Transformer Winding

2.7.1 Initial distribution of transient in winding

When a voltage surge arrives at a transformer winding, two harmful phenomena jeopardize the insulation of winding, which happen after a surge enters the transformer winding at different stages [28]:

1. Unbalanced distribution of voltage in the winding
2. Internal resonance of transformer

For studying the behaviour of winding against short rise time voltages it is helpful to divide the time after surge arrival into three different intervals [17, 29]:

Stage 1: Initial voltage distribution:

This interval lasts for a very short duration in the range of a few nano-seconds. During this time current penetrating the winding is not significant due to the transformer relatively high inductance. Therefore, the transformer can be modelled as a capacitive component during this period of time (Fig. 2. 15). During the initial period, each small length of the winding acts like a capacitor element (C_s) connected

to a capacitor to ground (C_g). It can be shown [29] that within the initial period of surge propagation, voltage at any point in winding (x) can be expressed as:

$$E = V \frac{\sinh\left(\frac{ax}{l}\right)}{\sinh a} \quad (2.19)$$

$$a = \sqrt{\frac{C_g}{C_s}}$$

V : Applied voltage

l : Length of winding

C_s : Series capacitance of winding

C_g : Ground capacitance of winding

Equation (2.19) shows that the voltage is not uniformly distributed through the winding, and C_g/C_s is not constant along the whole winding. It is clear that the terminals or first turns of the winding undergo a severe stress on their insulation. This non-uniformity is strongly dependent on the parameter a . If parameter a has smaller values or in other words, ground capacitance decreases and series capacitance increases, the voltage along the winding will be more uniformly distributed.

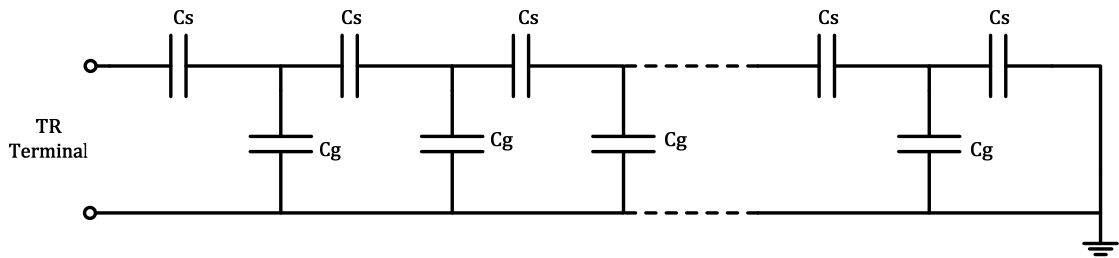


Fig. 2. 15 Model of transformer during initial voltage distribution

In actual power transformers, this parameter changes along the winding [29], therefore it can be observed that 60% of the voltage is distributed along the first 10% of the winding [29]. This non-uniform distribution of voltage within this period is illustrated in Fig. 2. 16a. At this state, striking surge can endanger the insulation between turns close to transformer terminals by imposing severe stress on insulation.

Stage 2: Transient voltage distribution

After a few micro-seconds, inductive and resistive characteristics of the circuit become dominant in determining the behaviour of winding against surge. Therefore, complicated oscillatory wave is created in the winding.

Stage 3: Final voltage distribution

At the end of transient state, when wave tail passes from the system, resistance of the circuit dominates the system response and consequently, as shown in Fig. 2. 16b the voltage distribution along the winding will be uniform.

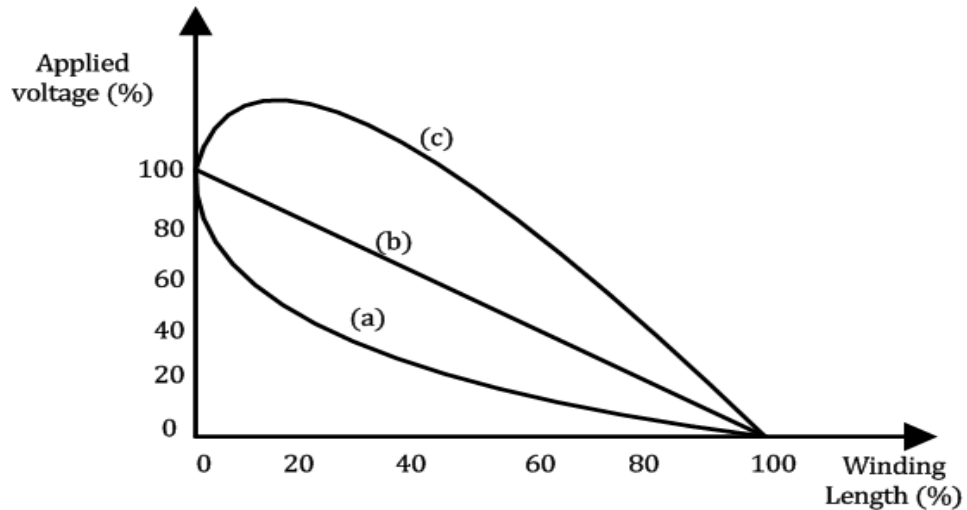


Fig. 2. 16 Voltage distribution in winding after arriving a surge
a) Initial state b) Final state c) Transient state

As the proposed technique is for a very short rise time of VFTO, initial and transient voltage distribution states are considered in this thesis. Several mitigation methods have been applied for protecting the winding insulation against electrical stress during initial voltage distribution as briefly elaborated below [29]:

- First method was to strengthen the insulation of the first few turns of the winding close to transformer terminal. This method has a significant drawback that necessitates careful design of insulation for windings, for this reason this method is no longer practical. The problem was that strengthening the insulation of the first few turns usually made the capacitance even more non-uniform and exaggerates the investigated issue rather than solving it.
- The common method that is currently used in industry is to install a metallic shield plate adjacent to coils for voltage grading; similar to the technique used for overhead transmission lines. The problem of non-uniform voltage distribution is originated from unbalanced passage of currents through ground capacitances in the equivalent circuit shown in Fig. 2. 15. Therefore, it is possible to compensate for the ground capacitance currents by locating two electrostatic plates in parallel to coils [30].
- Another widely used method is interconnecting the terminals of coils to make more uniform distribution of capacitance.

2.7.2 Internal resonance

The major concern of this study is the possibility of exciting the resonance frequencies of a transformer winding by a VFTO surge coming from the GIS, which

happens during the transient state of voltage distribution along a transformer winding. As stated before, during the transient state, the response of a winding is mostly determined by capacitance and inductance of the equivalent circuits, which is illustrated in Fig. 2. 17. In this figure, if points A and B are located at anti-nodes of standing wave pattern at some special frequencies, a maximum voltage occurs between them. This phenomenon is called “Internal Resonance” [31]. Anti-nodes may be at minimum voltage at particular frequencies, which is referred to “Internal Anti-resonance”. According to the definition presented in [31]:

- Terminal Resonance is the referred to a case with terminal maximum current or terminal minimum impedance.
- Terminal Anti-resonance is a case with terminal minimum current or terminal maximum impedance.
- Internal Resonance corresponds to a case with internal maximum voltage.
- Internal Anti-resonance corresponds to a case with internal minimum voltage.

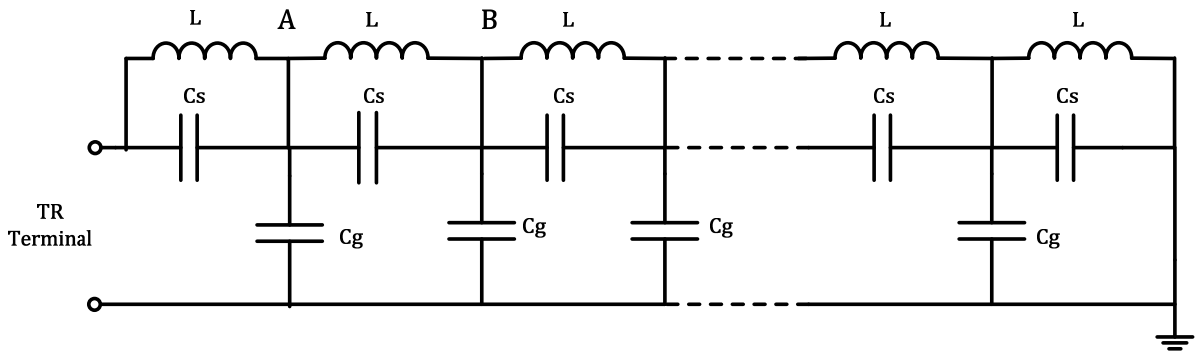


Fig. 2. 17 Model of transformer during fast and very fast transients

Any four terminal electrical network made of passive elements such as resistor, inductor and capacitor has some natural frequencies in which resonance may arise. The frequency, phase and magnitude of these resonances can be determined by both analytical and experimental methods. Analytical methods involve different methods to model the internal parts of transformer winding and study of winding behaviour at high frequencies. While experimental methods deal with Frequency Response Analysis (FRA) of a transformer, and proposing different measuring and testing methods based on winding transfer function for the purpose of finding the resonance frequencies [32]. Although several studies have been performed to introduce basic relationships of resonance frequencies of transformer with its technical specifications, resonance frequencies of transformers can be exactly found by detailed modelling of transformer winding or by performing measurements using a variable frequency source. Some empirical formulas for expressing the lowest resonance frequency of transformer are presented in [31]:

$$\begin{aligned}
\text{Hessen: } f(\text{kHz}) &= \frac{220\text{MVA}^{0.36}}{kV^{0.95}} \\
\text{Phillips: } f(\text{kHz}) &= \frac{325\text{MVA}^{0.275}}{kV^{0.95}}
\end{aligned}
\tag{2.20}$$

In which kV and MVA are voltage and apparent power of the transformer winding respectively. In order to find resonance frequencies of transformer in the present work, a detailed model of internal parts of the investigated transformer will be created.

For the purpose of analytical study of the resonance condition in power transformer and frequency dependence of the network, input impedance (V_{in}/I_{in}) or transfer function (V_{out}/V_{in}) can be evaluated [31]. For example, for analyzing the internal resonance we have to find the frequencies with maximum gain function between line terminal to ground and mid-winding to ground. Fig. 2. 18 shows a simplified model of power transformer winding consisting of five discs. The method of modelling a transformer winding will be discussed in chapter three. The transfer function at the connections between 1st and 2nd discs is also shown in Fig. 2. 19. It can be seen that there are resonance frequencies at 48, 70, 155 and 505 kHz and anti-resonance frequencies at 50, 80, 145 and 490 kHz. These frequencies and the magnitude of the transfer function are determined by the values of the passive components of the network.

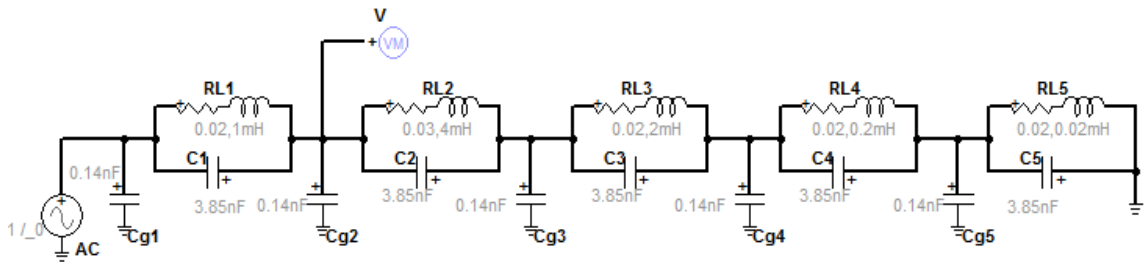


Fig. 2. 18 Simplified model of lumped parameter winding

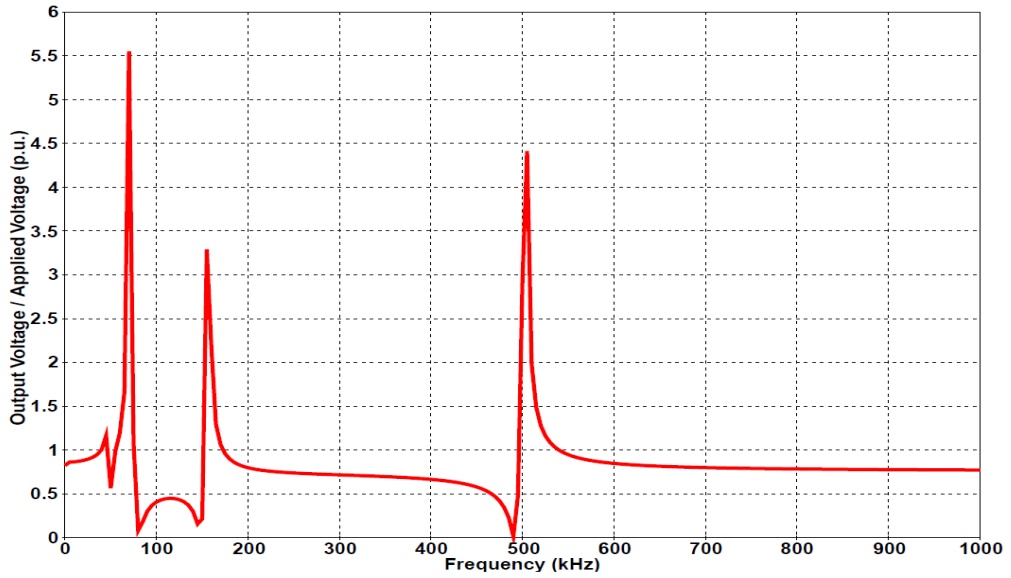


Fig. 2. 19 Gain function from terminal voltage to internal voltage [31]

Although, there are several resonance frequencies at the connection between 1st and 2nd disc, it doesn't mean that these resonance frequencies are exhibited at the terminal of the power transformer. Non-uniform insulation of winding causes the terminal response of transformer doesn't relate to internal response of a particular part of transformer winding.

As can be seen in Fig. 2.19, remarkable overvoltages occur as a consequence of resonance frequencies. Resonant frequencies of transformer winding can be explored by creating a mathematical model of the winding. Fig. 2. 20, and Fig. 2. 21 show that if a fast front surge (1.5/40 μ s standard lightning waveform) is applied to the network of Fig. 2. 18, the frequency spectrum of the voltage at the 1st and 2nd discs will exhibit large magnitude at resonance frequencies. Fig. 2. 21 shows the frequency spectrum of the voltage measured at the point shown in Fig. 2. 20 (between the 1st and 2nd discs of the winding) in the range of 40 to 80 kHz. It is noted that the voltage peaks locate exactly at frequencies 48 kHz and 70 kHz which are the resonance frequencies of the simplified model shown in Fig. 2. 19. In fact, Fig. 2. 21 illustrates how the input wave can excite the resonance frequencies of the winding and result in voltage peaks at these frequencies.

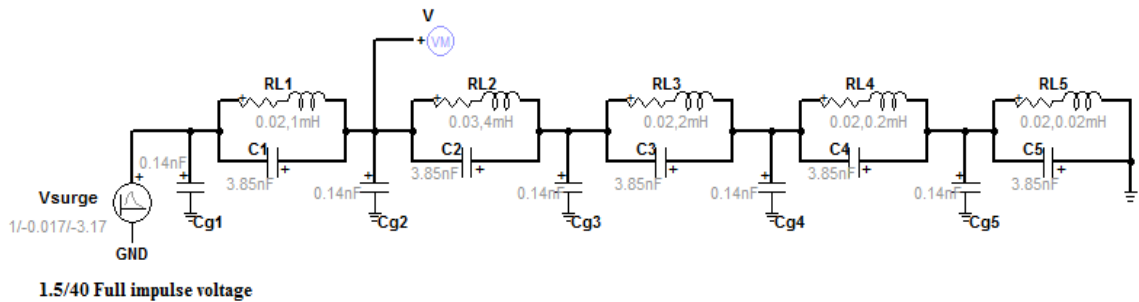


Fig. 2. 20 Circuit of Fig. 2. 19 with standard lightning surge applied as input voltage

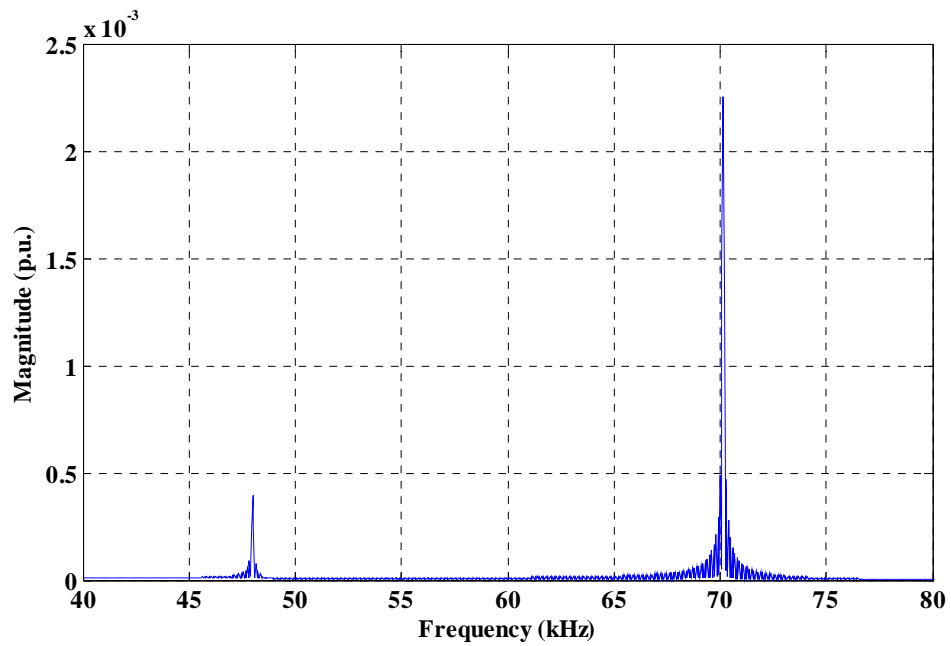


Fig. 2. 21 Frequency spectrum of voltage at connection between 1st and 2nd discs

The importance of studying resonance phenomena in power transformers is that the failure of power transformer insulation can be a result of voltage stresses at internal parts of the winding. Since the winding insulation of power transformers is non-restoring insulation, very careful measures should be adopted to avoid such internal overvoltages that endanger the insulation of transformer winding and consequently the whole transformer as the most important asset in high voltage substation.

3 Power System Modelling

This thesis is aimed at mitigating internal resonance of transformer due to VFTO surges originated from GIS; a schematic connection of GIS to power transformer is shown in Fig. 3.1. The internal resonance corresponds to the cases with maximum internal voltages in transformer winding [31], therefore the voltages between the turns of a transformer winding must be calculated. From the GIS side, the resonance in transformer winding is not noticeable due to the relatively high coupling between transformer windings. Thus, from GIS point of view, transformer can be modelled as a large capacitance. But for analysing the behaviour of a travelling surge inside transformer winding, each disc and turn of the winding must be modelled. Some experimental studies show that the resonance in the winding does not influence waveform of VFT in a GIS [33], it is concluded that the two phenomena: generating VFTO in GIS and interturn resonance in transformer winding can be investigated independently. In other words, in this study, each phenomenon is modelled separately and then studied altogether.

In this work, a real 400kV power plant substation was modelled in detail. This GIS plant is situated at about 100 km south of Caspian Sea in north of Iran, and is connected to a pumped-storage 1000MW power plant via a 400kV cable at a distance of 500m. According to Fig. 3. 2 Single Line diagram of substation the substation has four 400kV incoming lines from power plant unit, 250MVA transformers, and three 400kV outgoing transmission lines, all in a double busbar with bypass DS arrangement. Data required for modelling the substation components are collected from the technical specifications provided by the manufacturer of the gas insulated substation, and other high voltage equipment connected to GIS.

A detailed model of both GIS and transformer along with connecting cables is developed using EMTP-RV software. EMTP-RV (Electro-Magnetic Transient Program-Reconstructed Version) is advanced simulation software utilized for power system transient studies. In this study EMTP-RV, Version 3.0 is used to simulate all components of the investigated substation according to the guidelines of widely acceptable standards like CIGRE, IEC and IEEE [1, 9-11, 34]. Verification of the developed model is conducted using data collected from different published materials globally.

The arrangement of all equipment of the substation are according to the single line diagram of the 400kV substation shown in Fig. 3. 2 and Fig. 3. 3. The verification stage of this model is implemented by using data collected from previously published papers (such as amplitude of VFTO and VFTC, high frequency components and effects of different parameters on VFT) to compare the difference between the proposed model results and other results and hence tuning the model for better accuracy. It is worth mentioning that this study only focuses on internal very fast transients. Analysing external effects needs another comprehensive study.

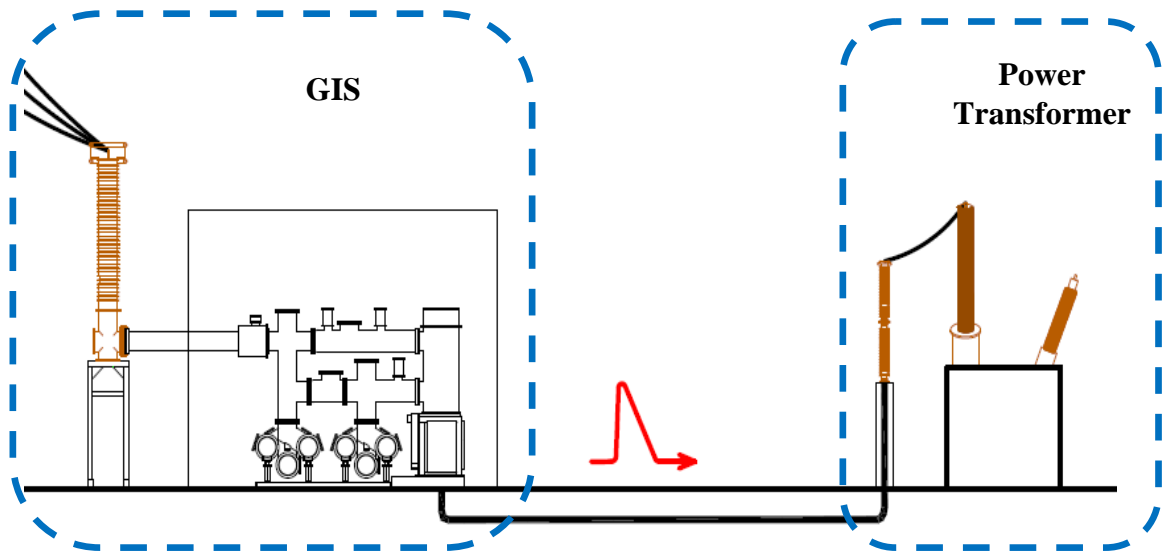


Fig. 3. 1 GIS to Power Transformer connection

Generally power system transients are transitions from one steady state condition to another. There are several causes for the generation of transients such as switching operation, short circuit, earth faults and lightning strikes. Due to transients, a travelling wave is produced after the occurrence of each event on transmission line, cable or GIS busbar. The frequency of transients is determined by the surge impedance of the travelling path and also transit time [11]. According to Table 3. 1, origins of transients are associated with particular frequency ranges. For the purpose of studying a special transient in the range of 100 MHz, modelling all components of power system is not essential. For this reason, only the components which have a decisive effect within that particular frequency range of transients are to be modelled and investigated in detailed consideration [34]. Since this study focuses on the highest frequency range with shortest rise-time oscillations, capacitive characteristics of components become predominant in system behaviour during transient state [34].

Table 3. 1 Origin of transients, associated with frequency ranges

Origin	Frequency range
Transformer energization Ferro-resonance	(DC) 0.1 Hz – 1 kHz
Load rejection	0.1 Hz – 3 kHz
Fault clearing	50/60 Hz – 3 kHz
Fault initiation	50/60 Hz – 20 kHz
Line energization	50/60 Hz – 20 kHz

Line reclosing	50/60 Hz – 20 kHz
Transient recovery voltage	50/60 Hz – 20 kHz
Terminal faults	
Short line faults	50/60 Hz – 100 kHz
Multiplies restrikes of CB	20 kHz – 1 MHz
Lightning surges	10 kHz – 3 MHz
DS operation in GIS	100 kHz – 100 MHz

3.1 GIS Modelling

Due to the origin and the travelling nature of a VFT, the GIS model has to include the equivalent circuit of lumped elements and distributed parameter lines. Generally, lumped parameter elements are used in cases related to transients that propagates instantaneously at every point of power system. In these cases, the behaviour of power system during disturbance is described by ordinary differential equations. While in distributed parameters, a time must be taken into consideration for disturbance wave to travel from one point to any other point in the power system. Thus, behaviour of the system is described by Telegraph equations [21, 22]. In order to model internal effects of VFT in GIS, only the internal mode is considered between GIS main conductor and enclosure that is assumed to be perfectly grounded. Other studies which intend to analyse external effects of VFT, must add a second mode known as external mode considering a transmission line for enclosure-ground route [11].

All equipment and components in GIS are modelled according to the arrangement shown in substation single line diagram of Fig. 3. 2. According to this single line diagram, all seven feeders including four transformer feeders and three outgoing line feeders are connected to the GIS main busbars in Double Busbar with Bypass DS arrangement [5]. All equipment surrounded by dashed line in the figure are encapsulated within GIS hall and are connected to other equipment outside the GIS hall such as Lightning Arrester (LA), Line Trap (LT) and Capacitive Voltage Transformer (CVT). Equipment in GIS are connected according to GIS single line shown in Fig. 3. 3. “IEEE modelling guideline for VFT in GIS” was applied for GIS Modelling in this work [11].

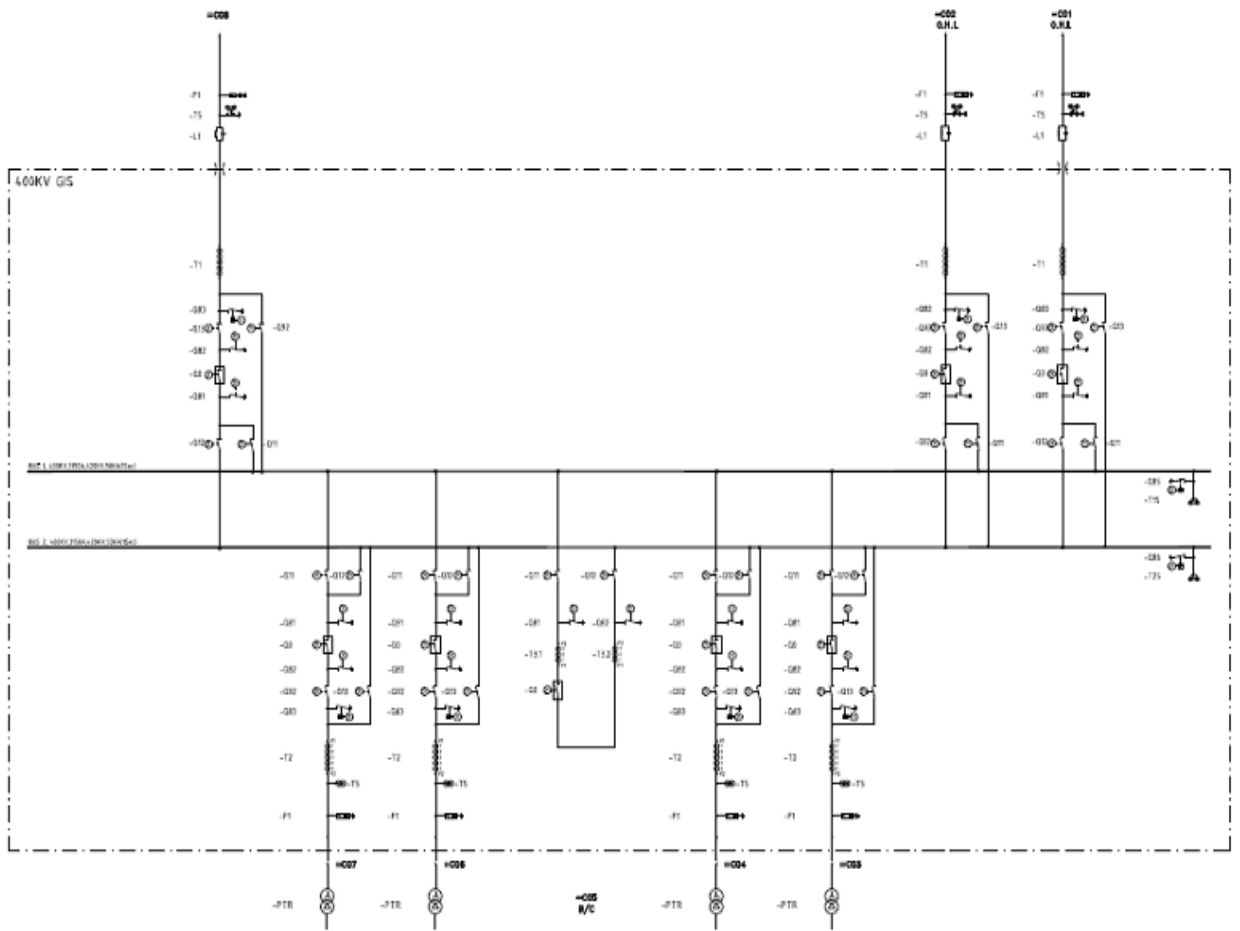


Fig. 3. 2 Single Line diagram of substation

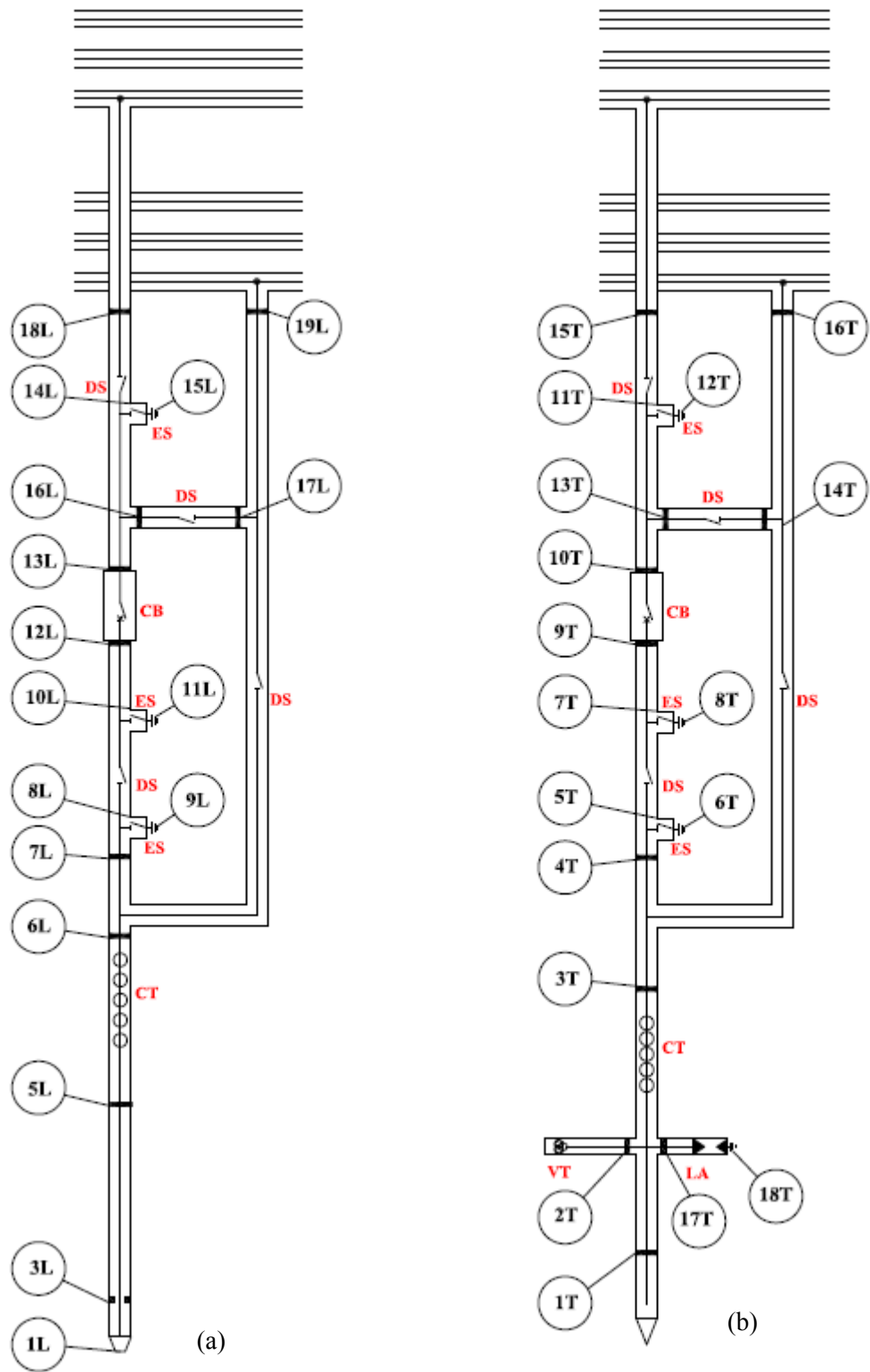


Fig. 3. 3 Arrangement of GIS compartments a) Line feeder b) Transformer feeder

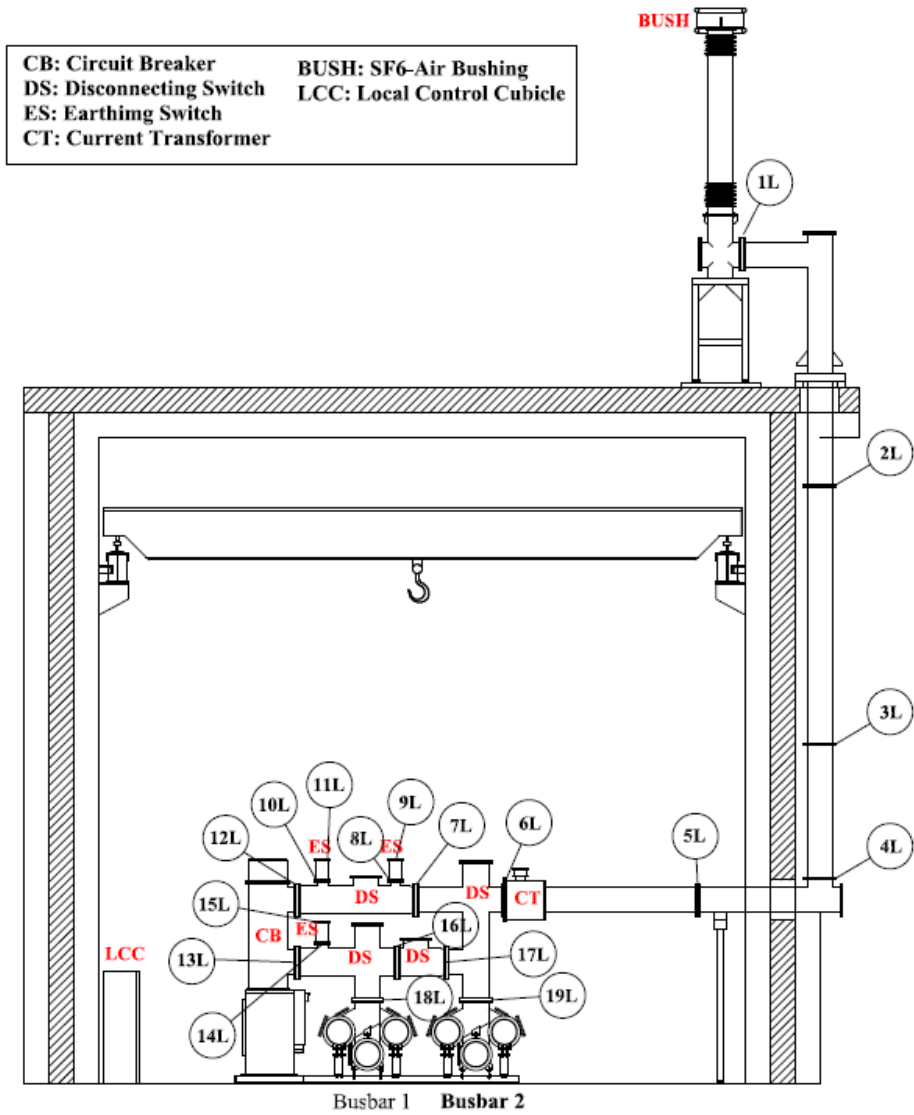


Fig. 3. 4 Section of GIS line feeder internal parts

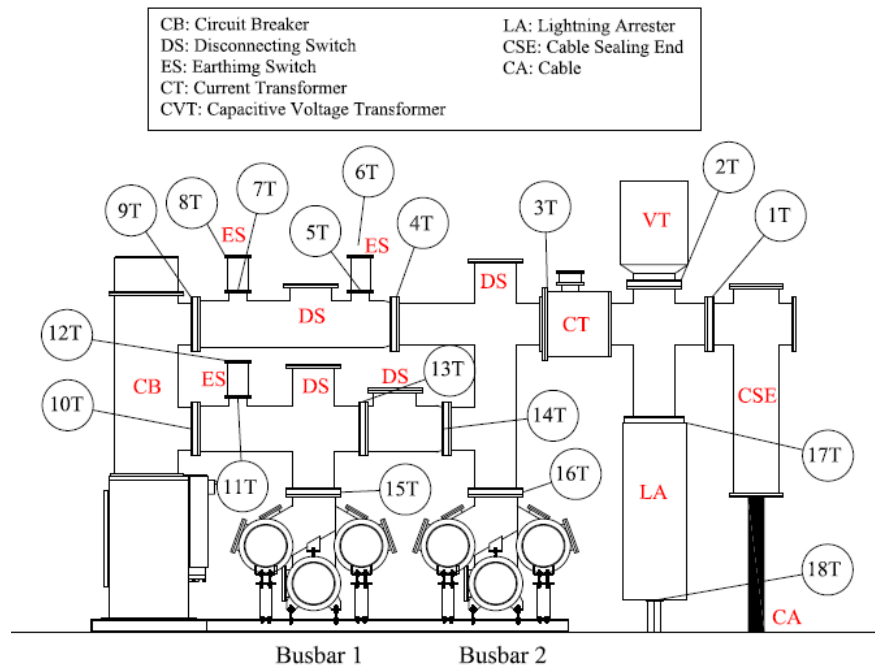


Fig. 3. 5 Section of GIS transformer feeder internal parts

Table 3. 2 Length and travel time of GIS sections

Feeder	Branch	Length	Travel time (ns)
Line Feeder	1L-2L	6.5 m	22.8
	2L-3L	5 m	17.5
	3L-4L	2.6 m	9.1
	4L-5L	2.8 m	9.8
	5L-6L	3.8 m	13.3
	6L-7L	1.7 m	5.7
	8L-9L	0.4 m	1.3
	7L-12L	2.4 m	8.0
	10L-11L	0.4 m	1.3
	12L-13L	1.3 m	4.4
	14L-15L	0.4 m	1.3
	13L-16L	1.9 m	6.4
	16L-17L	1 m	3.3
Trans. Feeder	1T-3T	1.9 m	6.7
	3T-4T	1.8 m	6.0
	5T-6T	0.4 m	1.3
	4T-9T	2.4 m	8.0
	7T-8T	0.4 m	1.3
	9T-10T	1.3 m	4.4
	10T-13T	0.4 m	1.3
	11T-12T	0.4 m	1.3
	13T-14T	0.4 m	1.3
	14T-15T	0.4 m	1.3

Each GIS section is modelled as a Constant Parameter (CP) lossless transmission line in EMTP with two important characteristics: surge impedance and travel time [9]. Sections with travel time less than 1 ns were ignored without decreasing modelling accuracy [11]. The input data was obtained from section drawings of GIS as shown in Fig. 3. 4, Fig. 3. 5 and Table 3. 2. Since the system is three symmetrical phases and each phase is located in a separate enclosure, single phase circuit was used to model the GIS. Each GIS stated in Table 3. 2 Length and travel time of GIS sections is simulated by its equivalent capacitance and inductance, which can be determined from its physical dimensions as follows [17]:

$$L = \frac{\mu_0}{2\pi} Ln \frac{R}{r} \quad (3.1)$$

$$C = \frac{2\pi\epsilon}{Ln \frac{R}{r}} \quad (3.2)$$

$$Z = \sqrt{\frac{L}{C}} = \frac{\sqrt{\epsilon\mu}}{2\pi} Ln \frac{R}{r} \approx 60Ln \frac{R}{r} \quad (3.3)$$

Where, C and L are the capacitance and inductance of a GIS busbar respectively, and according to Fig. 3. 6, r is the outside diameter of GIS busbar, R is the inner diameter of GIS enclosure and Z is the surge impedance. $R=246.1\text{mm}$ and $r=60\text{mm}$, $Z=84.7\Omega$ were considered in this study. Based on some empirical studies, propagation velocity of a travelling wave is about 95-96% of the speed of light [11]. Thus $v=285\text{m}/\mu\text{s}$ is considered here. Dimensions of GIS busduct in this study are presented in Table 3. 3 which is taken from GIS technical specification provided by the manufacturer (Hyosung Co., South Korea).



Fig. 3. 6 GIS bus duct cross section R: Inner diameter of GIS enclosure, r: Outside diameter of GIS bus duct

Table 3. 3 GIS Parameters

Parameter	Description
External radius of GIS conductor	60 mm
Internal radius of GIS conductor	42.5 mm
External radius of enclosure	254 mm
Internal radius of enclosure	246.1 mm

A short explanation about the representation of the most important substation and GIS components is illustrated below [11]:

3.1.1 Components of GIS model

Transmission line:

Overhead lines are considered to be of infinite length. Hence, it is modelled as a transmission line terminated with a resistance to ground of a value equal to the surge impedance of the overhead line (350Ω), so that there is no reflection from this end.

Surge Arresters (SA):

For successful conduction of arrester, the time taken for the residual voltage to reach the peak value shall be less than the time taken for the discharge current to reach its peak [35]. The problem for VFTO is that the front time is less than $1 \mu\text{s}$ and in this case, the arrester can't operate quickly and the arrester clamps the voltage after the occurrence of the current peak [36]. For modelling the surge arrester it is strongly recommended [11, 35] to include the inherent inductance of metal oxide blocks and inductance of lead conductor. Also stray capacitance and capacitance of arrester blocks must be considered [34, 37]. For this purpose, the method and the values suggested in [35] were implemented in this work. According to this method, lightning arrester was considered as two section modelled as lossless line considering the length of each arrester section connected with nonlinear resistance and capacitance between two sections. According to IEC modelling guideline [9] SA model as a capacitance to ground can have an acceptable result if overvoltage is less than SA protective level.

Circuit Breakers and Disconnecting Switches:

Generally closed switches including circuit breaker and disconnecting switch are modelled as a lossless line with their physical length and impedance that is calculated from (3.3).

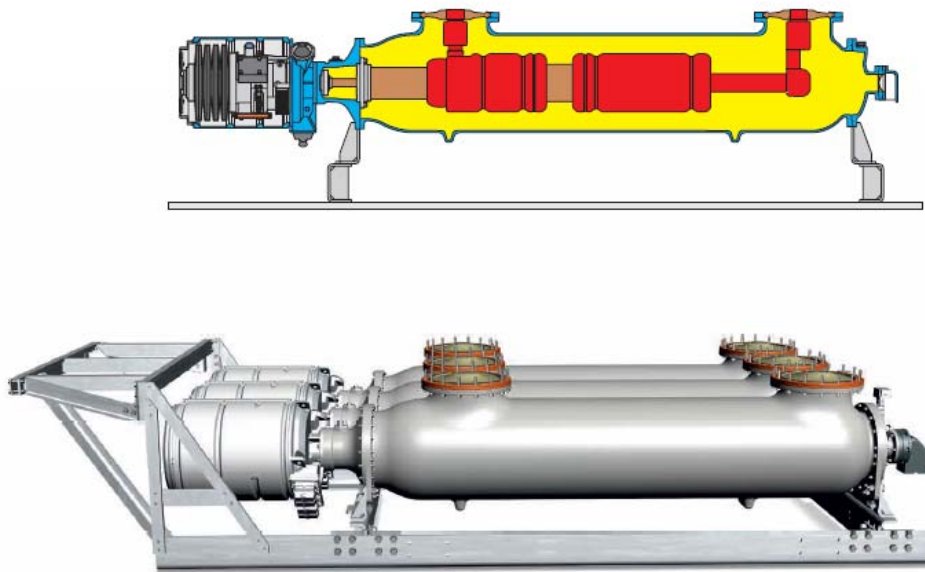


Fig. 3. 7 Circuit breaker with operating mechanism [ABB]

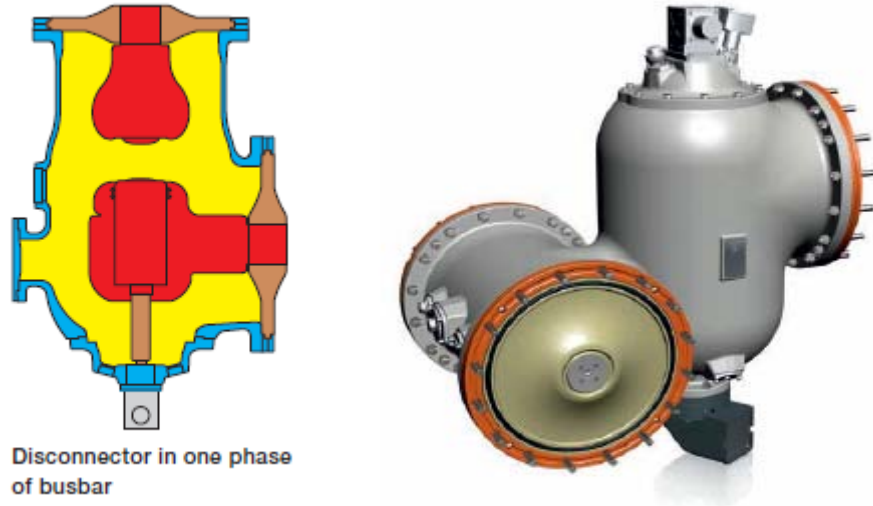


Fig. 3. 8 Disconnecting Switch [ABB]

Modelling an open switch is more complicated because of internal asymmetry of CB and DS construction. In this study switches are simulated as shown in Fig. 3. 9 according to their physical dimensions.

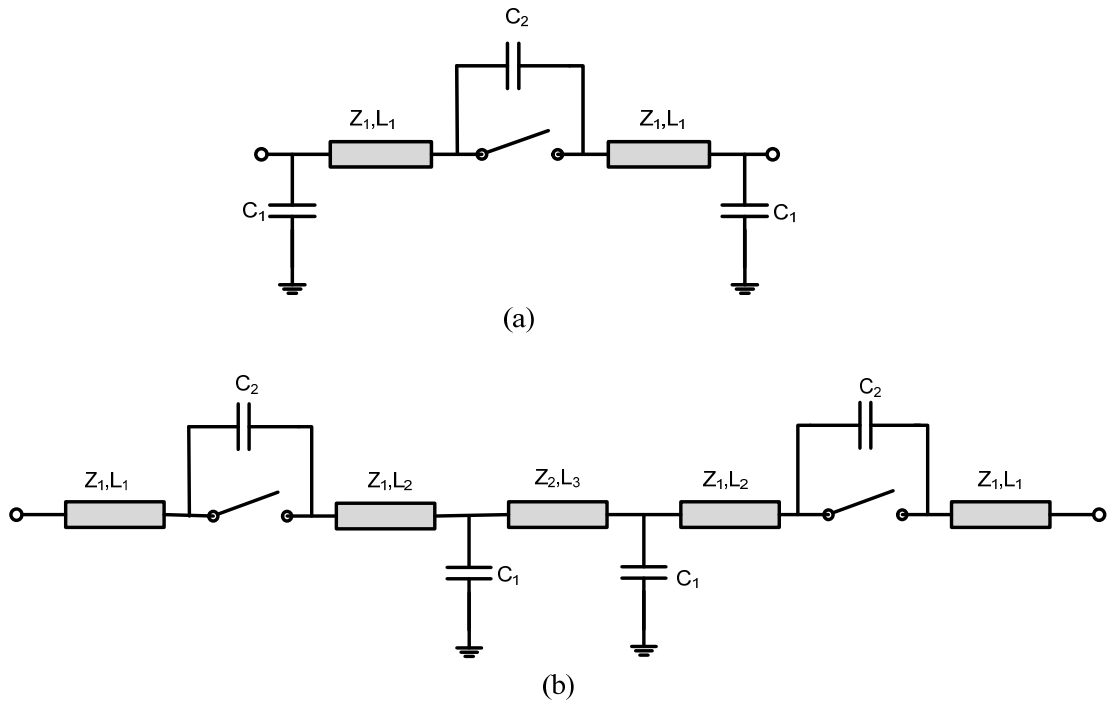


Fig. 3. 9 Equivalent circuit of switches a) DS: $Z_1=35 \Omega$, $L_1=50\text{cm}$, $C_1= 88\text{pF}$, $C_2=20\text{pF}$ b) CB: $Z_1=58 \Omega$, $Z_2=19 \Omega$, $L_1=56\text{cm}$, $L_2=93\text{cm}$, $L_3=40\text{cm}$, $C_1= 32\text{pF}$, $C_2=900\text{pF}$

The spark happening during the GIS disconnector closing operation, is modelled as a small fixed resistance connected in series with time varying resistance which decays exponentially. Small fixed resistance is considered as residual spark resistance. The mathematical equation for the above is given by [11]:

$$R(t) = r + R_0 e^{-t/T} \quad (3.4)$$

$r = 0.5 \Omega$ (final arc resistance) and $R_0 = 10^{12} \Omega$ (resistance of the gap while DS is opened)

$T = 1 \text{ ns}$ (time constant leading to the spark duration specific for the breakdown in SF_6)

This means that the voltage breakdown in SF_6 takes about 10 ns. The model created in EMTP for simulating the spark behaviour during operation is shown in Fig. 3. 10. As shown in this figure, an ideal switch was used for closing and opening operation which is connected in series to fixed and variable resistance. According to Fig. 2. 4, during closing operation, voltage at source side will decrease from 1 p.u. to 0.5 p.u. and voltage at the load side increases from 0 to 0.5 p.u.. On the other side, during opening operation, voltage at source side will increase from 0.5 p.u. to 1 p.u. and voltage at load side decreases from 0.5 p.u. to 0. In insulation breakdown, travelling waves propagate from failure location at both sides and the magnitude of voltage falls from 1 p.u. to 0. Therefore, considering 1 p.u. potential related to trapped charge on the load side of DS, for creating the input wave, voltage difference of 2 p.u. was applied between the two DS contacts to study the generated voltage as a worst case.

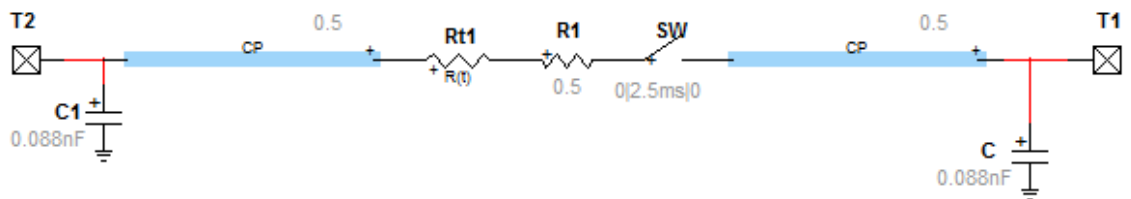


Fig. 3. 10 Model of operating DS in EMTP

SF_6 -Air Bushings and Cable Termination:

A gas to air bushing is designed to connect the main GIS conductor as an internal part of GIS to an overhead line conductor external to GIS (Fig. 3. 11a). It is constructed with several coaxial cylinders, whose lengths change gradually from the outermost to innermost of the bushing. When a travelling wave inside GIS arrives the bushing these capacitively graded layers form several transmission line, with different surge impedances, from GIS impedance to transmission line surge impedance. In other words, the bushing gradually changes the surge impedance from that of the GIS to that of the line [38]. Therefore, a model can consist of several transmission lines in series with gradually increasing surge impedances. A simplified model is suggested by [11] for modelling the bushing. According to this model, a transmission line with $Z=250\Omega$ was considered in this study. As shown in Fig. 2. 1 and Fig. 2. 2, SF_6 -air bushing is only installed in line feeders of GIS, which is designed to feed outgoing transmission lines, while transformer feeders are designed to feed the substation by transformer of generating plant. Therefore, they include a cable termination instead of gas to air bushing (Fig. 3. 11b). The same method can be used for modelling Cable Termination of GIS with impedance of $Z=70\Omega$ regarding the surge impedance of connecting cable.

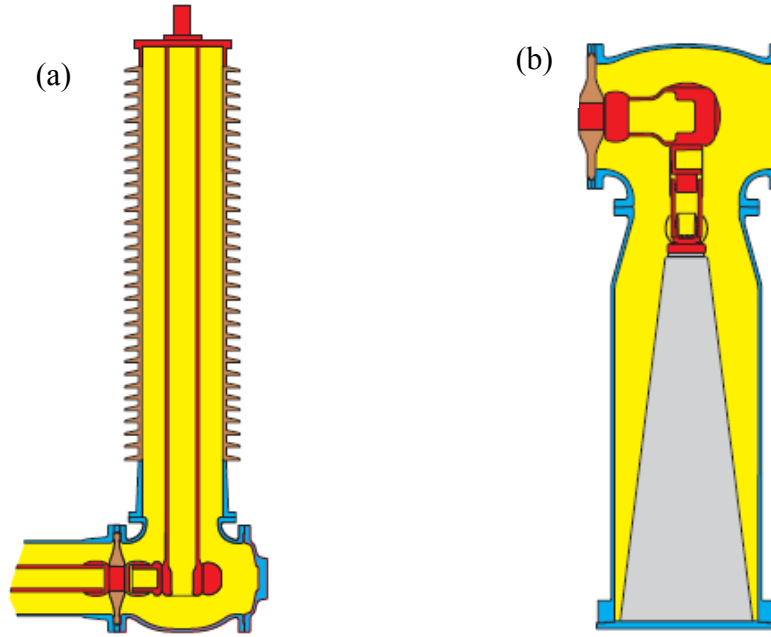


Fig. 3. 11 Schematic diagram of a) SF₆-Air Bushing b) Cable termination [ABB]

Power Transformer:

At very high frequencies of VFTO, capacitive characteristics of transformer winding becomes predominant and determine the behaviour of transformer during transient. Therefore, a transformer can be modelled as a network of capacitors connected in series between turns and coils and shunt between turns and coils to the ground and transformer tank [31]. The equivalent capacitance of transformer can be obtained from: [29]

$$C_{eff} = \sqrt{C_g C_s} \quad (3.5)$$

C_{eff} : equivalent capacitance of the capacitive model of transformer

C_g : equivalent series capacitance of the winding

C_s : equivalent ground capacitance of the winding

As explained in the introduction of chapter 3, and according to [29], it is common to model a transformer by an equivalent capacitor connected in series with a resistance representing loss in windings [33]. In this work the values and model recommended by IEEE guideline [11] are applied which also complies with the CIGRE guideline for modelling transients [34]. According to this model, the equivalent capacitance of transformer is connected in parallel with equivalent resistance and capacitance of transformer bushing. Fig. 3. 12 shows the considered model for the transformer.

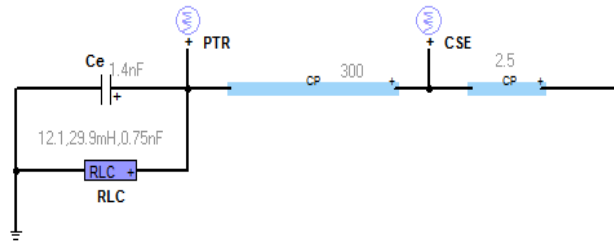


Fig. 3. 12 Model of power transformer in EMTD

Instrument transformer

Capacitive Voltage Transformer (CVT) is modelled as capacitance of 4.8 nF according to data sheet obtained from GIS supplier. The size was determined based on substation design requirements.

In order to study VFTO in GIS it is not essential to include Current Transformer (CT) in the model [11] because during high voltage switching operations in GIS, insulating gaps adjacent to CT usually flashover and travelling wave propagate through the created path. Thus current transformers are often neglected in most of the transient studies [11, 34] however in this study a capacitance of 300 pF was considered for CT model for more accurate representation [27, 39].

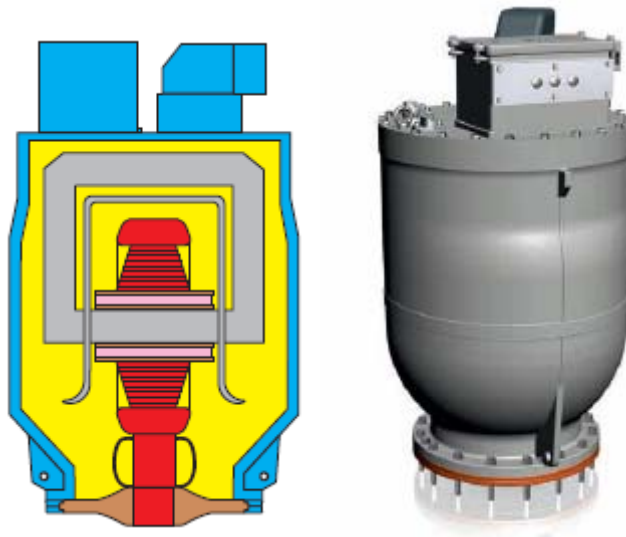


Fig. 3. 13 Capacitive Voltage Transformer [ABB]

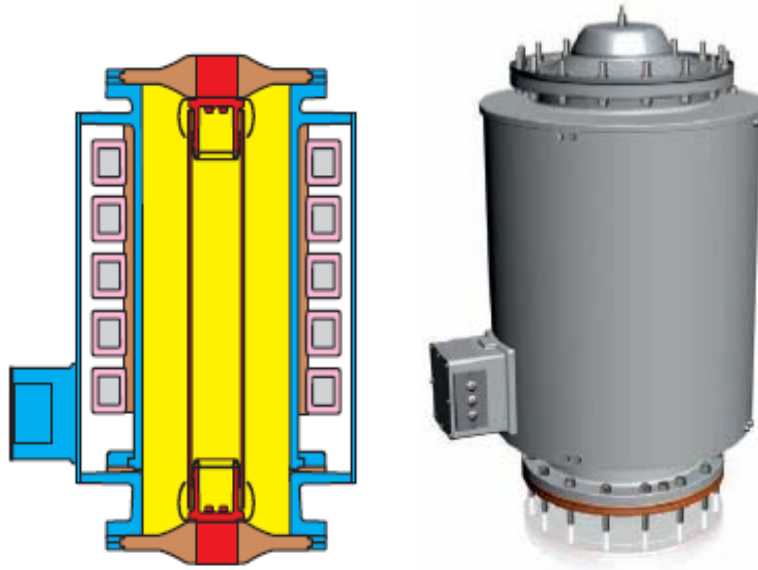


Fig. 3. 14 Current Transformer [ABB]

Spacer and Flanges


















For modelling all discontinuities in GIS, such as flanges, elbows and spacers, IEC and IEEE guidelines suggest to simulate them using a capacitor between 10 to 30 pF [9, 11]. In this study, capacitance of 15 pF was considered [27].

Cable

In this substation, the distance between the power transformer of a generating plant and GIS is about 500 m. For connecting the GIS to the power transformer at the generating plant, a 400kV XLPE cable with conductor cross section of 630 mm² is used. Based on the technical specification of cable received from cable supplier, the surge impedance of the cable line was calculated. In this study, a lossless line with $Z=60 \Omega$ and $v=165\text{m}/\mu\text{s}$ is considered to model the cable.

All models used in this study are mostly in accordance with models recommended by the IEEE guideline prepared by the Very Fast Transients Task Force of the IEEE Working Group on Modelling and Analysis of System Transients [11]. The parameters of the equivalent circuit can be summarized in Table 3. 4 [11].

Table 3. 4 Models recommended by IEEE guideline for modelling VFTO

COMPONENT	EQUIVALENT CIRCUIT	NOTES
Bus duct		Loss-free distributed parameter transmission line
Spacer		($C \approx 20$ to 30 pF)
Elbow		
Spherical shield		($C \approx$ few pF)
Surge arrester		
Closed switch		
Open switch		(n = number of breaking chambers)
Closed disconnect		
Open disconnect		
Disconnect during sparking		$r = r(t)$; $R =$ a few Ω $C =$ a few tens pF
Bushing (capacitive type)		n = number of equivalent shields (5 to 8) simulated
Bushing (gas filled)		$C =$ a few tens pF $Z_s \approx 250 \Omega$
Power transformer (termination)		parameters evaluated from the frequency response of the transformer
Current transformer		sometimes negligible
Capacitive voltage transformer		
Earth connection		
Aerial line or long cable (termination)		$r =$ surge impedance

3.1.2 Improved model of GIS by Maxwell 3D

Although the main approach taken by all VFTO studies involves modelling a GIS with equivalent circuits formed by distributed parameters, there is one problem with these simulations. The problem is that these methods are based on simple equations for calculating the inductance and capacitance of GIS conductor, thus they are not capable of representing all physical geometric changes along the travelling wave path. The necessity of including all small geometrical changes in GIS model will be critical if dielectric design of GIS is intended [40]. For this reason, a three dimensional (3D) simulation for the GIS is developed in this study to obtain more accurate equivalent circuit parameters using Maxwell electrostatic and magnetostatic equations. Some equipment in GIS such as CB and DS, which according to Figs 3.7 and 3.8, have small changes in geometry and shape of conductor and enclosure.

Maxwell® 3D software from ANSYS® Electromagnetic Suite, version 17.2.0 which is a high-performance interactive software package that uses finite element method (FEM) to solve three-dimensional electromagnetic field problems, such as electrostatic, magnetostatic, eddy current, and transient problems, is used in this study. Maxwell solves the electromagnetic field problems by solving Maxwell's equations in a finite region of space with appropriate boundary conditions and-when necessary with user-specified initial conditions in order to obtain a solution with guaranteed uniqueness. All solids modelled in the software are divided into a large number of small elements by adaptive meshing operation and in order to obtain the set of algebraic equations to be solved. The geometry of the problem is discretized automatically into small elements which called tetrahedral due to their shape and are produced by meshing operation.

The VFTO behaviour in a GIS has been simulated in EMTP-RV using equivalent circuits of power system components with distributed parameter, and solving the time domain circuit equations representing transient state of the network [11]. A VFTO can be described by Maxwell equation for electromagnetic travelling wave as well as circuit equation. According to the well-known “wave equation for vector potential”, travelling nature of electromagnetic wave is described by [41]:

$$\nabla^2 \mathbf{A} - \mu\epsilon \frac{\partial^2 \mathbf{A}}{\partial t^2} = -\mu \mathbf{J} \quad (3.6)$$

\mathbf{A} : magnetic vector potential

\mathbf{J} : current density

Therefore VFTO travelling electromagnetic wave can be formulated by magnetic vector potential [40]:

$$\nabla \times (\nabla \times \mathbf{A}) + \mu\sigma \frac{\partial \mathbf{A}}{\partial t} + \mu\epsilon \frac{\partial^2 \mathbf{A}}{\partial t^2} = 0 \quad (3.7)$$

μ : magnetic permeability of SF₆

ϵ : electric permittivity of SF₆

σ : conductivity

Now, $\mathbf{A}(\mathbf{r},t)$ is calculated by Maxwell 3D at each point (\mathbf{r}) and time (t). Electric and magnetic flux density can be calculated by [41]:

$$\mathbf{E} = -\frac{\partial \mathbf{A}}{\partial t} \quad (3.9)$$

$$\mathbf{B} = \nabla \times \mathbf{A} \quad (3.10)$$

Fig. 3. 15 shows the Maxwell 3D model of the GIS busduct at both sides of the DS for the purpose of calculating the travelling electromagnetic waves. This model includes main GIS conductor, DS contacts, enclosures, spacers and elbows considering all geometric changes. Model of DS in GIS is shown in Fig. 3. 16. As can be seen in the DS and elbow models in Fig. 3. 17, it is possible to model all geometric details of GIS conductors, insulations and enclosure.

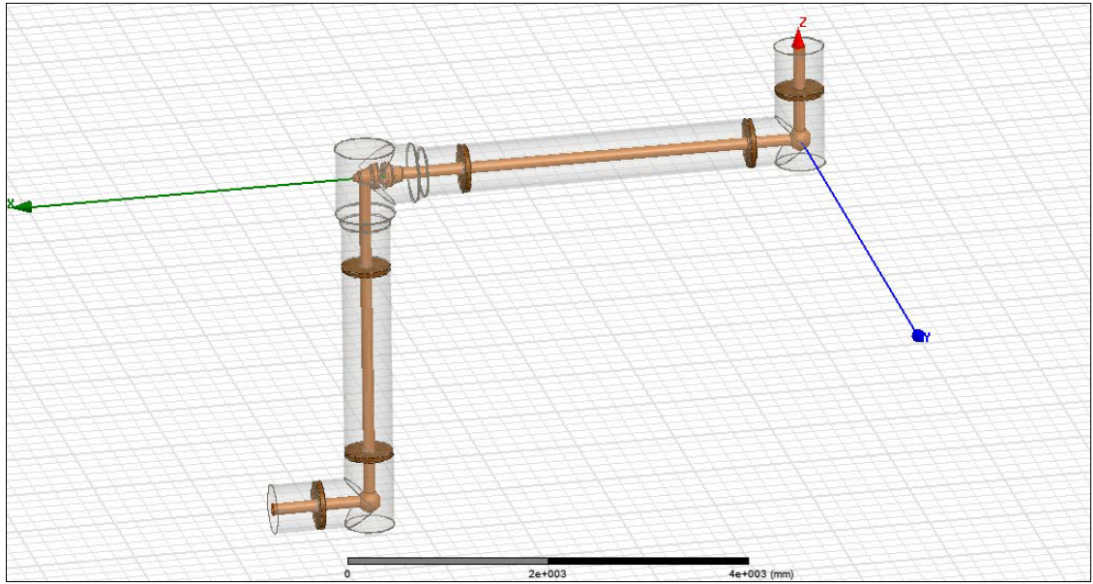


Fig. 3. 15 GIS Model in 3D Maxwell

For modelling the insulation breakdown during DS operation, a spark channel can be represented by a solid small cylinder connected between two contacts of the DS which material is defined with time varying conductivity [11]. As explained in section 2.3.1, during DS operation, spark channel is formed between the two contacts within a time (τ). Within this time, in case that DS is closing, resistance of the channel decays considerably which is described by equation (3.4). Therefore for modelling the spark, it can be assumed that the conductivity of the cylindrical solid varies between 0 and $\sigma_0 = 1000$ S/m (conductivity in conducting state) during about 10ns according to previous experimental study [42]. Conductivity of spark during closing and opening operations which start at t_0 can be described by the below exponential functions:

$$\sigma_{\text{opening}}(t) = \sigma_0 e^{-(t-t_0)/\tau} \quad (3.11)$$

$$\sigma_{\text{closing}}(t) = \sigma_0(1 - e^{-\frac{t-t_0}{\tau}}) \quad (3.12)$$

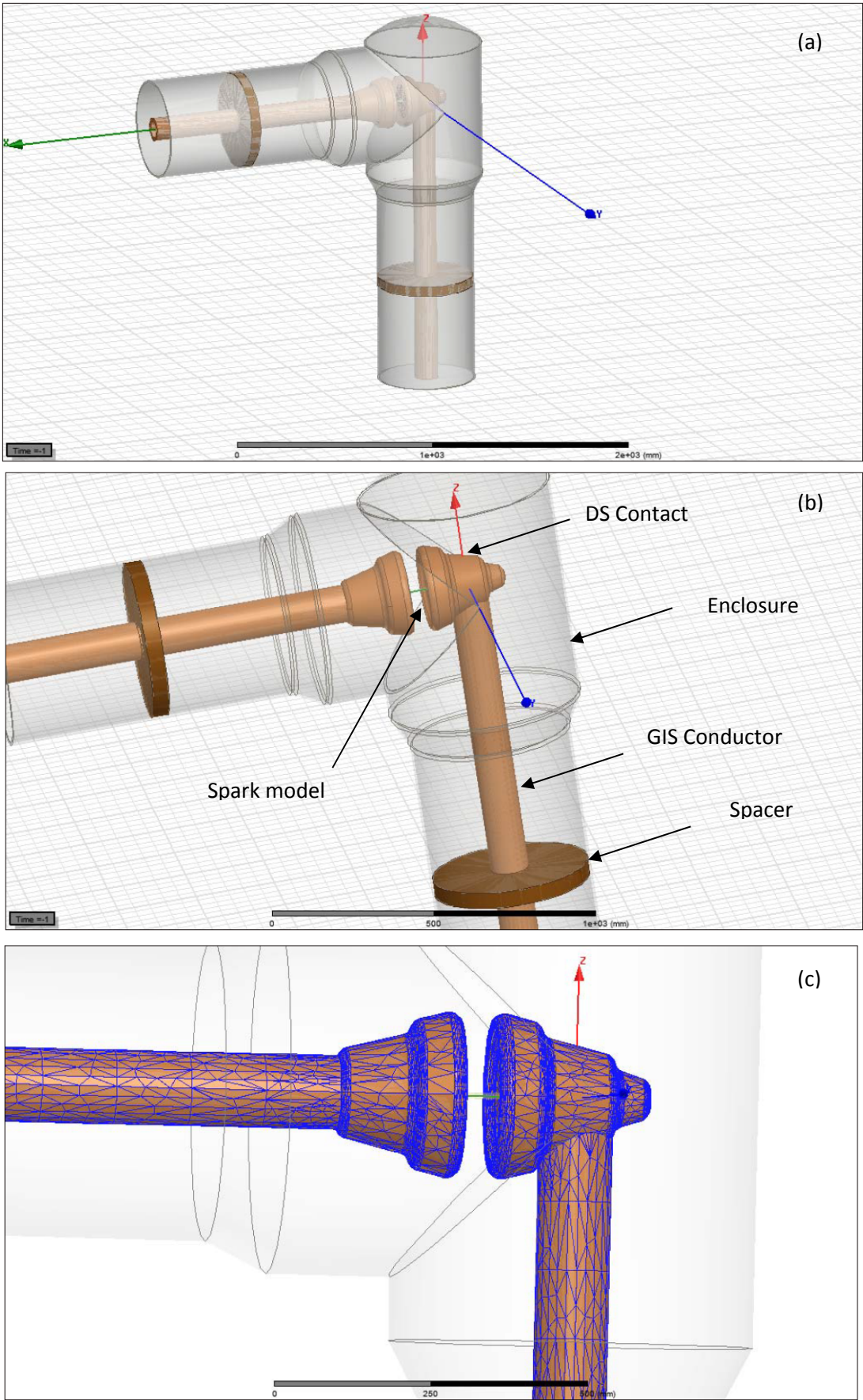


Fig. 3. 16 DS Model in Maxwell a) enclosure view b) model components c) mesh operation on GIS conductors applied by Maxwell

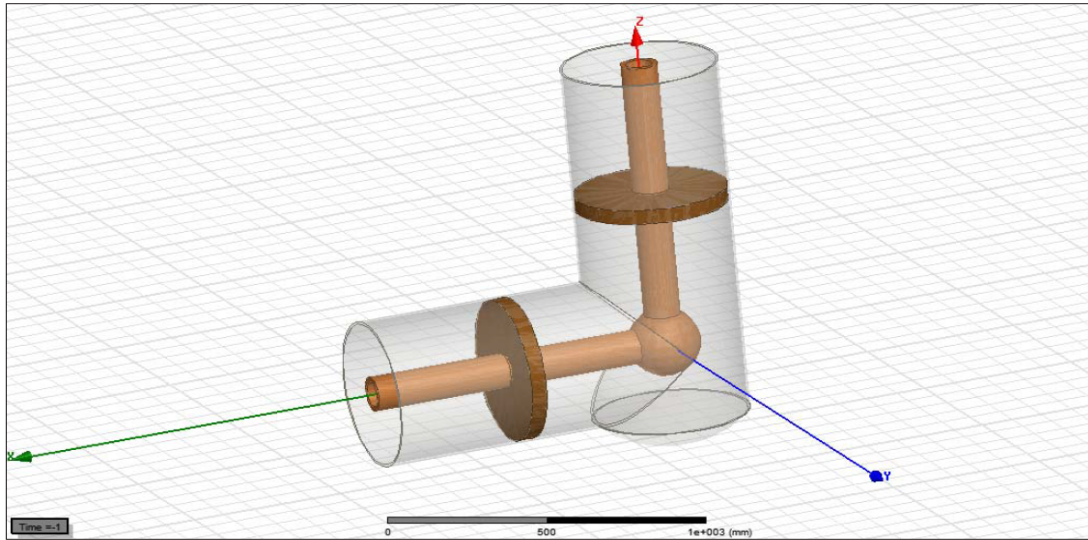


Fig. 3. 17 Model of elbow

Maxwell 3D simulation was performed for a GIS section shown in Fig. 3. 15 connecting a power transformer with source voltage of +1 p.u. and the initial voltage of -1 p.u. due to trapped charge at the load side of the DS which is actually an open circuit breaker. Fig. 3. 18 shows the magnitude of magnetic field in GIS, resulted from solving Maxwell equations, at the moment that spark ignites.

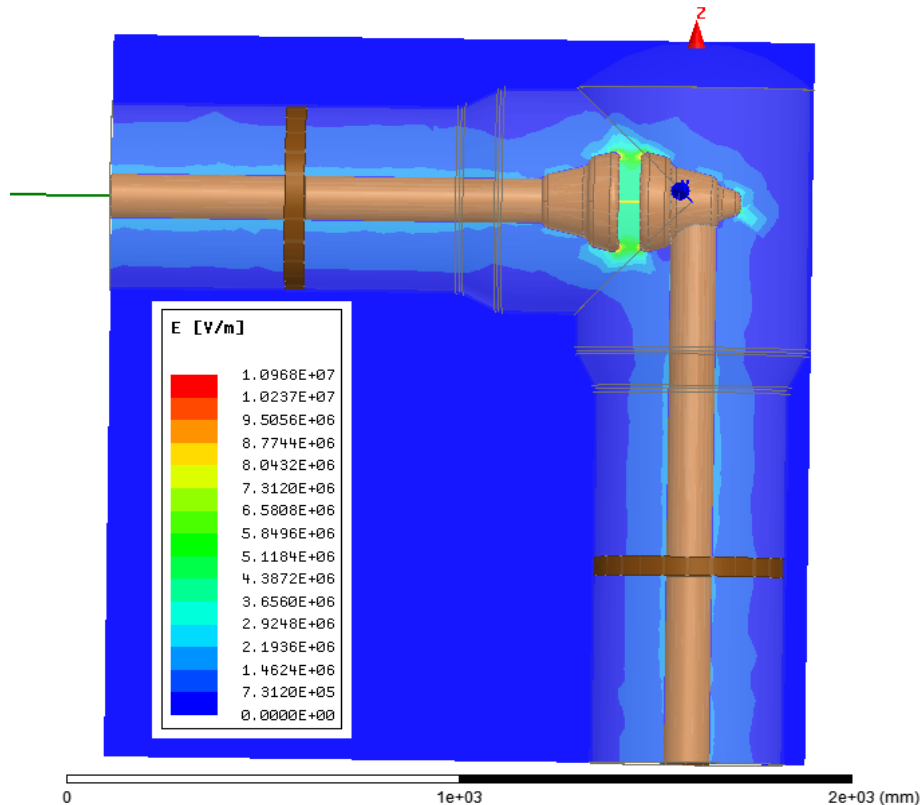


Fig. 3. 18 Magnitude of electric field around DS contacts

According to the report published in [40], a typical small 3D model of GIS needs at least 15 h to be run for each case on a PC with 32 GB RAM. Also Maxwell 3D usually needs the objects to be modelled exactly according to their real dimensional

and physical details with accurate boundary conditions, which means that 3D models are usually too complex to be implemented in comparison with two dimensional or circuit based models. It can be concluded that although 3D Maxwell can be utilized to mimic real system operation, EMTP-RV model is suitable enough for the investigated studies in this thesis. For this reason, in this study GIS models are created and studied in EMTP using equivalent circuit parameters obtained from 3D modelling in Maxwell.

For the purpose of calculating the capacitance and inductance of GIS conductor, electrostatic and magnetostatic solvers equipped with Ansys software are used. According to described procedure, improved model of circuit breaker and disconnect switch are shown in Fig. 3. 19 and Fig. 3. 20 respectively. Capacitive elements are calculated by running the electrostatic solver of Maxwell 3D, where a voltage V is applied on GIS conductor, while the voltage level is maintained at a level of zero on the stainless steel enclosure. The electrostatic solver computes static (DC) electric fields. The energy stored in the electrostatic field (W_{ij}) between the two elements can be calculated as follows [43]:

$$W_{ij} = 0.5 \int_{Vol} D_i \times E_j dVol \quad (3.13)$$

Where W_{ij} is the electrical field energy between 3d elements i and j

D_i is the electrical flux density of element i

E_j is the electrical field intensity of element j

Vol is the volume of the conductor

The capacitance C_{ij} between two elements i and j can then be calculated as:

$$C_{ij} = 2 \times \frac{W_{ij}}{V^2} \quad (3.14)$$

Inductive elements are calculated by running the magnetostatic solver of Maxwell 3D where a current I is applied on GIS conductor entering from one side and outgoing from the other side while the voltage level is maintained at a level of zero on the stainless steel enclosure. The magnetostatic solver computes static (DC) magnetic fields. Inductive components are calculated based on the average of the magnetic field energy (W_{ij}) and the corresponding peak current passing through the conductor (I) as follows [43]:

$$W_{ij} = 0.5 \int_{Vol} B_i \times H_j dVol \quad (3.15)$$

$$L_{ij} = 2 \times \frac{W_{ij}}{I^2} \quad (3.16)$$

Where W_{ij} is the electrical field energy between 3d elements i and j

B_i is the magnetic flux density of element i

H_j is the magnetic field intensity of element j

Vol is the volume of conductor.

To compute the resistance, the simulator calculates the ohmic loss (P_{loss}) after a field solution has been computed [43]:

$$P_{loss} = \left(\frac{1}{2\sigma}\right) \int_{Vol} J \cdot J dVol \quad (3.17)$$

where σ is conductor conductivity

J is the current density

Then:

$$R = P_{loss}/I^2 \quad (3.18)$$

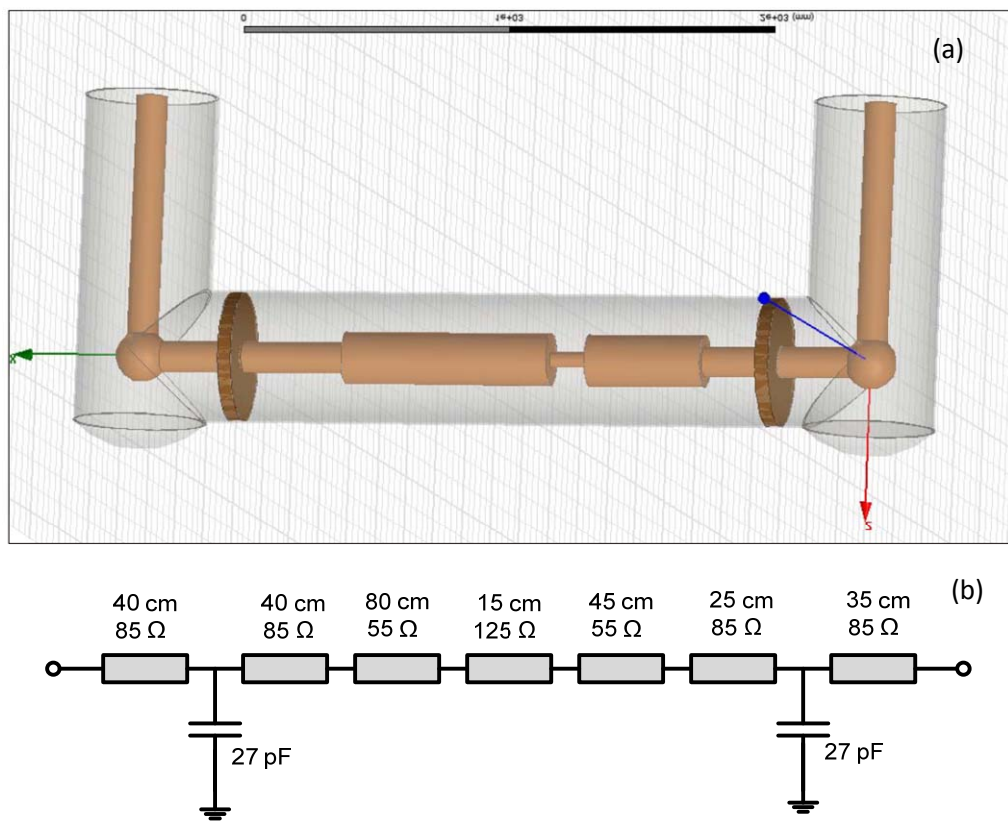


Fig. 3. 19 Closed CB model a) 3D model in Maxwell b) Equivalent circuit

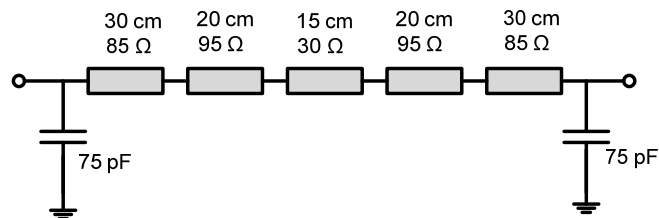


Fig. 3. 20 Equivalent circuit of closed DS obtained from Maxwell according to Fig. 3. 16

3.1.3 GIS Overall Model

Fig 3.15 illustrates the model of GIS in EMTP in which the values of various equipment parameters are obtained from 3D Maxwell simulation.

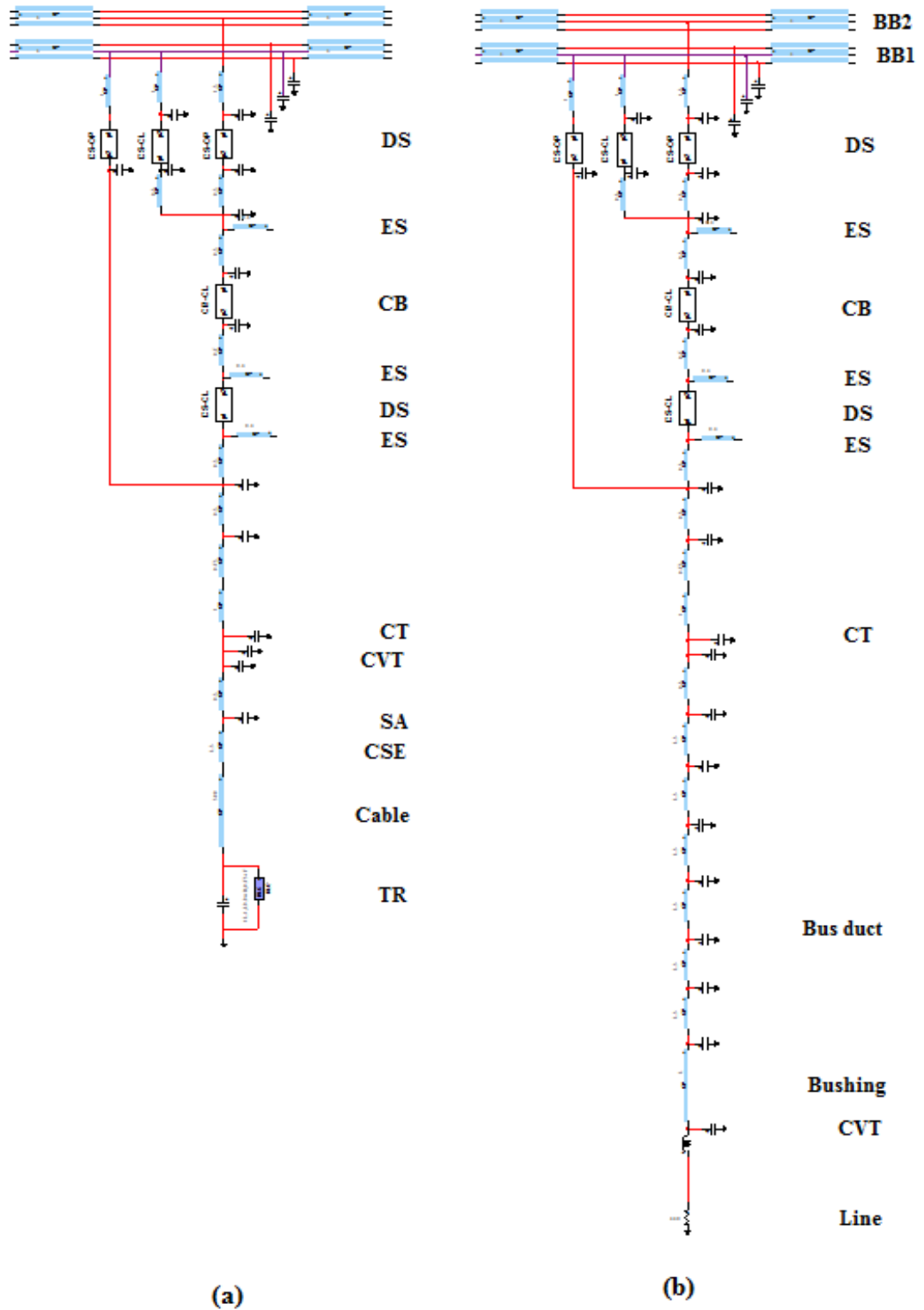


Fig. 3. 21 Substation model in EMTP a) Transformer feeder b) Line feeder

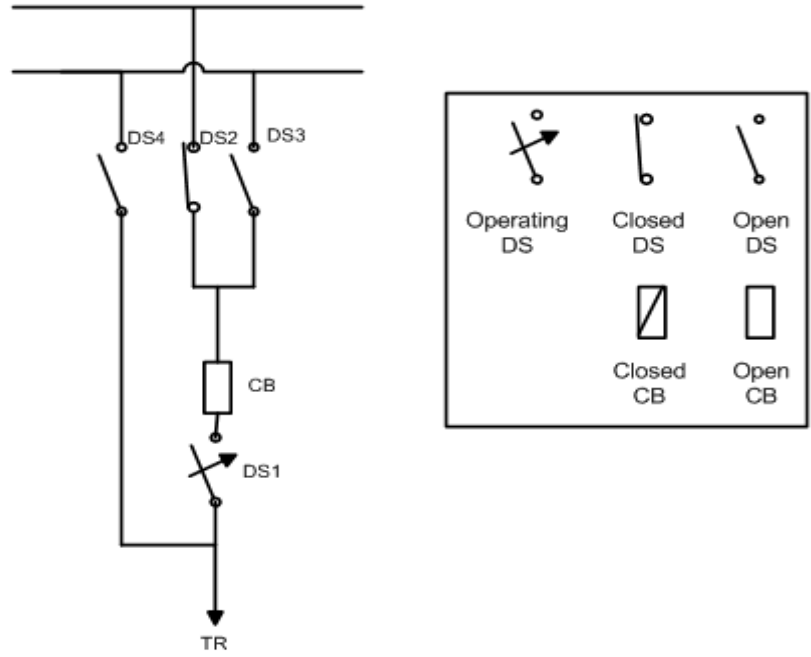
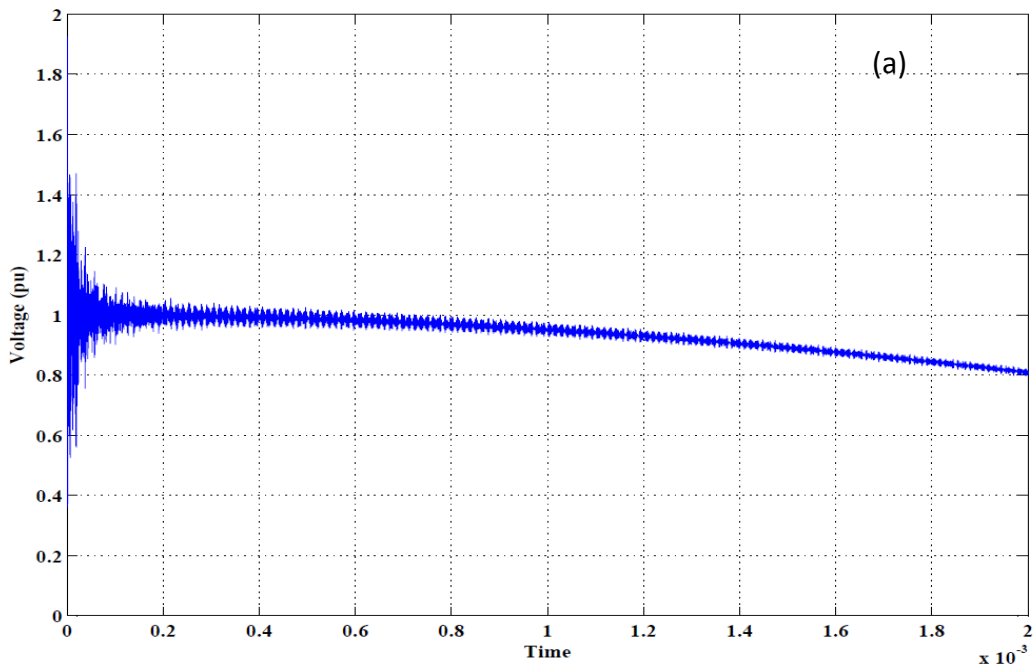


Fig. 3. 22 Configuration of switches in transformer feeder

A VFTO waveform can be obtained at different points in the substation. Considering the state of transformer feeder as shown in Fig. 3. 22, DS3 and DS4 are in open condition and DS2 is in closed condition. DS1 is assumed to be operating at $t=0$. In fact, this condition results in the most severe overvoltage on the transformer due to closing operation in GIS because T in (17) has the least value. The voltage waveform at the transformer terminals is shown in Fig. 3. 23 within short duration of $50 \mu\text{s}$ and relatively long duration of 2 ms. Also frequency spectrum of voltage waveform is shown in Fig. 3. 24.



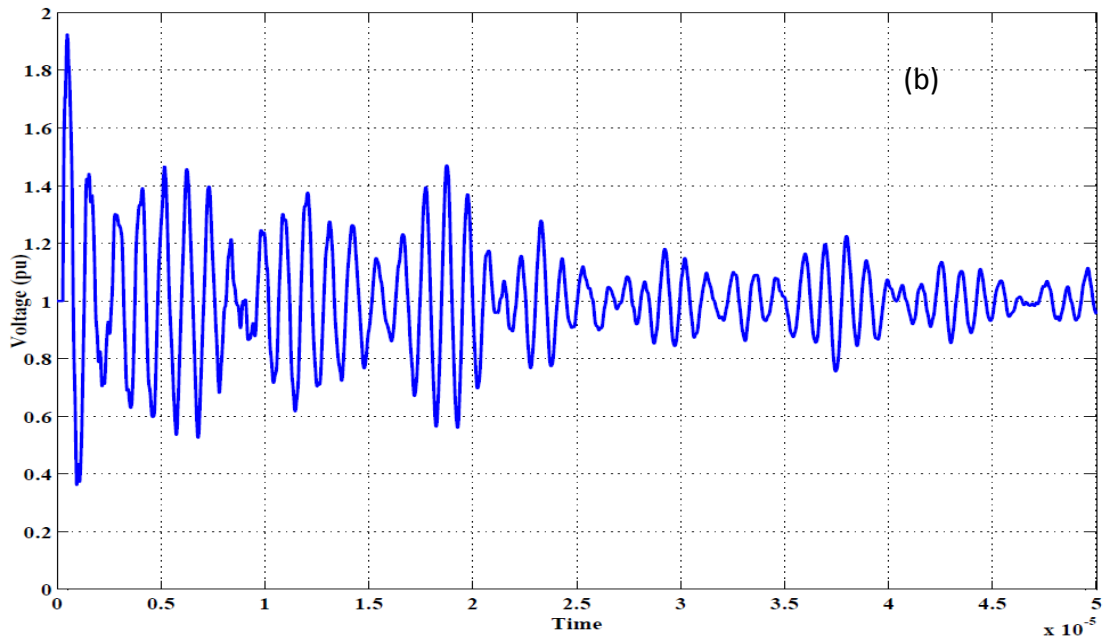


Fig. 3. 23 VFTO waveform at transformer a) During 2 ms b) During 50 μ s

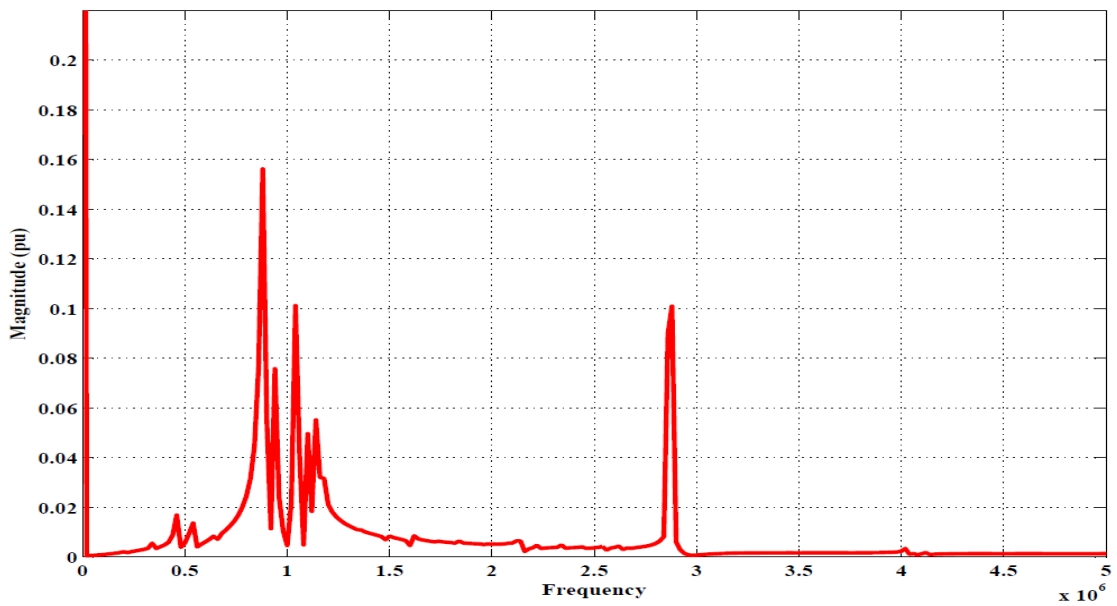


Fig. 3. 24 Frequency spectrum of VFTO at transformer

3.1.4 Effect of SF₆ degradation on VFTO

GIS insulation aging can reduce the dielectric strength of SF₆ due to frequent operation of disconnecting switches and circuit breakers, which will result in some catastrophic failures if a reliable monitoring system is not applied to assess the quality of SF₆ regularly [44]. During the arcing time and with very high temperature of about 20,000 K, the gas breaks down and although SF₆ is chemically stable material, it decomposes into low number fluorine molecules such as SF₂, which are extremely toxic and corrosive [45]. Corona discharge could be one of the other reasons for

creating impurities in a GIS insulation medium [46]. Normally, arced gas may contain the following [47]:

- The inert gas CF_4 generated by arc erosion of polymers
- Corrosive gaseous decomposition products (approximately 100 ppmv to 200 ppmv) as residues
- Solid decomposition products, mainly metal fluorides and tungsten oxifluorides, usually referred to as switching dust

In addition to the above described impurities, air and moisture ingress in GIS may have a deteriorating effect on the insulation medium [47]. Very high levels of humidity increase the possibility of water molecules condensing into the liquid phase, adversely affecting the dielectric withstand strength of GIS and significantly increasing the possibility of flashover. Therefore, humidity in GIS should be maintained at a level that does not condense in the form of liquid water over the entire range of the expected operating temperatures and gas pressures. Also, the formation of corrosive and toxic decomposition by-products occurs in reactions between moisture and dissociated SF_6 found in the high energy arcs during normal switching operations. Higher concentrations of humidity can result in higher concentrations of decomposition by products [47]. These by-products cause corrosion and may degrade insulators and other internal components within the GIS, and pose a safety hazard. Maximum permissible levels for impurities in GIS insulation are presented in IEC standard [48] as shown in Table 3. 5.

Table 3. 5 Maximum permissible impurity level in GIS insulation

Impurity	Specification
Air	2 g/kg
CF_4	2400 mg/kg
H_2O	25 mg/kg
Mineral oil	10 mg/kg
Total acidity expressed in hydrogen fluoride (HF)	1 mg/kg

Since gas insulated substations have been extensively used in power networks over recent decades with SF_6 as insulating medium in an environment with large number of switching operations, and frequent strikes due to their higher reliability and safety, special attention must be given to the condition monitoring of SF_6 in gas insulated substations.

The dielectric strength of insulation system is characterized based on two fundamental specification of the insulating medium [49]: permittivity and conductivity. While the permittivity affects insulation system behaviour during electrical transient conditions, electric conductivity plays an essential role to specify

the dielectric strength of the insulating system. SF₆ degradation is usually accompanied with a change in both insulation permittivity and conductivity which results in a change in the capacitance between the GIS main conductor and enclosure. This change in capacitance value can be specified by [50]:

$$\epsilon^* = \frac{\epsilon}{\epsilon_0} = \epsilon_r - j\epsilon'' = \epsilon_r - j\frac{\sigma}{\omega} = \frac{C(\omega)}{C_0} \quad (3.19)$$

where ϵ , ϵ^* and ϵ_r refer to the total, complex and relative permittivity, respectively, and ϵ_0 is the absolute permittivity of vacuum. σ is the electrical conductivity (S/m) and ω is the angular frequency (Rad/sec).

Equation (3.19) clarifies that the GIS capacitance is significantly dependent on dielectric permittivity and conductivity. Any change in these factors will be reflected as a kind of change in the capacitance value. Therefore, according to equation (3.3), the surge impedance of GIS changes dependently, and then the VFTO surge could have a different waveshape. In this section, the impact of aging and degradation of SF₆ on VFTO waveform is investigated. Three different levels are defined for SF₆ degradation, as presented in Table 3. 6 which are slight, moderate and significant variation in gas dielectric characteristics based on 10%, 20% and 30% change in permittivity of SF₆ respectively. The impact of gas degradation on VFTO high frequency dominant components is studied for each degradation level. It is worth mentioning that there is no published study on the exact relation between the moisture or aging level and the permittivity of SF₆.

Table 3. 6 SF₆ Degradation Level

Level	Base	slight	moderate	Significant
Relative permittivity	1	1.1	1.2	1.3

Fig. 3. 25 shows the effect of changing the health condition of SF₆ on the frequency contents of the VFTO waveform. The blue curve is corresponding to the base case with its original permittivity value. As compared to the frequency spectrum of the base case, it is clear that the dominant high frequencies shift to the right for various degradation levels of the SF₆ gas. The reason can be explained based on equations described in section 2.5. As mentioned before, the surge impedance of GIS conductor decreases with the increment of dielectric permittivity of SF₆. Thus according to Fig. 2. 14, the slope of the crossing line decreases and ω_i increases consequently. It means that dominant high frequencies shift even higher. Furthermore, according to equation (2.18), the amplitude of these high frequency components are reduced due to increment in ω_i .

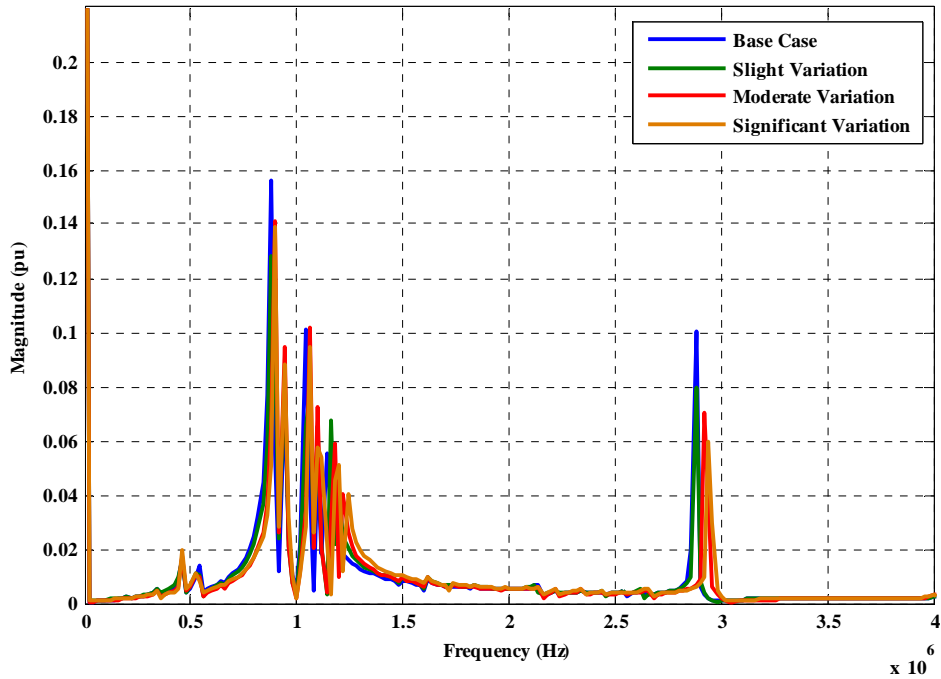


Fig. 3.25 Frequency spectrum of VFTO at different SF₆ health conditions

3.2 Transformer Modelling

There have been several methods presented for modelling the high frequency behaviour of transformer. In this section, the theoretical background of common important models of transformer are investigated, then one is selected to be applied in this study. Regardless of which model is chosen for representing the transformer winding, inductive, capacitive and resistive components of transformer are required to be included in transformer model and for this reason, detailed geometrical and dimensional information of internal parts of transformer are required for determining these parameters. Since core of power transformer behaves as a barrier against magnetic flux of windings at very high frequencies and does not allow the flux to penetrate into the core, core is neglected in the model of transformer for VFTO studies [17].

3.2.1 High Frequency Transformer Models

Generally HF transformer models are divided into two categories: Black Box Models and Grey Box Models [51].

Black Box Model is important especially for insulation coordination of power network and is used for studying the voltage and current waves travelling towards the transformer or departing it. This model is obtained from measuring the voltage and current at transformer terminals according to some predefined test in time or frequency domain. Since this model is derived from tests and measurements

regardless of detailed information of internal construction of transformer including core and windings, it is called the black box model because in contrary to other transformer models, this model doesn't need any data on internal parts.

Grey Box Model is suitable for analysing the resonance phenomenon inside power transformer and is necessary if detailed calculation of electrical stresses in transformer winding and voltage distribution along conductors is required [51]. This model can be divided into two different models: RLC Ladder Network Model and MTL Model [52].

3.2.1.1 Grey Box Model

Based on main presented transformer HF models, the Black Box model is not an appropriate model for the study of internal resonance of transformer. According to section 2.7, for calculating the behaviour of incident wave in transformer winding, a surge propagation along the winding can be illustrated as Fig. 3. 26. This figure shows a unit length of transformer winding in which:

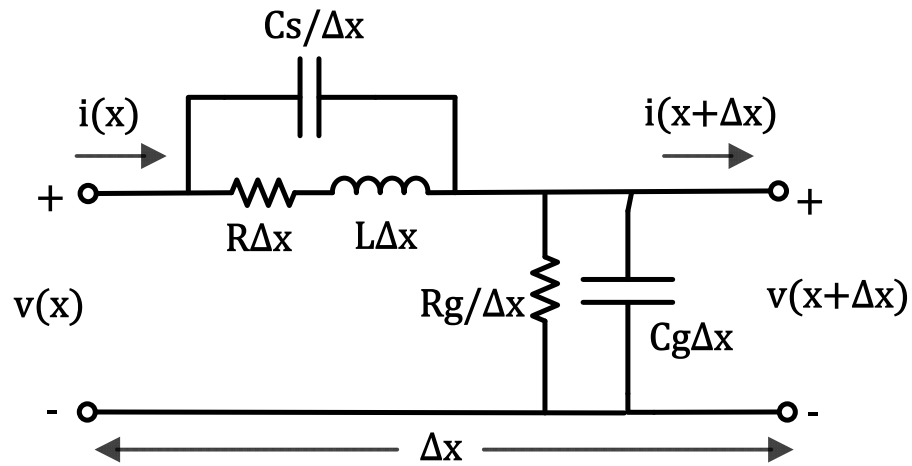


Fig. 3. 26 Equivalent circuit per unit length of transformer winding

C_s is the series capacitance of the winding

C_g is the ground capacitance of the winding

R is series resistance of the winding

R_g is shunt resistance of C_g

L is series inductance of the winding

Depending on what type of elements are implemented to create the model shown in Fig. 3. 26, the next step in simulation procedure will be specified. If lumped parameter elements of R , L and C are used for this purpose, a model can be developed known as RLC Ladder Network Model and if distributed parameter elements are used based on transmission line theory, a model called as Multiconductor Transmission Line (MTL) Model can be created [17]. They are also known as Lumped Parameter Model or Distributed Parameter Model [17].

RLC Ladder Network (Lumped) Model

The RLC ladder model is the most common and effective model used for studying fast front transients in transformer [53]. In this model, R, L, G (conductance) and C are lumped together to form a unit length of conductor or segment. The whole winding can be built in simulation by connecting all these segments to form a large network made of R, L and C.

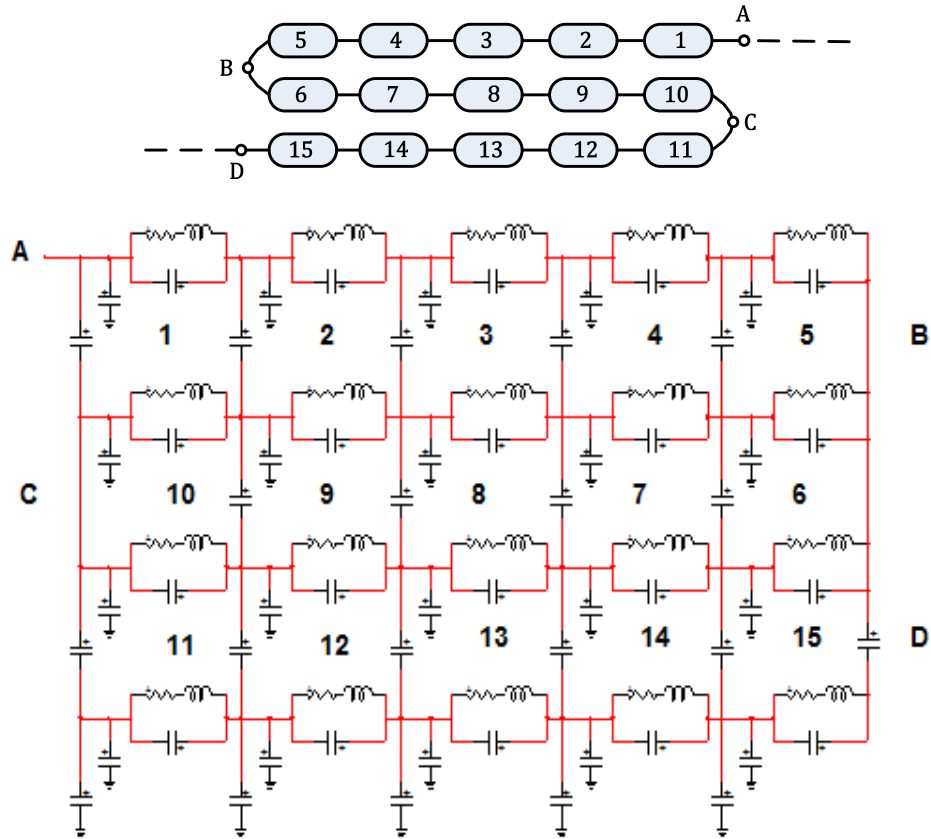


Fig. 3. 27 Equivalent RLC Network Model of winding

At first step in this model, a minimum segment length has to be specified. It is very important to choose a proper length for lumped parameter modelling. Regarding the front time of fast transient surges and length of winding conductor in transformer, it is sufficient to choose a disc length as the segment in the RLC model in order to study fast transients [17]. But since very fast transient surge has a very short rise time and can be reflected along disc length for several times, it is not sufficient to consider a disc length as the segment. In the case of very fast transient, this model can be applied but all turns must be represented. Fig. 3. 27b shows the details of RLC model in EMTP for a small part of winding shown in Fig. 3. 27a. This figure shows a part of winding consisting of three discs, each disc is made of five turns. Point A is the line terminal and the winding continues to point D. Each turn can be modelled by a series of resistance and inductance connected to series and parallel capacitances representing the capacitance between adjacent turns and also between turns and ground. This procedure must be done for the whole turns of transformer which result in very complicated networks of resistor, inductor and capacitors. This detailed model can be

reduced to a simple model for better calculation which is fully explained in [31]. It can be reduced to an RLC ladder network like the model shown in Fig. 2. 17.

This model can be described by the following equations [17]:

$$\mathbf{I}(s) = \mathbf{Y}(s) \cdot \mathbf{V}(s) \quad (3.20)$$

$$\mathbf{Y}(s) = s\mathbf{C} + \mathbf{G} + \frac{1}{s}\mathbf{H} \quad (3.21)$$

Where

$\mathbf{Y}(s)$ is the nodal admittance matrix of the circuit

$\mathbf{I}(s)$ is the nodal current vector

$\mathbf{V}(s)$ is the nodal voltage vector

\mathbf{C} , \mathbf{G} and \mathbf{H} are the nodal capacitance, nodal conductance and inverse nodal inductance matrices respectively.

If the input surge is applied to node n, voltage values at all nodes can be calculated as:

$$\begin{bmatrix} 0 \\ \vdots \\ I_n \end{bmatrix} = [\mathbf{Y}]_{n \times n} \begin{bmatrix} V_1 \\ \vdots \\ V_n \end{bmatrix} \quad (3.22)$$

$$\rightarrow V_i = [\mathbf{Y}]_{i,n}^{-1} I_n \quad (3.23)$$

Multiconductor Transmission Line (MTL) Model

If it is required to produce a model for studying the wave propagation along the winding, it is necessary to implement distributed parameter model. Multiconductor Transmission Line model describes the behaviour of travelling wave at any points of the winding based on differential equations of transmission line theory [54]. This method was first presented in [55] as a complete analytical solution alternative to other existing method at that time for calculating stresses on transformer winding resulted from voltage impulses. After that, MTL model was developed and extended to study the interturn insulation failures in large AC machine windings [56]. MTL model was successfully applied in [30, 57-59] for investigating the effect of very fast transient in transformer winding.

As shown in Fig. 3. 28, in this model, each disc or turn is modelled as a single transmission line. This model includes the behaviour of travelling waves in winding and propagation phenomenon, while the lumped parameter method ignores it [57]. Based on the well-known Telegrapher equations, voltage and current at any point x on transformer winding can be expressed by [60]:

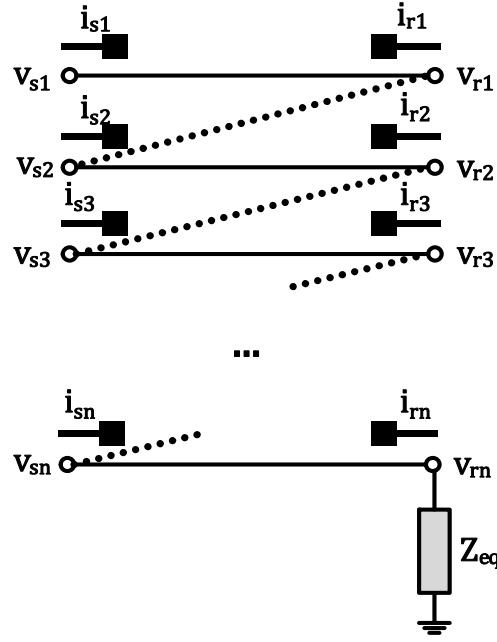


Fig. 3. 28 Equivalent MTL Model of winding

$$\frac{d\mathbf{V}(x)}{dx} = -\mathbf{Z} \cdot \mathbf{I}(x) \quad (3.24)$$

$$\frac{d\mathbf{I}(x)}{dx} = -\mathbf{Y} \cdot \mathbf{V}(x) \quad (3.25)$$

Here, $\mathbf{V}(x)$ and $\mathbf{I}(x)$ are voltage and current matrices respectively.

$$\begin{aligned} i_{r(i)} &= -i_{s(i)} \\ v_{r(i)} &= v_{s(i+1)} \end{aligned} \quad (3.26)$$

$$\begin{bmatrix} I_S \\ I_R \end{bmatrix} = \begin{bmatrix} Y_0 \coth(Pl) & -Y_0 \operatorname{csch}(Pl) \\ -Y_0 \operatorname{csch}(Pl) & Y_0 \coth(Pl) \end{bmatrix} \begin{bmatrix} V_S \\ V_R \end{bmatrix} \quad (3.27)$$

In which l is length of the line and:

$$I_S = \begin{bmatrix} i_{s1} \\ \vdots \\ i_{sn} \end{bmatrix}, I_R = \begin{bmatrix} i_{r1} \\ \vdots \\ i_{rn} \end{bmatrix}, V_S = \begin{bmatrix} v_{s1} \\ \vdots \\ v_{sn} \end{bmatrix}, V_R = \begin{bmatrix} v_{r1} \\ \vdots \\ v_{rn} \end{bmatrix}$$

$$\mathbf{P}^2 = \mathbf{ZY}, \mathbf{Y}_0 = \mathbf{Z}^{-1}\mathbf{P}$$

Therefore above equations can be formulated as:

$$\begin{bmatrix} i_{s1} \\ \vdots \\ i_{rn} \end{bmatrix} = [\mathbf{Y}]_{(n+1) \times (n+1)} \begin{bmatrix} v_{s1} \\ \vdots \\ v_{rn} \end{bmatrix} \quad (3.28)$$

By substituting (3.26) in (3.27) and some matrix operations [60], (3.28) can be expressed as:

$$\begin{bmatrix} i_{s1} \\ 0 \\ \vdots \\ 0 \end{bmatrix} = [T]_{(n+1) \times (n+1)} \begin{bmatrix} v_{s1} \\ v_{s2} \\ \vdots \\ v_{rn} \end{bmatrix} \quad (3.29)$$

Thus voltage values at all nodes can be calculated:

$$\begin{bmatrix} v_{s1} \\ v_{s2} \\ \vdots \\ v_{rn} \end{bmatrix} = [T]_{(n+1) \times (n+1)}^{-1} \begin{bmatrix} i_{s1} \\ 0 \\ \vdots \\ 0 \end{bmatrix}$$

$$\text{Assume } [F] = [T]^{-1} \rightarrow v_{si} = F_{i1} i_{s1} \quad (3.30)$$

Applying above formulas to all turns of transformer winding results in a very large matrix. In order to solve this problem, [30] suggested a simpler solution based on MTL model. The suggestion is that instead of applying MTL model to all turns, simulation can be performed in two steps (according to Fig. 3. 29):

- Step 1- Each disc shall be represented by an extended single transmission line model in order to find the voltage values at the disc's end. The calculated voltage at each disc's end is used as input for the next step.
- Step 2- Each disc shall be represented by multiconductor transmission line model to calculate the voltage values at each turn's end. The voltage calculated for each disc at previous step is used as applied voltage of coils in this step. This step shall be applied for each turn independently.

As explained before, since the high voltage stress in winding is more severe at first few turns of the winding, MTL model is only considered for the first disc of the transformer winding.

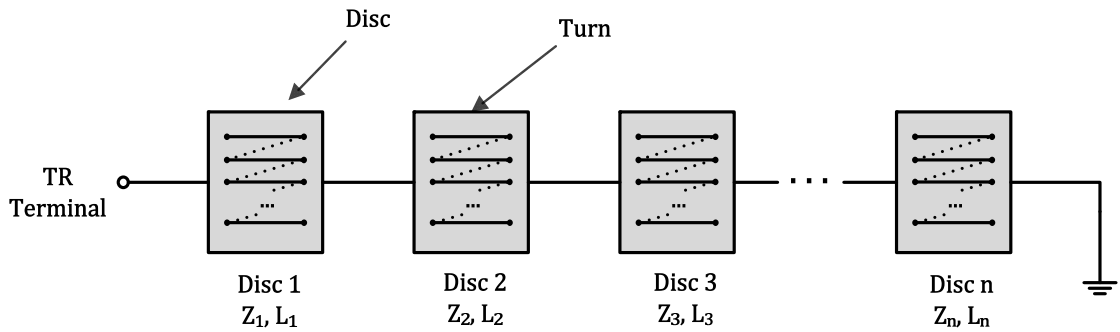


Fig. 3. 29 Combined single transmission line and multiconductor transmission line model of winding

Considering all procedures required for modelling transformer winding in either lumped or distributed parameter, it can be concluded that while the lumped parameter method is more straightforward to simulate the winding and needs simpler computation, the distributed parameter model has the advantage over lumped model due to its capability to include the propagation of travelling wave along the transformer winding. Reference [52] compared the results of simulations by lumped and distributed parameters with measurements carried out on a 220/35kV, 50 MVA

transformer and concluded that RLC ladder model is more correlated to the frequency range of $10 \text{ kHz} < f < 1 \text{ MHz}$ while MTL model is more suitable for frequency range of $1 \text{ MHz} \leq f \leq 5 \text{ MHz}$. Therefore, lumped parameter model has good accuracy for studying fast transient and distributed parameter model is recommended for very fast transient studies. For this reason, in this study, the MTL model is applied to study transformer internal resonance.

3.2.2 Determination of Parameters

Parameters for transformer models can be determined by Finite Element Method (FEM) or analytical methods. FEM method is used for the highest accuracy for calculating the parameters [61]. On the other hand, analytical method, which is used in this work, has acceptable accuracy [62].

Parameters are strongly dependent on the geometrical and dimensional features of winding. Construction of core and winding in a transformer play an important role in determining the parameters. The windings of power transformer are generally formed in two shapes: Layer type and Disc type [29]. As shown in Fig. 3. 30, in layer type windings, turns are wound in axial direction to form several coaxial cylinders around the core while in disc type windings turns are wound in radial directions to form several discs located on top of each other. The transformer investigated in this study is of disc type. Some specification of conductor and winding used in this study to compute R, L and C parameters are mentioned in Table 3. 7.

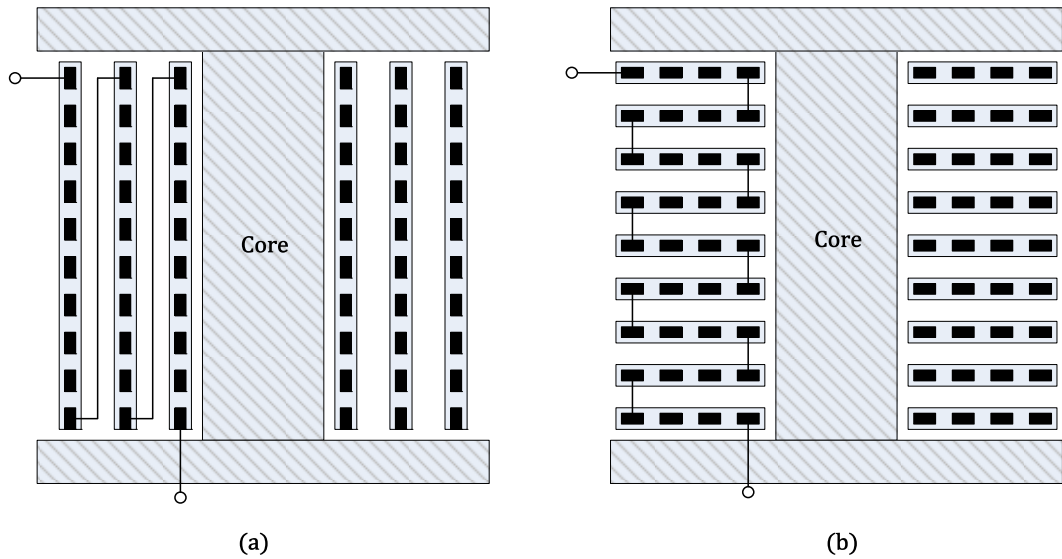


Fig. 3. 30 Type of transformer winding a) Layer type b) Disc type

Table 3. 7 Technical specification of transformer winding

Item	Value
S : Conductor cross section	120 mm^2
h : Conductor height	15 mm
w : Conductor width	8 mm
Number of discs	90

Number of turn per disc	20
a : Turn average length (m)	5.65 m
σ : Conductor conductance	5.85×10^7 S/m
μ : Conductor permeability	1.256×10^{-6} H/m
ϵ_0 : free space permittivity	8.85×10^{-12} F/m
ϵ_p : relative permittivity of paper	4.2
ϵ_{pb} : relative permittivity of pressboard	4.4
ϵ_{oil} : relative permittivity of oil	2.2
v : Surge velocity	143 m/ μ s
t_p : Distance between turns	3 mm
t_d : Distance between discs	8 mm
R_i : inner radius of disc	62.5 cm
R_o : Outer radius of disc	117.5 cm

3.2.2.1 Capacitance

According to the parallel plate capacitor formula, C_t (capacitance between turns) is obtained from [17, 63]:

$$C_t = \frac{\epsilon_0 \epsilon_p \pi D_m (w + t_p)}{t_p} \quad (3.31)$$

Where:

ϵ_0 : Permittivity of free space

ϵ_p : Relative permittivity of insulation

D_m is average diameter of winding

w : Width of conductor

t_p : distance between turns

Therefore interturn capacitance per unit length is:

$$C_t = \frac{\epsilon_0 \epsilon_p (w + t_p)}{t_p} \quad (3.32)$$

C_d (capacitance between discs) is calculated as [17, 63]:

$$C_d = \epsilon_0 \left(\frac{k}{\frac{t_p}{\epsilon_p} + \frac{t_d}{\epsilon_{oil}}} + \frac{1-k}{\frac{t_p}{\epsilon_p} + \frac{t_d}{\epsilon_{pb}}} \right) \pi D_m (R + t_d) \quad (3.33)$$

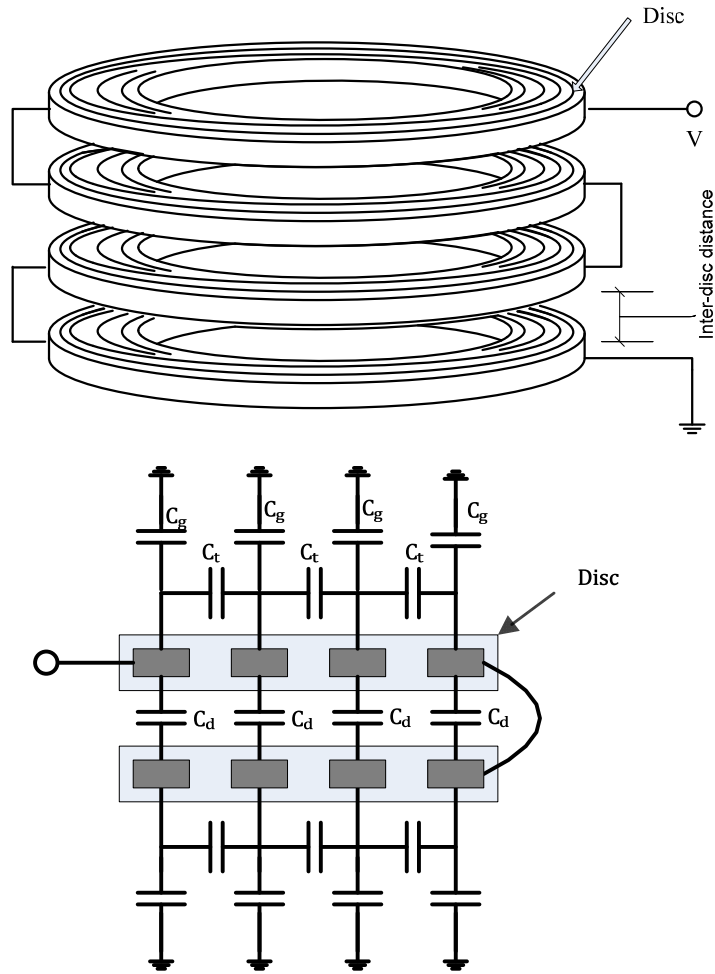


Fig. 3. 31 Representing capacitance between turns and discs

For the same reason mentioned above, the inter-disc capacitance per unit length will be:

$$C_d = \epsilon_0 \left(\frac{k}{\frac{t_p}{\epsilon_p} + \frac{t_d}{\epsilon_{oil}}} + \frac{1-k}{\frac{t_p}{\epsilon_p} + \frac{t_d}{\epsilon_{pb}}} \right) (R + t_d) \quad (3.34)$$

k is a fraction of circumferential space between adjacent discs occupied by oil = 0.7 (Fig. 3. 32)

R is the winding radial depth = $w = 8$ mm

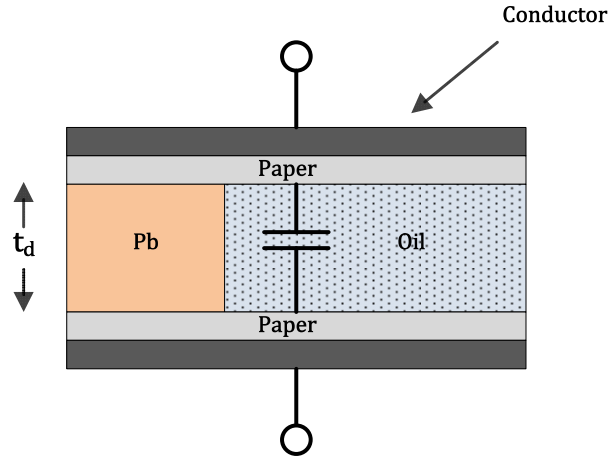


Fig. 3. 32 Composition of inter-disc capacitance

Regarding the values of parameters specified in Table 3. 7 Technical specification of transformer winding:

C_i : interturn capacitance = 770.3 pF (136.3 pF/m)

C_d : inter-disc capacitance = 223.5 pF/turn (39.55 pF/m)

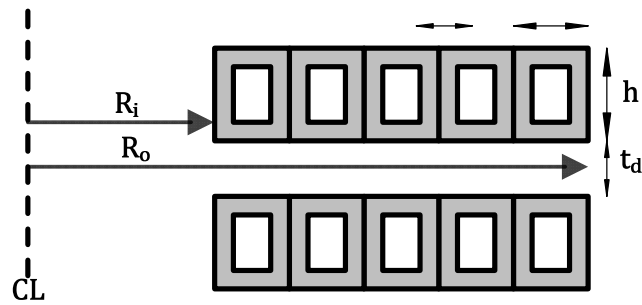


Fig. 3. 33 Cross section of discs

Also the capacitance of winding to ground (C_g) can be computed as [62, 64]:

$$C_g = \frac{2\pi\epsilon_0\epsilon_r h}{\ln\left(\frac{R_{disc}}{R_{core}}\right)} \quad (3.35)$$

R_{disc} : Inner radius of the disc

R_{core} : Radius of the iron core= 55 cm

Using the values in Table 3. 7, we have: $C_g=27\text{pF}$

For MTL modelling we need capacitance values per meter, thus: $C_g=27/5.65=4.85$ pF/m. The results of capacitance calculation are shown in Table 3. 8.

Table 3. 8 Calculated capacitances

For disc to disc modelling	
Inter-disc capacitance 4.47 nF (changes at different discs)	Disc-Ground capacitance 4.85 pF/m
For turn to turn modelling	
Inter-turn capacitance 770 pF	Turn-Ground capacitance 4.85 pF/m

3.2.2.2 Inductance

Inductance of winding is calculated according to [64]:

$$L_s = \mu_0 N^2 \pi R \left[\frac{1 + \frac{2}{3}\beta + \frac{1}{6}\beta^2}{f_1(\alpha + \beta)} + f_2(\alpha + \beta) \right] \quad (3.36)$$

Where:

$$f_1(\alpha + \beta) = [0.905 + \alpha + 0.72\beta - 0.195e^{-\frac{\alpha+\beta}{0.32}} + \beta(0.234 + 0.116e^{-\frac{\beta}{2.1}})e^{\frac{\alpha}{3.3+1.5\beta-2.3\beta/(1+0.28\beta^2)}}]$$

$$f_2(\alpha + \beta) = 0.38e^{-16(\alpha+\beta)} + 0.48e^{-68(\alpha+\beta)} \quad (\alpha + \beta) \geq 0.02$$

Or

$$f_2(\alpha + \beta) = \frac{1}{\pi} \ln \left(\frac{0.058}{\alpha + \beta} \right) + 3(\alpha + \beta) \quad (\alpha + \beta) < 0.02$$

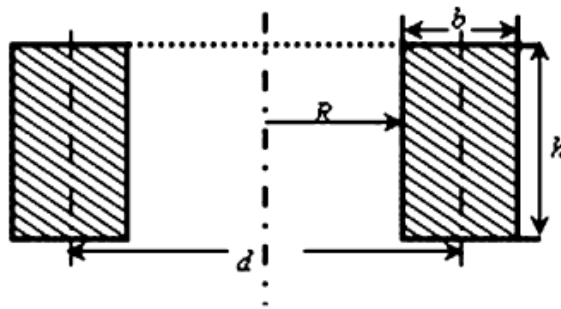


Fig. 3. 34 Cross section of winding conductor

$$\alpha = \frac{h}{R} = 0.017$$

$$\beta = \frac{b}{R} = 0.009$$

$$f_1(\alpha, \beta) = 0.7518$$

$$f_2(\alpha, \beta) = 0.3326$$

$$L_s = 5.93 \mu H/m$$

3.2.2.3 Resistance

Finally, resistance of winding can be obtained by [59]:

$$R = \frac{1}{2(w + h)} \sqrt{\frac{\pi f \mu}{\sigma}} \quad (3.37)$$

According to the provided details in Table 3. 7: $R=40 \mu\Omega/m$ at 50Hz

3.2.3 Resulted transformer model

For the two step method utilized in this study, each disc is considered as a transmission line as shown in Fig. 3. 35. According to the information provided in Table 3. 7, total number of discs is 20, therefore, twenty transmission lines were considered in EMTP to represent all discs of winding. For this purpose, Frequency Dependent (FD) line (FDline object) of EMTP was used. Then a sinusoidal power supply with an amplitude of 1 voltage unit was connected to the line terminal and the case was run in frequency domain. As described before, after calculation of inter-disc voltage, each disc can be selected for 2nd step for determining interturn voltages. Similar procedure and model is implemented for 2nd step but the specification of the line including length and interturn capacitance change. The output of 1st step is used as input to the circuit created in 2nd step. Voltage results between 1st and 2nd turns of the first disc is shown in Fig. 3. 36.

As illustrated in Fig. 3. 37 Frequency spectrum of VFTO at the terminal of transformer the dominant frequencies of VFTO locate at 0.87 MHz, 1.04 MHz and 2.88 MHz, but according to Fig. 3. 36, the amplitude of the voltage between 1st and 2nd turns of the first coil of winding at 0.87 MHz and 1.04 MHz is negligible in comparison with the amplitude at 2.88 MHz. Thus, high frequency components at 0.87 MHz and 1.04 MHz cannot endanger the transformer winding, but there is a high risk frequency at 2.88 MHz that occurrence of internal resonance is highly probable, this means that at this frequency dominant frequency of VFTO coincides with one of the resonance frequencies of interturn voltage. Consequently:

Amplitude of VFTO component at 2.88 MHz = 0.101 p.u.

➔ Amplitude of interturn voltage at 2.88 MHz = 23.7 kV (Fig. 3. 38)

Although there is no standard available on the insulation levels of windings against VFTO, several studies have been carried out to determine insulation withstanding level against nonstandard waveshapes. One published study [58] suggests that the interturn insulation level can be considered as 1.5% of basic insulation level (BIL) of transformer insulation which results in 19.5 kV (0.015×1300 kV). It is obvious that the emerged voltage between two turns in the first disc of the investigated transformer in this study exceeds the maximum permissible value. Therefore it is desired to

suppress the voltage to a value below 19.5 kV which means a suppression percentage of 56%.

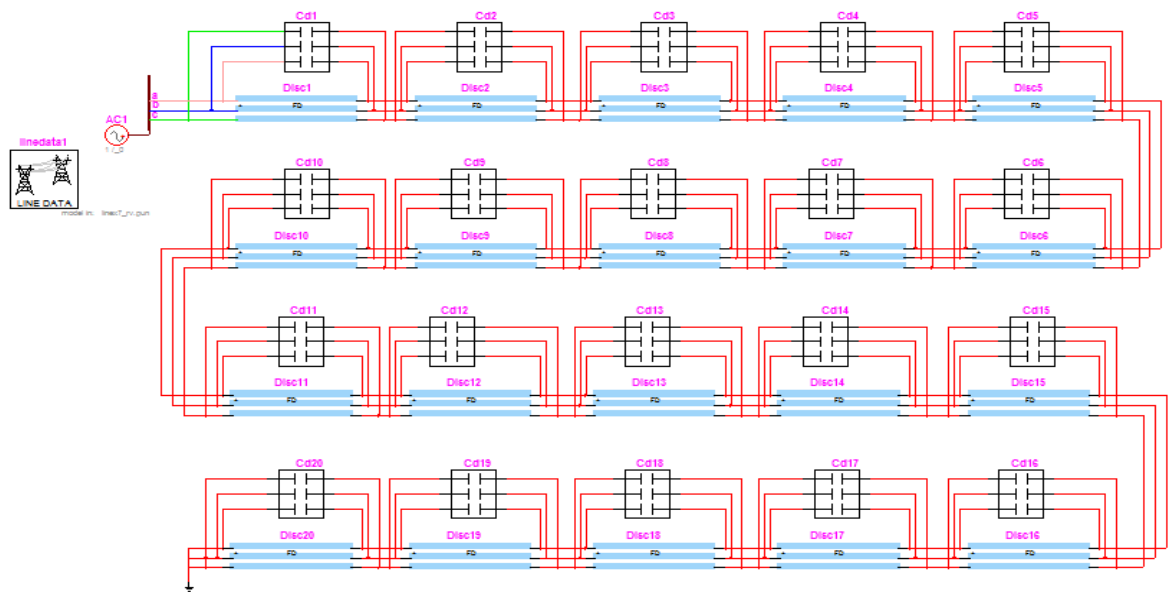


Fig. 3. 35 Winding model at 1st step

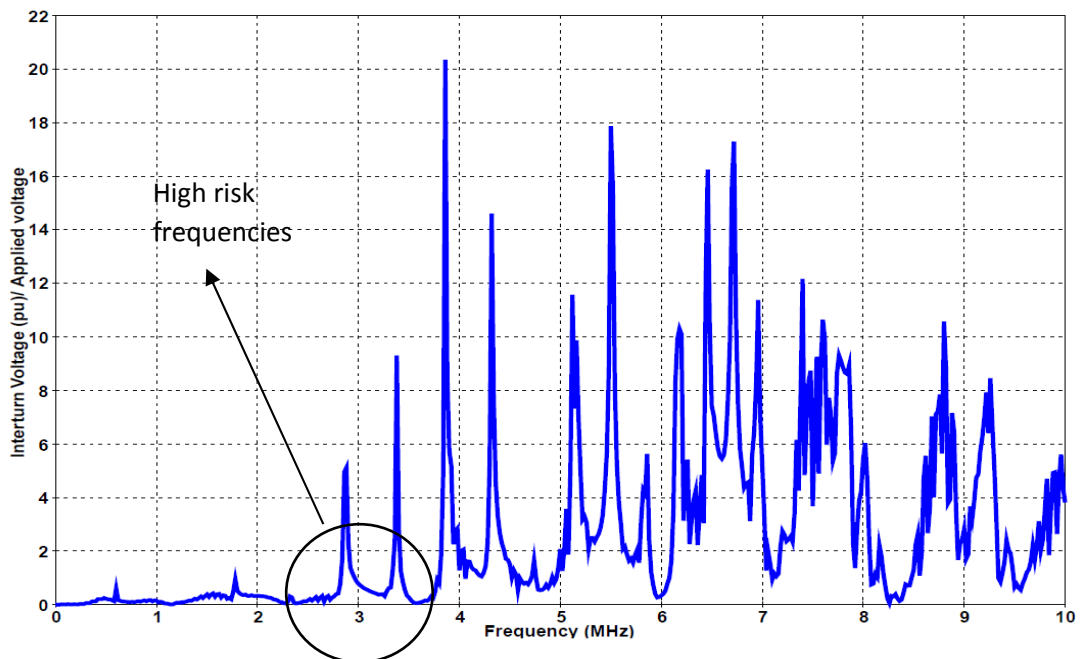


Fig. 3. 36 Frequency spectrum of voltage between 1st& 2nd turn of the 1st coil per applied voltage

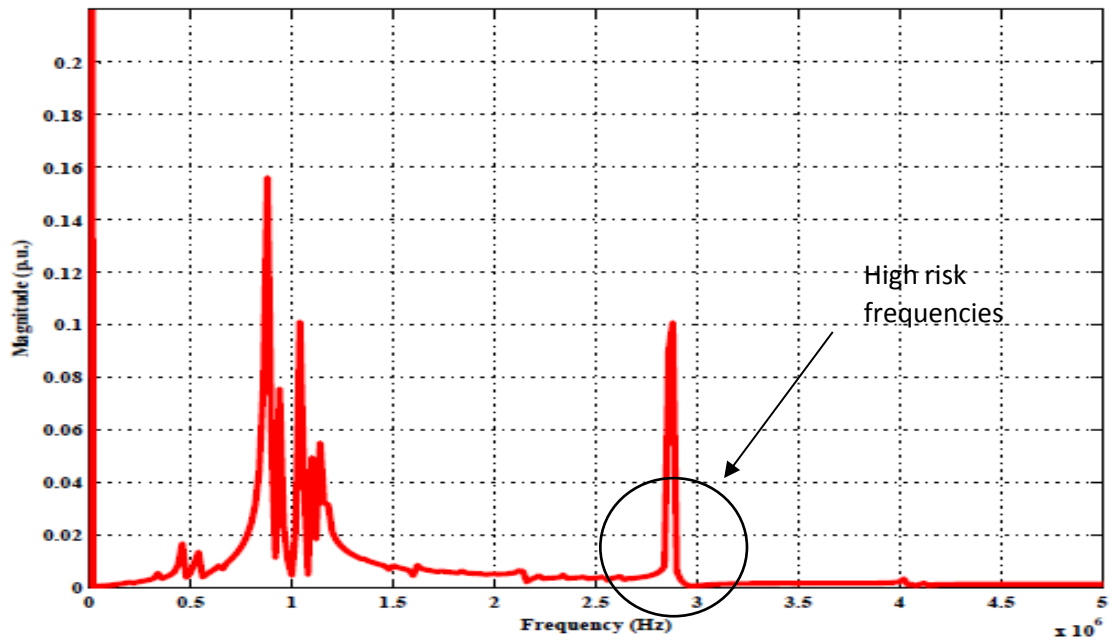


Fig. 3. 37 Frequency spectrum of VFTO at the terminal of transformer

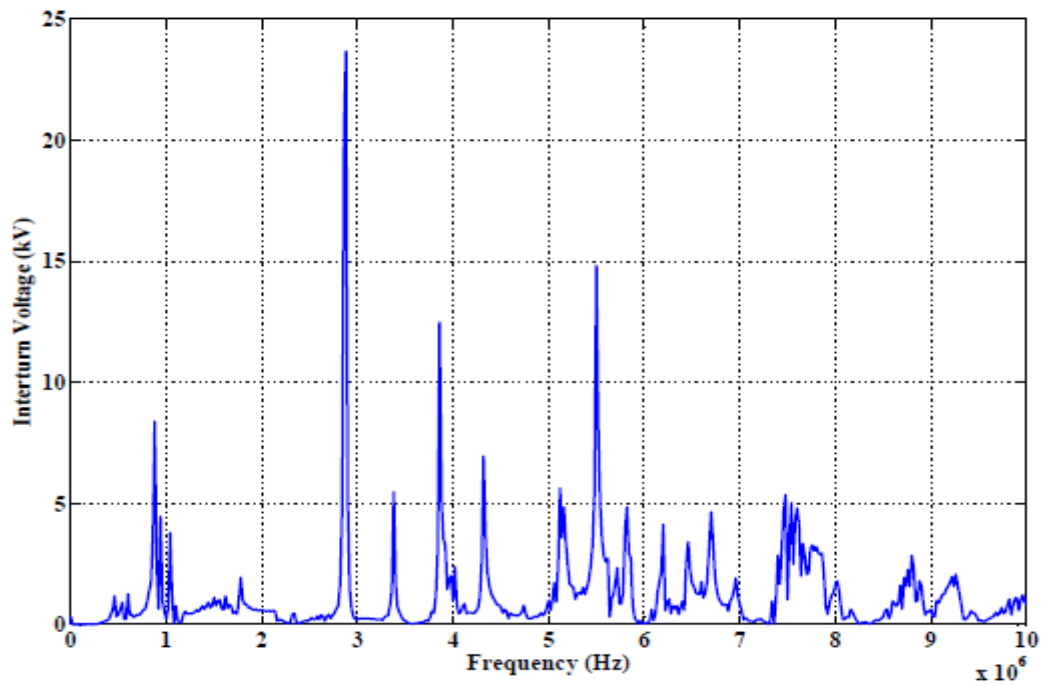


Fig. 3. 38 Frequency spectrum of voltage between 1st& 2nd turn of the 1st coil

4 VFTO Surge Suppression

4.1 RC Surge Suppressor

Based on the suppressing effect of the capacitor on high frequency components of VFTO, the main target in this study is to achieve a voltage waveform at terminal of power transformer where the amplitude at high risk frequency doesn't exceed the maximum permissible value of interturn insulation. Generally, resistive components can be connected to C for consuming the energy stored in VFTO surge and any RC branch in different topologies provide very small impedance at high frequencies while they show a large impedance at the power frequency which could be ideal regarding concerns about losses during normal operation. Fig. 4. 1 and Fig. 4. 2 show proposed topologies for RC surge suppressors and their related impedance characteristics. According to Fig. 4. 2, the three proposed topologies provide low impedance at high frequencies, but the elements in 2nd and 3rd order suppressors can be set to provide minimum impedance at particular frequency while 3rd order has maximum impedance at another frequency.

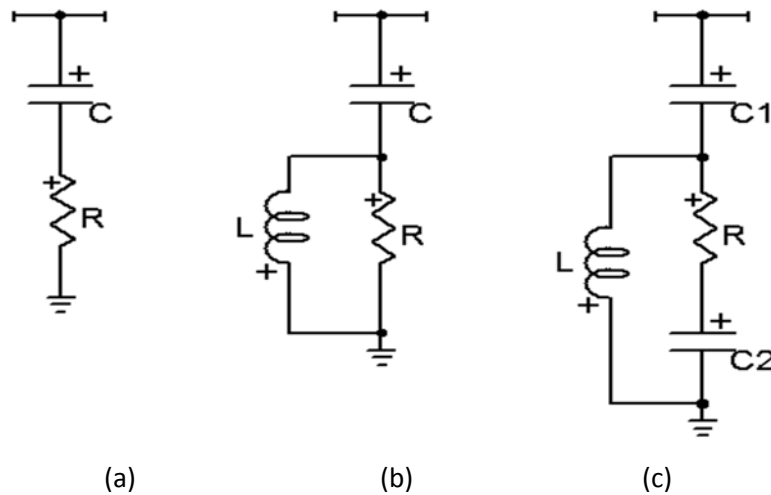


Fig. 4. 1 Proposed topologies for RC surge suppressor (a) 1st order (b) 2nd order (c) 3rd order

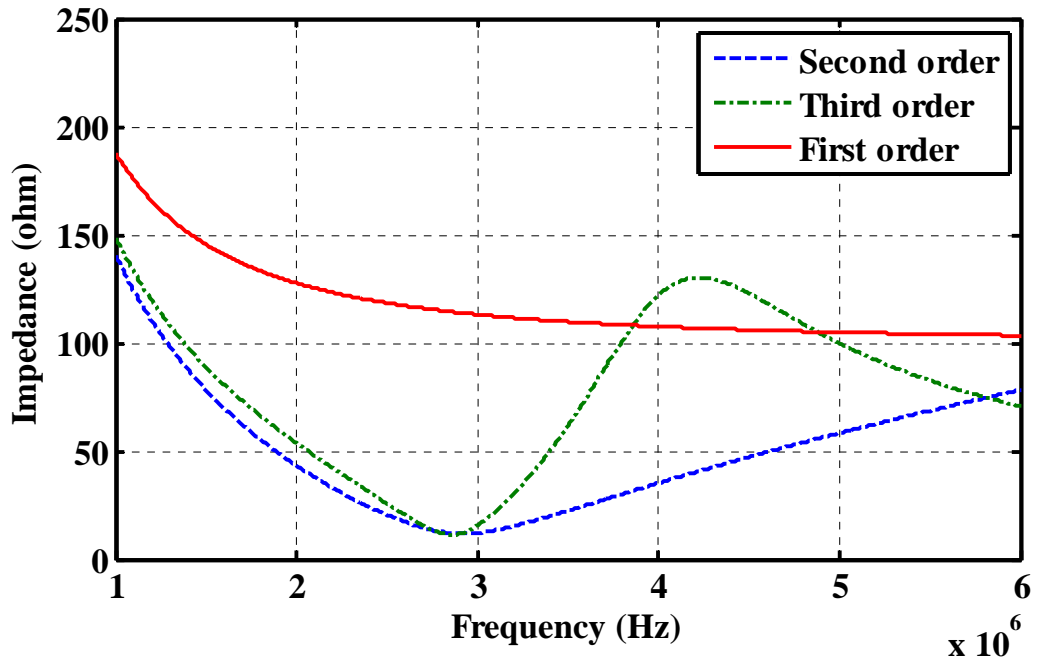


Fig. 4. 2 Frequency response of proposed suppressor; 1st order (C=1nF, R=500Ω);2nd order (C=1nF, R=510Ω, L=26μH);3rd order (C=1nF, R=50Ω, L=13μH)

These topologies are taken from the topology of passive filters used in industrial applications for the purpose of filtering undesired harmonics and compensating reactive power [65, 66]. In this study, the efficiency of these arrangement of RC components for the purpose of suppressing high frequency dominant components of VFTO is investigated. Therefore, in this chapter, different arrangement of RC suppressors are considered to be installed in parallel with the transformer terminals connected to the GIS.

4.1.1 First Order Surge Suppressor

Fig. 4. 3 and Fig. 4. 4 Show the impedance curve of 1st order surge suppressor with constant C, and constant R respectively.

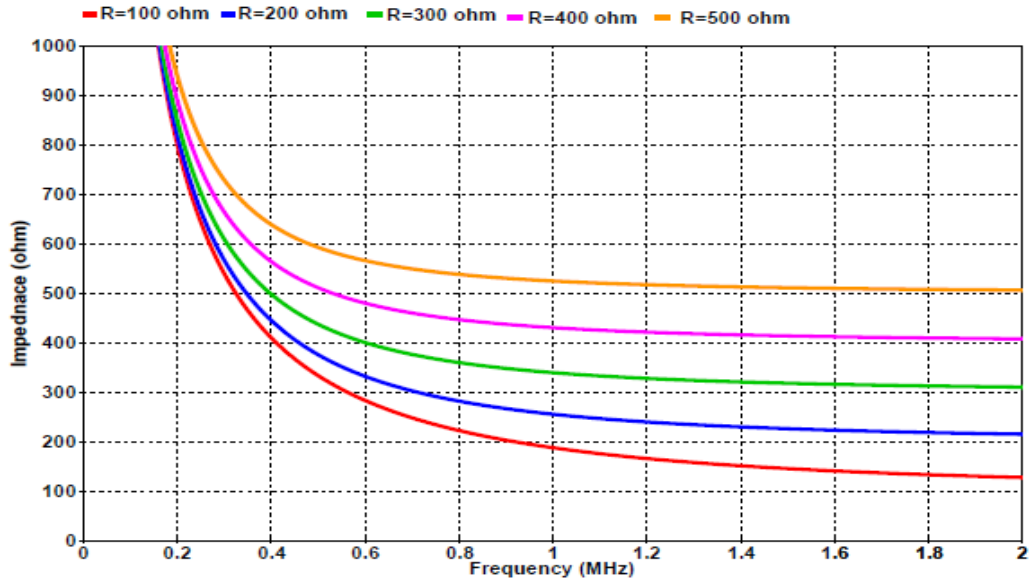


Fig. 4. 3 Frequency response of first order suppressor with $C=1\text{nF}$ and different R values

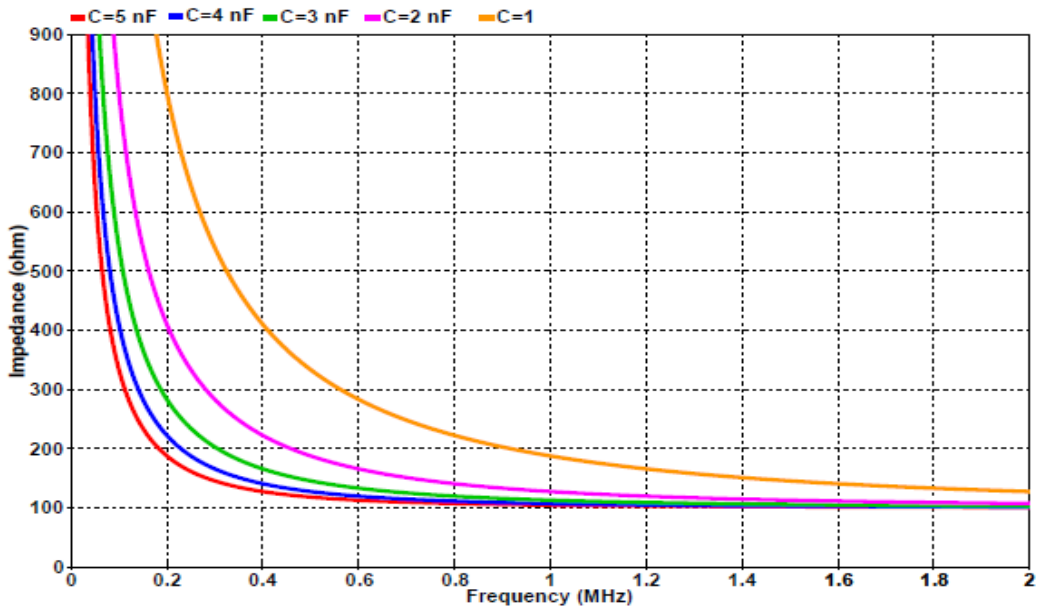


Fig. 4. 4 Frequency response of first order suppressor with $R=100\Omega$ and different C values

It can be seen that the impedance of shunt branch at high frequencies approaches to the value of R. Also suppressors with larger values of C provide lower impedance.

4.1.2 Second Order Surge Suppressor

In this suppressor, a capacitor is connected in series with a parallel branch of R and L. At very high frequencies, it behaves like a first order suppressor with a small impedance but at lower frequencies it behaves like a tuned filter because inductor has smaller value at lower frequencies and can bypass the resistor. As shown in Fig. 4. 2, second order suppressor can provide a min impedance at particular frequency and the suppressor can be tuned to this particular frequency. This frequency can be obtained from calculating the impedance of RC suppressor impedance shown in Fig. 4. 5:

$$Z = (R \parallel jL\omega) + \frac{1}{j\omega C} \quad (4.1)$$

$$Z = \frac{RL^2\omega^2}{R^2 + L^2\omega^2} + j\left(\frac{R^2L\omega}{R^2 + L^2\omega^2} - \frac{1}{C\omega}\right) \quad (4.2)$$

By defining two auxiliary parameters: m & f_0 , the behaviour of the surge suppressor can be described by these two parameters.

$$m = \frac{L}{R^2C} \quad (4.3)$$

$$f_0 = \frac{1}{2\pi RC} \quad (4.4)$$

If $x = \frac{f}{f_0}$ then:

$$Z = \frac{Rm^2x^2}{1 + m^2x^2} + jR\left(\frac{mx}{1 + m^2x^2} - \frac{1}{x}\right) \quad (4.5)$$

$$x = \omega RC \quad (4.6)$$

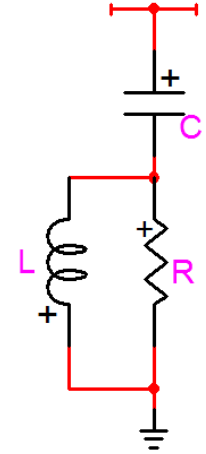


Fig. 4. 5 Second order surge suppressor

It can be shown that m indicates the sharpness of impedance curve at the tuning frequency [65]. For calculating the suppressor elements, at a given C value, m is decided to choose appropriate values for R and L . For this purpose, with known C and m , minimum value of Z in (4.5) must be found. The x_{min} resulting in Z_{min} is corresponding to desired frequency which can be a dominant frequency of VFTO. Now R can be obtained from:

$$R = \frac{x_{min}}{2\pi f_{min}C} \quad (4.7)$$

And L can be calculated from:

$$L = mR^2C \quad (4.8)$$

The procedure required for determining the suppressor elements according to a desired minimum frequency is shown in Fig. 4. 6. Also, impedance curve of second order surge suppressor with different R , L and C values are shown in Fig. 4. 7 and Fig. 4. 8. From Fig. 4. 7 it is found that by changing R and L (consequently m) f_{min} can be set to a desired value and from Fig. 4. 8 it is clear that by reducing m , sharpness of tuning improves. In this figure, suppressors are tuned at 870 kHz which is one of the dominant frequencies of VFTO according to Fig. 3. 24.

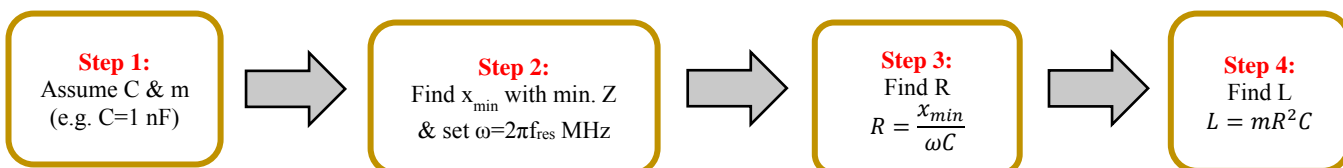


Fig. 4. 6 Determining the elements of surge suppressor

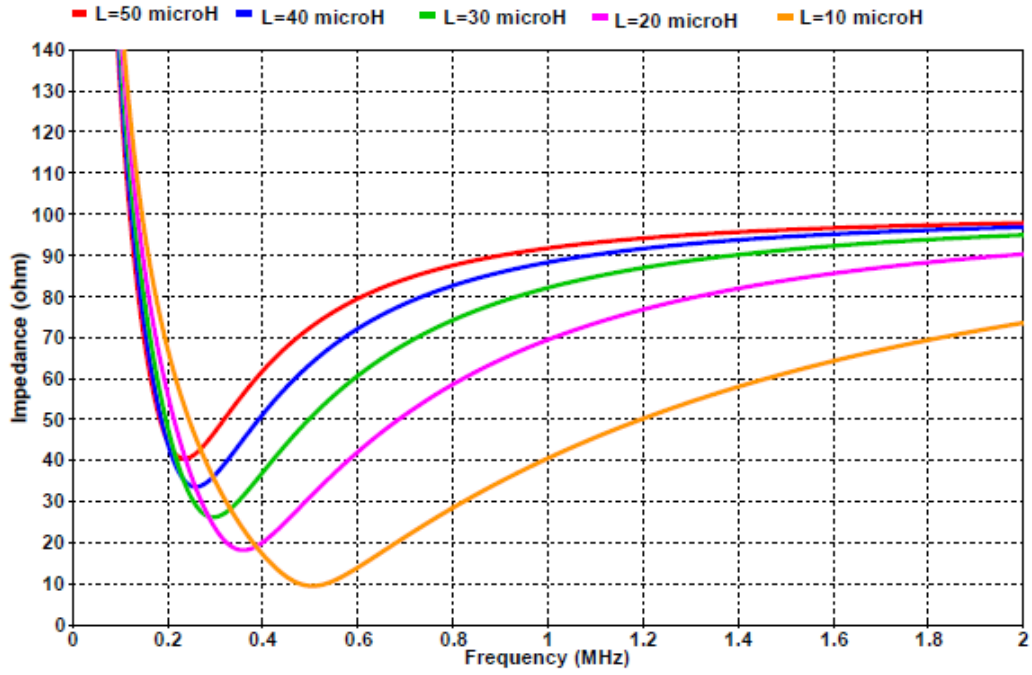


Fig. 4. 7 Impedance curve of 2nd order suppressor with $C=10\text{nF}$, $R=100\Omega$, varying L

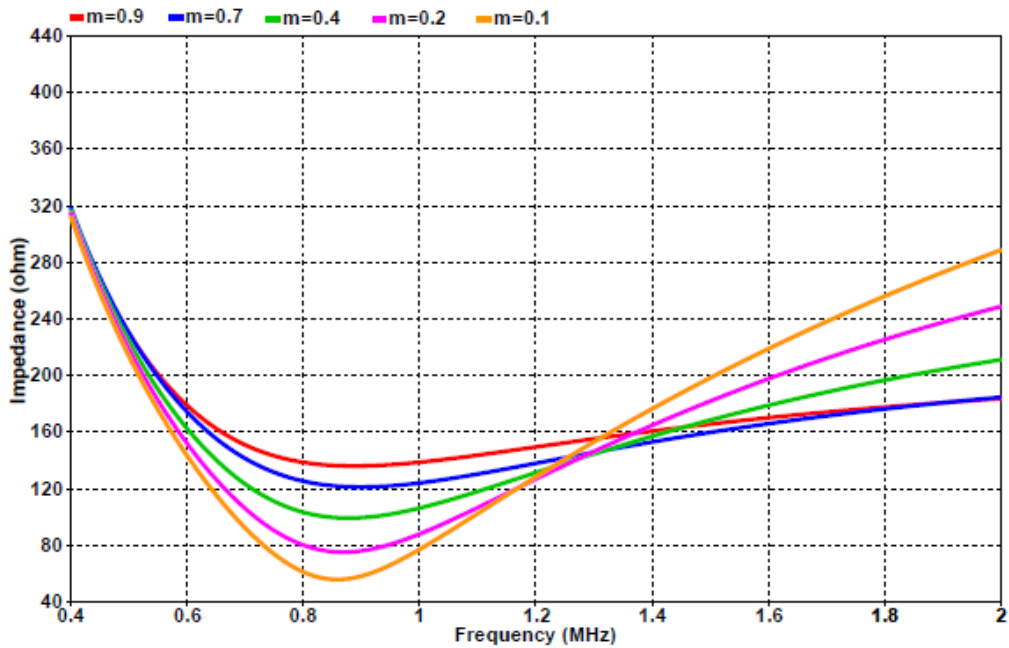


Fig. 4. 8 Impedance curve of 2nd order suppressor with $C=1\text{nF}$, varying m

4.1.3 Third Order Surge Suppressor

Third order surge suppressor consists of a capacitor connected in series with a parallel connection with RL branch as shown in Fig. 4. 9. Similar to the second order surge suppressor, at very high frequencies, it behaves as a first order suppressor which has a small impedance but at lower frequencies it is a single tuned filter with two capacitors C_1 and C_2 which make a tuning frequency with minimum impedance value and one anti-resonance peak at a frequency higher than tuning frequency [67]. Third

order suppressor has less loss at normal operation because another capacitor is connected in series with R and resistive branch exhibits larger impedance even than 2nd order suppressor at normal operation.

The procedure needed for determining the suppressor elements is similar to the second order suppressor. Given the C value for each suppressor, values of R and L are calculated to set the minimum impedance at a particular frequency with the desired tuning sharpness, which is represented by m .

$$Z = \left(R + \frac{1}{j\omega C} \right) \parallel jL\omega + \frac{1}{j\omega C} \quad (4.9)$$

$$Z = \frac{RL^2C^2\omega^4}{R^2C^2\omega^2 + (\omega^2LC - 1)^2} + j \left(\frac{R^2LC^2\omega^3 - \omega L(\omega^2LC - 1)}{R^2C^2\omega^2 + (\omega^2LC - 1)^2} - \frac{1}{C\omega} \right) \quad (4.10)$$

$$\Rightarrow Z = \frac{Rm^2x^4}{x^2 + (mx^2 - 1)^2} + jR \left(\frac{mx^3 - m^2x^3 + mx}{x^2 + (mx^2 - 1)^2} - \frac{1}{x} \right) \quad (4.11)$$

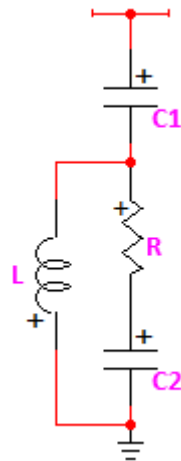


Fig. 4. 9 Third order surge suppressor

The impedance curves of a third order surge suppressor with different R , L and C values are shown in Fig. 4. 10 and Fig. 4. 11. The value of m in 2nd order suppressor is below 1, and the impedance curve of 2nd order suppressor doesn't show any minimum value at any frequencies for m greater than 1. There is no limitation for m in third order suppressor. Changing m can change the sharpness of the notch appeared in impedance curve of the third order suppressor. From Fig. 4. 10 it is found that by changing R and L (consequently m) f_{min} can be set to a desired value and from Fig. 4. 11 it is clear that suppressor with $m=10$ is sharper at tuning frequency than $m=0.1$, however suppressor will have larger Z_{min} . In this figure, suppressors are tuned at 870 kHz which is one of dominant frequencies of VFTO according to Fig. 3. 24.

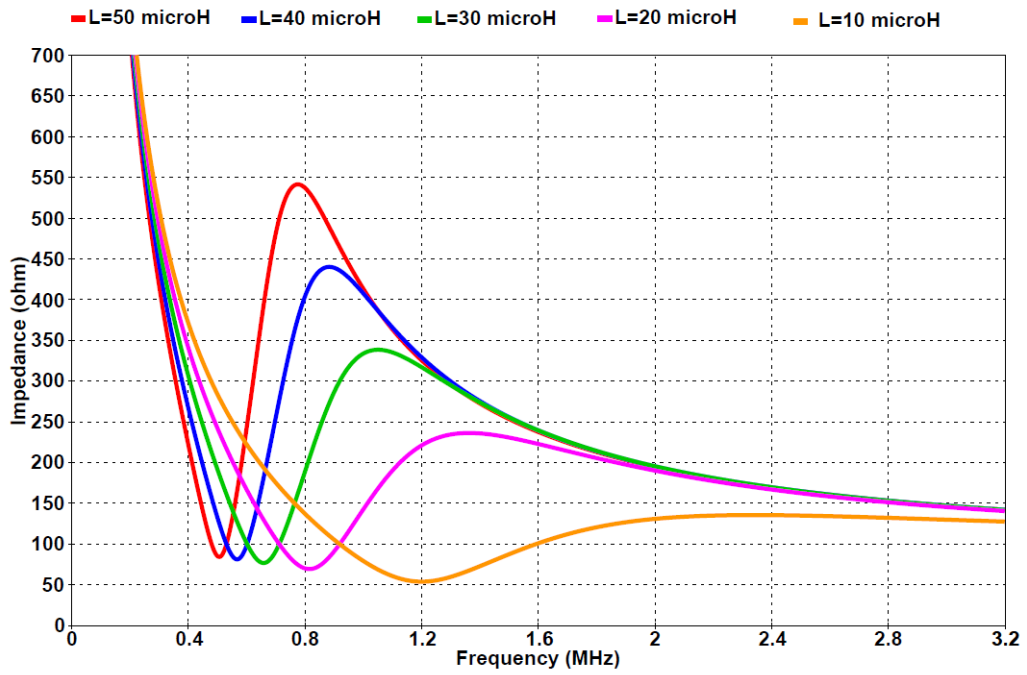


Fig. 4. 10 Impedance curve of 3rd order suppressor with $C=1\text{nF}$, $R=100\Omega$, varying L

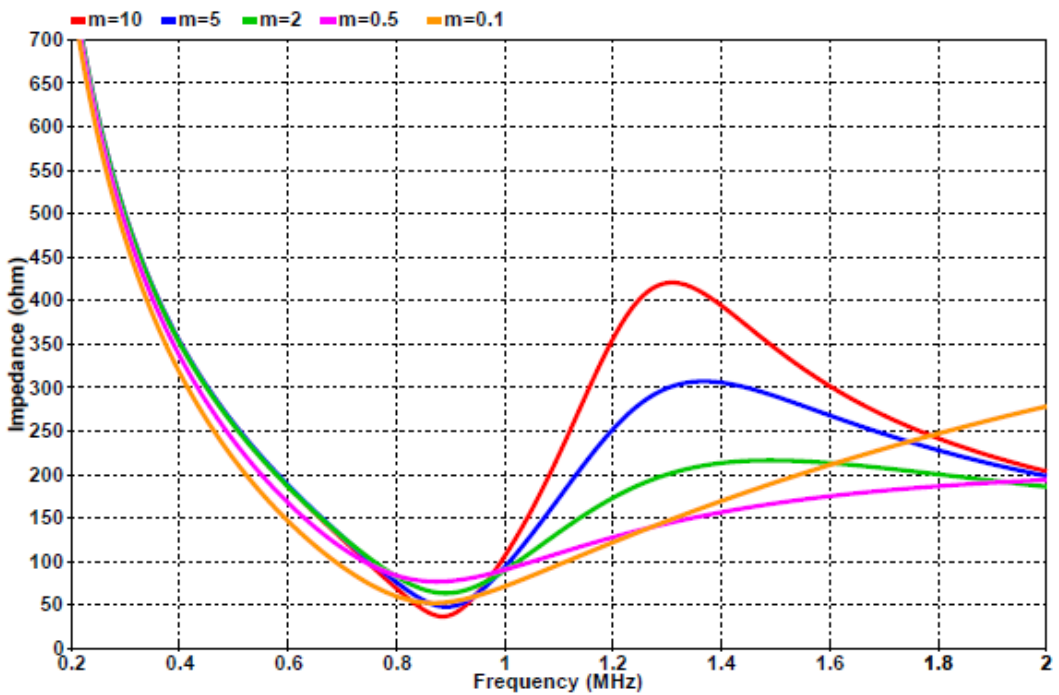


Fig. 4. 11 Impedance curve of 3rd order suppressor with $C=1\text{nF}$, varying m

As an example, for designing second order and third order suppressors with $C=2\text{ nF}$ (assumed) to be tuned at two frequencies 0.87MHz and 2.88MHz elements of surge suppressor are determined as shown in Table 4. 1.

Table 4. 1 Calculated elements of 2nd order suppressor

Parameter	Case 1 Tuned at 0.87 MHz	Case 2 Tuned at 2.88 MHz
f_{min}	0.87 MHz	2.88 MHz
C	2 nF	2 nF
m	0.1	0.2
x_{min}	3.2	2.25
R	293 Ω	62 Ω
L	17 μ H	1.5 μ H

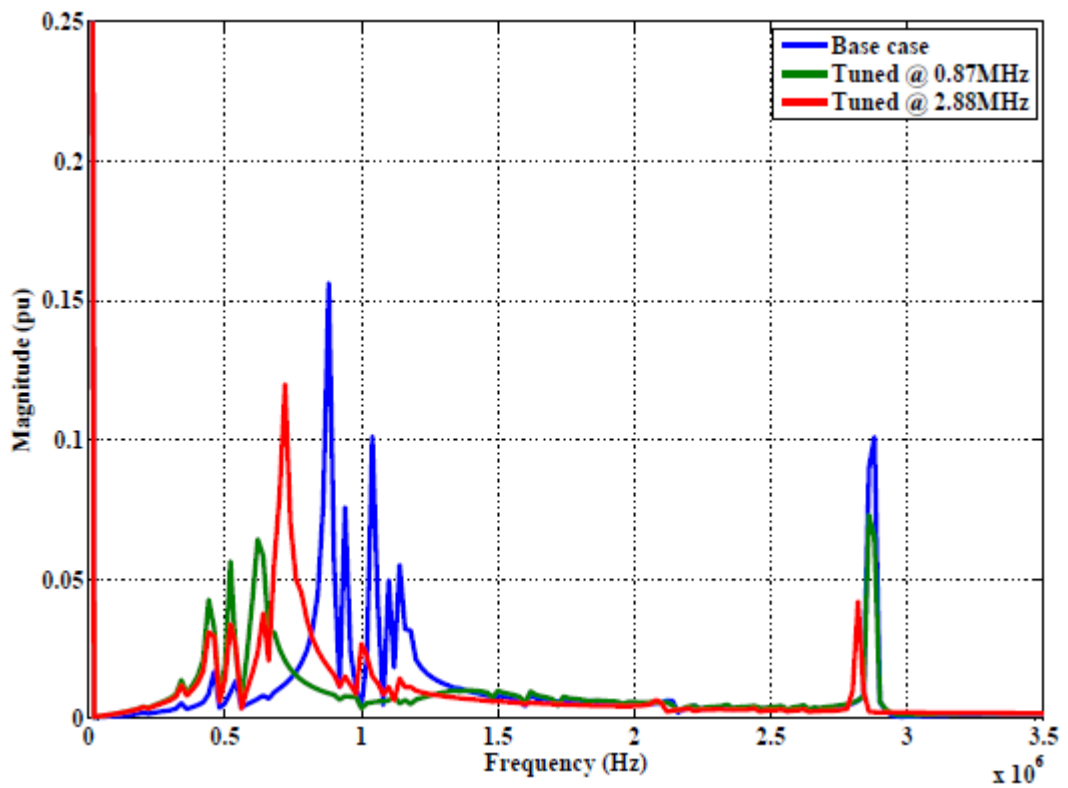
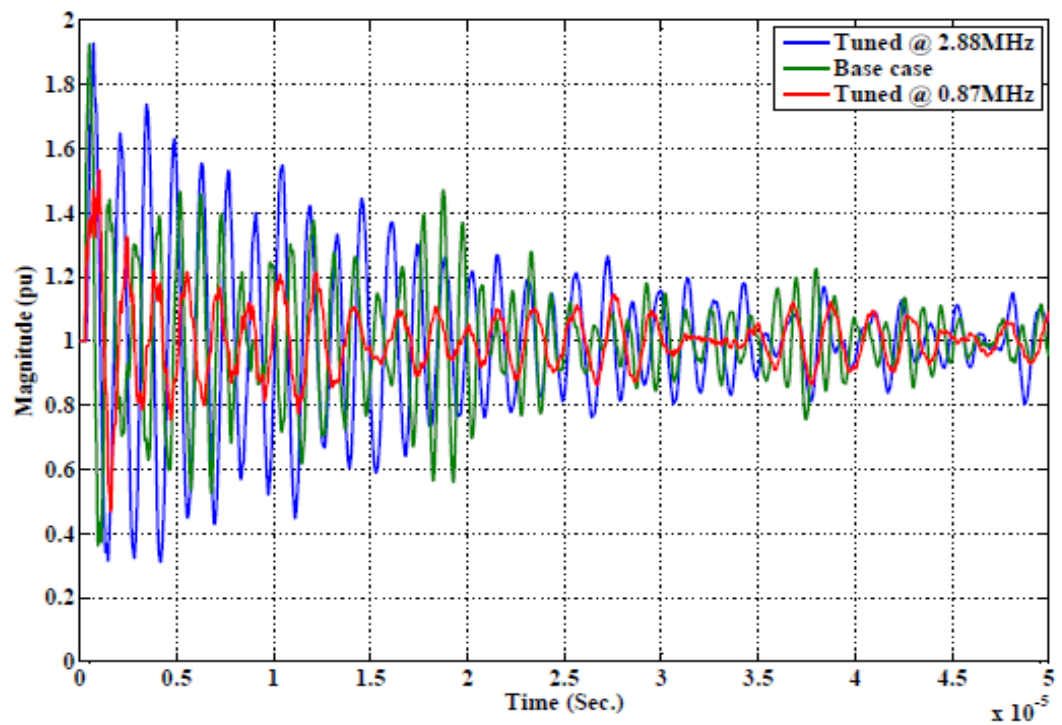


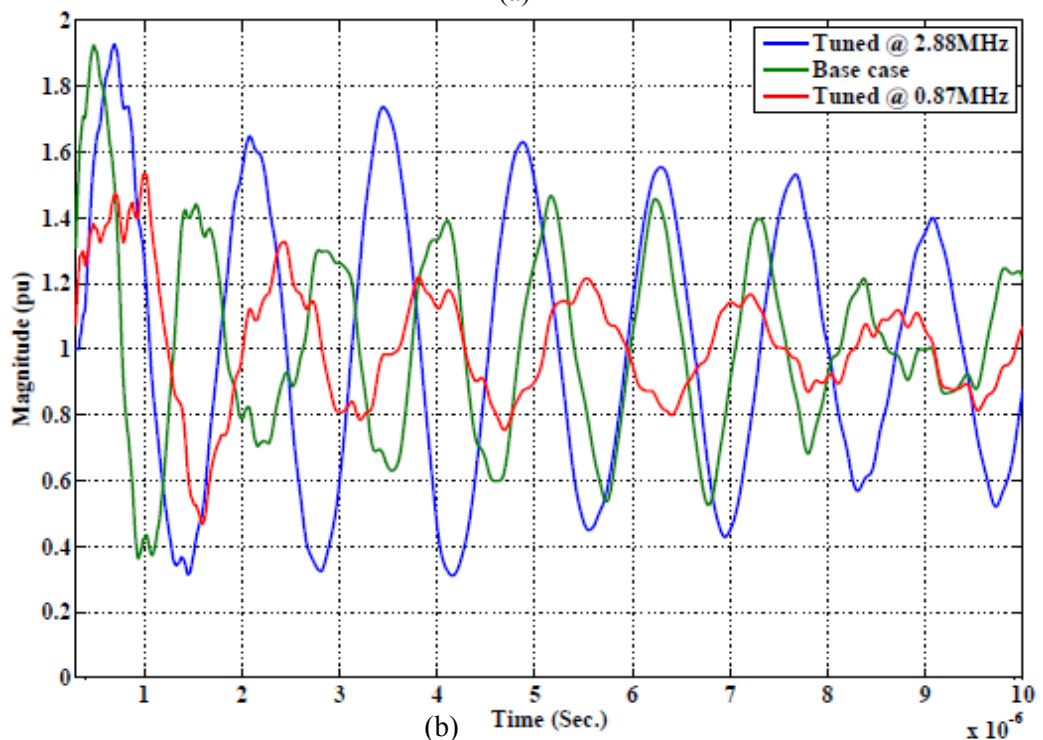
Fig. 4. 12 Frequency spectrum of VFTO after adding 2nd order suppressor

Fig. 4. 12 compares the frequency spectrum of VFTO surge at the transformer terminals in three different cases. Base case is the original state of VFTO without any surge suppressor while two other cases include a second order surge suppressor parallel to the transformer. In one case, the second order suppressor is tuned at 0.87 MHz, which is a dominant frequency with the largest magnitude; and in another case, it is tuned at 2.88 MHz, which is another dominant frequency but high risk frequency because it coincides with transformer's resonance frequency. It is evident that by adding a suppressor tuned at 0.87 MHz, this dominant frequency is suppressed considerably (reduced from 0.16 p.u. to 0.06 p.u.) and there is a reduction in amplitude of 2.88 MHz from 0.01 p.u. to 0.007 p.u. (about 30%), while by adding a suppressor tuned at 2.88 MHz, there is significant suppression at 2.88 MHz (from

0.01 p.u. to 0.004 p.u.) about 60%, but the dominant frequency at 0.87 MHz isn't suppressed as much as previous case.



(a)



(b)

Fig. 4. 13 Amplitude of VFTO after adding 2nd order suppressor a) During 50 μ s b) During 10 μ s

Fig. 4. 13 illustrates the maximum amplitude of VFTO at three defined cases within 50 μ s, and a zoomed view in 10 μ s. It is seen that voltage magnitude in the case with the second order surge suppressor, tuned at 0.87 MHz, is suppressed by 20%

(reduction in magnitude from 1.93 p.u. to 1.53 p.u.), while the suppressor tuned at 2.88 MHz doesn't cause any remarkable change in voltage magnitude. The enlarged view is brought here for comparing the surge front steepness in three cases. It is clear that surge suppressor tuned at 0.87 MHz reduced the maximum rate of rise of VFTO, while the suppressor tuned at 2.88 MHz has the same steepness of the original surge. It is concluded that suppressor tuned at 0.87 MHz had a positive effect on overall magnitudes of VFTO, its front steepness and how it attenuated the high risk frequency of VFTO at 2.88 MHz. Although the suppressor tuned at 2.88 MHz had considerable suppressing effect on the amplitude of high risk frequency at 2.88 MHz, its suppression on overall VFTO magnitudes and front steepness is not sensible.

4.2 Indices to Assess Suppressing Performance

Based on the definition of insulation strength presented for the purpose of insulation coordination studies, the crest value of applied voltage and time to crest are two most important factors specifying the insulation strength [68]. As explained before, the major concern in this study is the failure of insulation between turns of transformer resulting from internal resonance caused by VFTO surge, therefore insulation strength against high frequencies of VFTO plays an important role although VFTO causes high voltage stress on terminal insulation of transformer or bushing which can be attenuated by adding a shunt capacitor at transformer terminal.

To find the most appropriate RC surge suppressor for the purpose of suppressing high frequency components of VFTO, a set of design criteria is introduced to compare the effectiveness of different arrangements to be installed at the transformer terminal. These criteria represent the capability of suppressor to suppress following parameters:

- High risk frequencies of VFTO (factor K_1)
- Maximum amplitude of VFTO (factor K_2)
- Maximum amplitude of VFTC (factor K_3)
- Rate of rise of VFTO (factor K_4)

Four different indices are defined to be considered as criteria:

$$K_1 = \frac{V_{res}}{V_{0res}} \quad (4.12)$$

V_{res} : Voltage amplitude at resonance frequency of transformer

V_{0res} : Voltage amplitude at resonance frequency of transformer at original case

$$K_2 = \frac{V_{max}}{V_{0max}} \quad (4.13)$$

V_{max} : Maximum VFTO amplitude

V_{0max} : Maximum VFTO amplitude at original case = 1.92 p.u.

$$K_3 = \frac{I_{max}}{I_{0max}} \quad (4.14)$$

V_{max} : Maximum VFTC amplitude

V_{0max} : Maximum VFTC amplitude at original case = 7.06 kA

$$K_4 = \frac{ROR_{max}}{ROR_{0max}} \quad (4.15)$$

V_{max} : Maximum Rate of Rise of VFTO waveform

V_{0max} : Maximum Rate of Rise of VFTO waveform at original case = 3.99 p.u./ μ s

Putting aside the first criterion as the most important factor which must be met in suppressor design, the maximum amplitude of VFTO, and its rate of rise, represent two phenomena which could damage the insulation of equipment connected to GIS, especially in extra high voltage levels in which maximum amplitude of VFTO gets closer to BIL [12]. In contrary to fast front transient and slow front transient, there is no standard waveform for very fast front transient specified by IEC or IEEE [9], as shown in Fig. 4. 14, maximum rate of rise in present work is defined as the ratio of VFTO peak (V_{max}) to time-to-crest of VFTO (T_f) [69].

VFTO is always associated with VFTC that can induce harmful transients in the secondary equipment of substation such as protection relays, control cables and low voltage instruments. Simulation results revealed that attenuating VFTO amplitude is accompanied with increasing VFTC amplitude at transformer terminal which may be harmful to the control and instrumental devices connected to the transformer, therefore in suppressor selection procedure, a suppressor with least magnification of VFTC maximum amplitude must be selected.

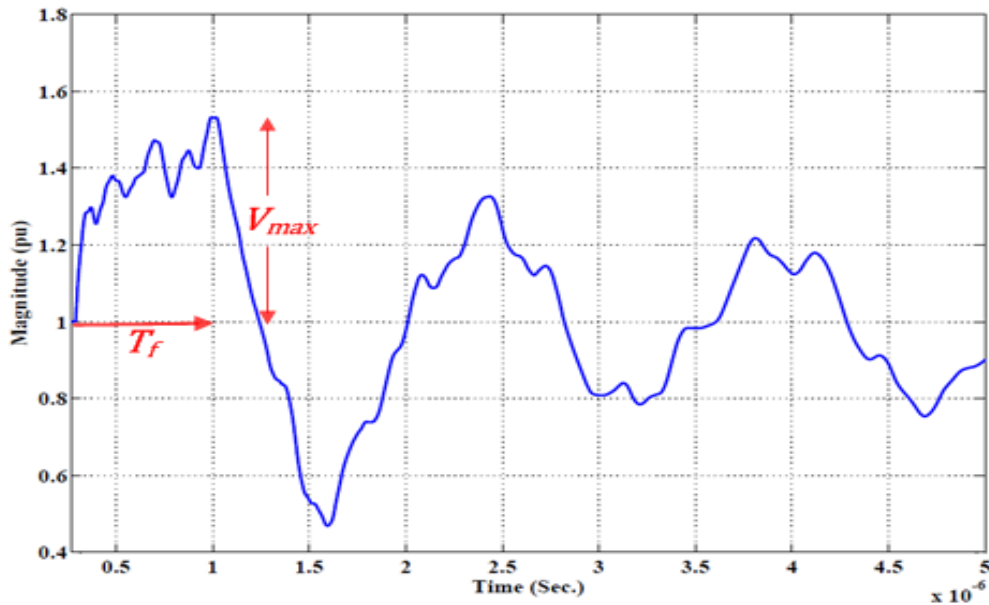


Fig. 4. 14 Maximum rate of rise of VFTO

4.3 Investigation Procedure for Selection of Surge Suppressor

On the first step, an acceptable range for capacitor size has to be determined. According to Fig. 4. 16, the capacitor required to be installed at the terminal of power transformer has to be formed by some capacitor units connected in series and parallel. There are several capacitor sizes available to be installed in a capacitor bank such as 7.2 kV, 12 kV, 24 kV and 36 kV [70]. As described below, if the capacitor units with lower voltage level are selected, the number of required units and also installation detail change, however the procedure for selecting the capacitor unit is the same for all voltage levels and doesn't influence this study. For this study, 24 kV capacitor units with capacitance of 0.1 μF are considered [70]. Dimensional drawings of capacitor unit presented by Vishay is shown in Fig. 4. 15. For the purpose of using 24kV capacitor units in 400kV power system, two requirements regarding insulation coordination must be met:

1. Maximum continuous voltage of each branch must be greater than the highest system voltage. Highest system voltage in this study is 420 kV and rated voltage of selected capacitor unit is 24kV. Therefore each branch must have at least 18 units. ($420 \text{ kV} / 24 \text{ kV} = 17.5 \rightarrow m \geq 18$)
2. Lightning Impulse Withstand Voltage (LIWL) of each branch of capacitor units must be greater than BIL of network. LIWL of each selected unit is 125 kV and BIL=1300 kV, Therefore each branch must have at least 11 units. ($1300 \text{ kV} / 125 \text{ kV} = 10.4$)

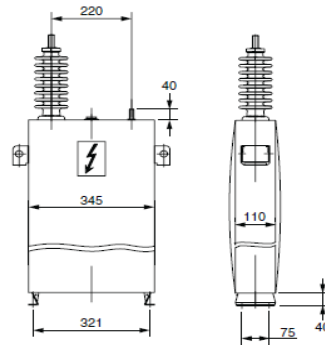


Fig. 4. 15 24 kV capacitor unit

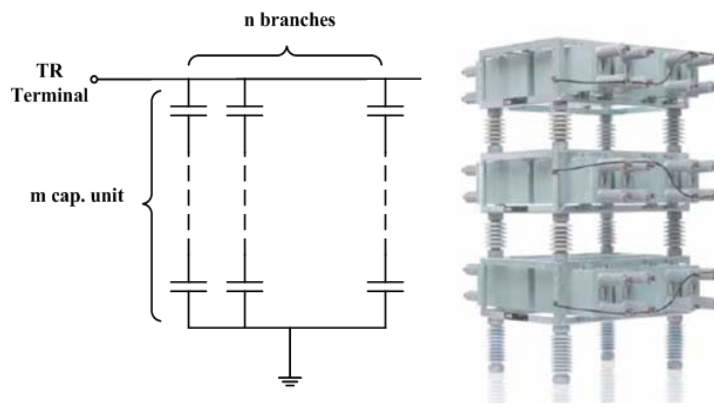


Fig. 4. 16 Arrangement of capacitor unit in a capacitor bank

Therefore, the minimum number of units in each branch is considered to be 18 and the capacitance of each branch is $0.1\mu\text{F} / 18 = 5.56\text{ nF}$. The minimum capacitor value of surge suppressor corresponds to the case with the maximum number of units all connected in series, regarding mechanical strength of the required structure for installing the capacitor bank. At most ten racks are considered to be installed in one capacitor bank, which can withstand eight capacitor units mounted on each rack (based on ABB catalogue for capacitor banks [71]). Several equivalent capacitances can be obtained by connecting the capacitor units in different arrangements with minimum value of 1.39 nF corresponding to the case with 72 units (4 parallel branches of 18 series connected). Also, the maximum capacitor value of surge suppressor corresponds to the case with all four branches connected in parallel which result in $4 \times 5.56\text{nF} = 22.24\text{nF}$. It is obvious that other equivalent capacitances can be obtained by selecting any integer number of capacitor units more than 18 to be connected in series, but for investigating the performance of suppressors, the capacitance values specified in Table 4. 2 are technically sufficient in this study. Therefore in this table, each branch is considered as 18 units connected in series. According to this table, available capacitances are: 1.39, 1.85, 2.78, 3.70, 4.17, 5.56, 7.41, 8.33, 11.11, 16.67 and 22.22 nF.



Fig. 4. 17 420 kV capacitor installation in Norway supplied by ABB [71]

Table 4. 2 Equivalent capacitance of different arrangement of capacitor units

Combinations	Total number of units	$C_{eq.}(nF)$
1 branch	18	5.56
2 branches connected in series	36	2.78
2 branches connected in parallel	36	11.11
3 branches connected in series	54	1.85
3 branches connected in parallel	54	16.67
2 parallel branches connected in series with 1 branch	54	3.70
2 parallel branches connected in parallel with 1 branch	54	8.33
4 branches connected in series	72	1.39
4 branches connected in parallel	72	22.22
3 parallel branches connected in series with 1 branch	72	4.17
3 parallel branches connected in parallel with 1 branch	72	7.41
2 parallel branches connected in series with 2 branch	72	5.56

The main undesired consequence of connecting a capacitor in parallel with the power network is the overcompensation resulting from injected reactive power at power frequency. In this study, injected reactive power at the case with maximum C size is $Q = \frac{V^2}{X_C} = 1.15$ MVAR. Since the apparent power of transmission line connected to the GIS in this study is about 600MW, injected reactive power is about 0.2% of the line capacity which can be neglected. Thus available capacitor values for possible arrangements are specified in Table 4. 2 Equivalent capacitance of different arrangement of capacitor units. The resistance of the 1st order suppressor can be any value, and components of 2nd order suppressor can be specified according to the procedure described in the previous section. For this purpose, at each capacitor size, resistor and inductor are tuned to provide minimum impedance at a particular frequency with desired tuning sharpness (m). Given the C value, different values are considered for m then R and L are calculated for each m and C . At next step, all four indices K_1 , K_2 , K_3 and K_4 are calculated for each case. K_1 is the key factor to design the surge suppressor. Its value must be less than the minimum suppression level, which is required to reduce the amplitude of VFTO high risk frequency to maximum permissible amplitude. In the case of 1st order suppressor, resistance values are selected to be in the range of calculated range for 2nd and 3rd suppressors for better comparison. The 2nd and 3rd suppressors are compared in two situations aimed to suppress 0.87 MHz and 2.88 MHz as dominant frequencies, and the high risk frequency of VFTO respectively. Therefore, five different groups of cases are defined as introduced in Table 4. 3.

Table 4. 3 Investigated cases

Group	Description	Number of cases
G1	First order suppressor	55
G2	Second order suppressor tuned at 0.87 MHz	55
G3	Second order suppressor tuned at 2.88 MHz	55
G4	Third order suppressor tuned at 0.87 MHz	55
G5	Third order suppressor tuned at 2.88 MHz	9

At final stage, all cases of five different groups are compared. Regarding five different R values for each of eleven capacitor sizes, each group consists of 55 different cases. Since calculated values for R and L in group 5 are practically not applicable, 9 cases are investigated in this group, thus 229 different cases must be investigated in total. The procedure required for selecting the best suppressor is illustrated in the flowchart shown in Fig. 4. 18 that is explained in the following steps:

Step 1- Define the minimum and maximum values of capacitor size

Step 2- Select one group to be investigated

Step 3- Select min C size to start

Step 4- Determine the size of suppressor components. If it is 1st order suppressor, we can choose any resistance values and for 2nd order or 3rd order, we can calculate R and L values based on selected C and m .

Step 5- Compare K_I with the maximum permissible value. If yes, go to step 6. If not, change the values of R or C and go to step 4 as another case. In analysing each group, different R values are first investigated for each C size. Then C value is increased if all R values are investigated.

Step 6- Other indices have to be calculated

Step 7- Check whether maximum capacitor size has been reached or not. If not, increase the capacitor size and go to step 4. If yes, go to step 7.

Step 8- Check whether any other arrangements have to be investigated or not. If yes, go to step 2 and if not, go to step 9.

Step 9- Sort all cases according to calculated indices for comparing the performance of suppressors.

Step 10- Analyse the surge suppressors in terms of their loss at power frequency and cost and eliminate the cases which have similar performance to other existing cases but are more expensive or lossy.

Step 11- Select the best case regarding index evaluation results.

4.4 Procedure Results

All 229 cases were run in EMTP and the results of simulations and calculated K_1 - K_4 are presented in Table 4. 4. Results of obtained values for K_1 in groups 1-4 is shown in Fig. 4. 19. There is a dashed line indicating the minimum required suppression factor. It is clear that all cases above this dashed line must be eliminated. All cases in groups 3 and 5 located below the line means that surge suppressors designed to be tuned at high risk frequency meet the minimum requirement for suppressing internal resonance of transformer. Fig. 4. 20 to Fig. 4. 23 show calculated K_1 - K_4 for the remaining 157 cases. Fig. 4. 20 shows that suppressors tuned at 2.88 MHz are more suitable for reducing the amplitude of high risk frequencies. In all five groups, K_1 decreases gradually by increasing C size and 2nd order suppressor tuned at 2.88 MHz has the best performance in suppressing the high risk frequency of VFTO and suppressors tuned at 0.87 MHz have the worst performance.

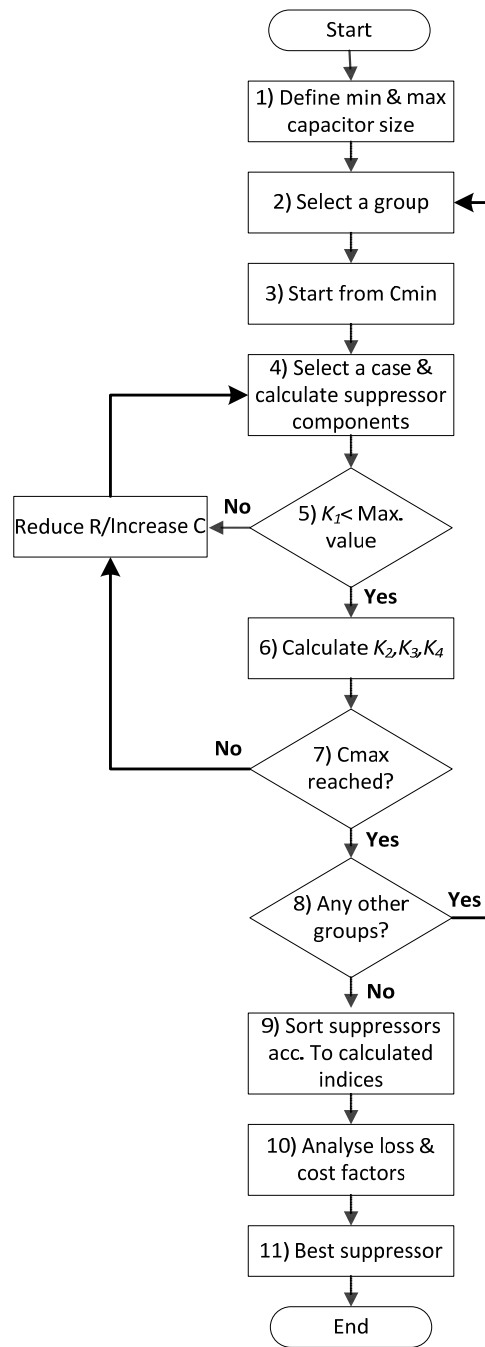


Fig. 4. 18 Algorithm for selecting the best surge suppressor

Table 4. 4 Results of simulation for all cases

1st order Suppressor																				
C (nF)	1.39					1.85					2.78					3.70				
R (Ω)	397.6	174.9	127.2	89.5	49.7	298.7	131.4	95.6	67.2	37.3	198.8	87.5	63.6	44.7	24.8	149.4	65.7	47.8	33.6	18.7
K1	0.83	0.75	0.71	0.67	0.63	0.80	0.71	0.66	0.60	0.62	0.75	0.62	0.58	0.58	0.57	0.71	0.57	0.55	0.54	0.51
K2	0.92	0.88	0.88	0.89	0.93	0.90	0.85	0.87	0.89	0.93	0.85	0.84	0.86	0.89	0.93	0.82	0.83	0.85	0.87	0.91
K3	1.06	1.11	1.13	1.16	1.20	1.07	1.14	1.16	1.20	1.25	1.11	1.19	1.22	1.27	1.33	1.14	1.24	1.28	1.32	1.39
K4	0.92	0.83	0.70	0.71	0.67	0.89	0.80	0.62	0.64	0.65	0.85	0.58	0.60	0.62	0.64	0.81	0.57	0.59	0.60	0.61
C (nF)	4.17					5.56					7.41					8.33				
R (Ω)	132.5	58.3	42.4	29.8	16.6	99.4	43.7	31.8	22.4	12.4	74.6	32.8	23.9	16.8	9.3	66.3	29.2	21.2	14.9	8.3
K1	0.69	0.56	0.54	0.52	0.48	0.63	0.53	0.50	0.46	0.46	0.57	0.49	0.46	0.45	0.46	0.55	0.47	0.45	0.45	0.45
K2	0.80	0.82	0.84	0.86	0.90	0.77	0.80	0.81	0.85	0.90	0.75	0.78	0.82	0.86	0.91	0.74	0.79	0.83	0.87	0.92
K3	1.15	1.26	1.30	1.35	1.42	1.19	1.32	1.36	1.41	1.49	1.24	1.38	1.43	1.48	1.55	1.26	1.40	1.46	1.51	1.58
K4	0.75	0.57	0.58	0.58	0.60	0.54	0.55	0.54	0.47	0.50	0.52	0.38	0.40	0.42	0.44	0.51	0.38	0.40	0.42	0.43
C (nF)	11.11					16.67					22.22									
R (Ω)	49.7	21.9	15.9	11.2	6.2	33.2	14.6	10.6	7.5	4.1	24.9	10.9	8.0	5.6	3.1					
K1	0.53	0.45	0.44	0.44	0.42	0.48	0.44	0.43	0.41	0.38	0.45	0.42	0.41	0.39	0.35					
K2	0.70	0.80	0.83	0.86	0.90	0.71	0.79	0.83	0.87	0.92	0.70	0.81	0.84	0.87	0.91					
K3	1.32	1.47	1.52	1.57	1.64	1.41	1.57	1.68	1.79	1.92	1.48	1.81	1.92	2.04	2.20					
K4	0.49	0.38	0.39	0.40	0.42	0.33	0.28	0.29	0.30	0.32	0.25	0.28	0.29	0.30	0.28					

2nd Order Suppressor (f=0.87 MHz)																				
C (nF)	1.39					1.85					2.78					3.70				
R (Ω)	1316.1	579.1	421.2	296.1	164.5	988.9	435.1	316.4	222.5	123.6	658.1	289.5	210.6	148.1	82.3	494.4	217.6	158.2	111.2	61.8
K1	0.95	0.84	0.79	0.75	0.69	0.92	0.80	0.74	0.71	0.65	0.84	0.71	0.66	0.63	0.56	0.78	0.64	0.61	0.57	0.52
K2	0.79	0.78	0.79	0.80	0.84	0.88	0.82	0.78	0.80	0.84	0.97	0.91	0.87	0.84	0.83	1.00	0.95	0.92	0.89	0.84
K3	1.08	1.10	1.11	1.12	1.14	1.11	1.13	1.14	1.15	1.18	1.16	1.18	1.19	1.21	1.25	1.20	1.23	1.24	1.26	1.30
K4	0.37	0.78	0.79	0.55	0.59	0.41	0.38	0.37	0.55	0.59	0.46	0.44	0.42	0.41	0.57	0.48	0.46	0.44	0.43	0.41
C (nF)	4.17					5.56					7.41					8.33				
R (Ω)	438.7	193.0	140.4	98.7	54.8	329.0	144.8	105.3	74.0	41.1	246.9	108.6	79.0	55.5	30.9	219.6	96.6	70.3	49.4	27.5
K1	0.74	0.61	0.58	0.54	0.50	0.68	0.57	0.55	0.51	0.47	0.60	0.52	0.49	0.48	0.45	0.51	0.45	0.45	0.44	0.44
K2	1.00	0.96	0.93	0.90	0.86	0.98	0.96	0.94	0.92	0.89	0.94	0.93	0.92	0.92	0.90	0.95	0.92	0.91	0.90	0.89
K3	1.22	1.25	1.26	1.29	1.33	1.28	1.31	1.32	1.35	1.39	1.34	1.38	1.39	1.41	1.46	1.38	1.40	1.42	1.44	1.49
K4	0.48	0.46	0.45	0.44	0.42	0.47	0.46	0.44	0.44	0.43	0.44	0.44	0.44	0.43	0.42	0.33	0.43	0.43	0.43	0.42
C (nF)	11.11					16.67					22.22									
R (Ω)	164.7	72.5	52.7	37.0	20.6	109.7	48.3	35.1	24.7	13.7	82.3	36.2	26.3	18.5	10.3					
K1	0.47	0.44	0.44	0.44	0.43	0.50	0.48	0.47	0.45	0.43	0.47	0.44	0.41	0.40	0.39					
K2	0.99	0.97	0.95	0.94	0.91	0.97	0.96	0.95	0.94	0.93	0.98	0.97	0.96	0.95	0.94					
K3	1.57	1.59	1.58	1.58	1.58	1.96	1.93	1.92	1.91	1.91	2.25	2.24	2.23	2.23	2.22					
K4	0.35	0.34	0.33	0.33	0.32	0.34	0.33	0.33	0.33	0.32	0.28	0.27	0.27	0.27	0.26					

2nd Order (f=2.88MHz)																				
C (nF)	1.39					1.85					2.78					3.70				
R (Ω)	397.6	174.9	127.2	89.5	49.7	298.7	131.4	95.6	67.2	37.3	198.8	87.5	63.6	44.7	24.8	149.4	65.7	47.8	33.6	18.7
K1	0.36	0.44	0.45	0.47	0.52	0.33	0.42	0.44	0.46	0.49	0.29	0.37	0.40	0.44	0.49	0.26	0.34	0.37	0.41	0.46
K2	0.99	0.99	0.99	0.99	0.99	1.00	1.00	1.00	1.00	1.00	0.99	0.99	0.99	0.99	0.99	1.01	1.00	1.00	0.99	0.98
K3	1.25	1.25	1.25	1.25	1.25	1.30	1.30	1.30	1.30	1.31	1.37	1.38	1.38	1.39	1.40	1.42	1.44	1.44	1.45	1.47
K4	0.69	0.71	0.71	0.71	0.71	0.70	0.70	0.70	0.70	0.69	0.68	0.68	0.68	0.66	0.66	0.58	0.57	0.57	0.57	0.56
C (nF)	4.17					5.56					7.41					8.33				
R (Ω)	132.5	58.3	42.4	29.8	16.6	99.4	43.7	31.8	22.4	12.4	74.6	32.8	23.9	16.8	9.3	66.3	29.2	21.2	14.9	8.3
K1	0.24	0.31	0.34	0.38	0.44	0.17	0.23	0.26	0.30	0.37	0.19	0.23	0.26	0.29	0.36	0.16	0.20	0.23	0.26	0.32
K2	1.01	1.01	1.00	1.00	0.99	1.00	0.99	0.99	0.99	0.99	1.00	1.00	1.00	1.00	0.99	0.99	0.99	0.99	0.99	0.99
K3	1.44	1.46	1.47	1.48	1.50	1.50	1.53	1.53	1.55	1.56	1.57	1.59	1.60	1.61	1.63	1.60	1.62	1.63	1.64	1.65
K4	0.58	0.57	0.57	0.57	0.56	0.57	0.48	0.48	0.48	0.48	0.49	0.49	0.48	0.48	0.47	0.47	0.47	0.47	0.47	0.46
C (nF)	11.11					16.67					22.22									
R (Ω)	49.7	21.9	15.9	11.2	6.2	33.2	14.6	10.6	7.5	4.1	24.9	10.9	8.0	5.6	3.1					
K1	0.19	0.22	0.25	0.27	0.32	0.15	0.17	0.19	0.20	0.24	0.20	0.21	0.22	0.23	0.26					
K2	0.98	0.98	0.98	0.98	0.98	0.99	0.99	0.99	0.99	0.99	0.99	0.99	0.99	0.98	0.98					
K3	1.74	1.73	1.73	1.73	1.73	2.07	2.08	2.08	2.08	2.08	2.35	2.36	2.36	2.37	2.38					
K4	0.42	0.41	0.38	0.38	0.38	0.35	0.35	0.34	0.34	0.34	0.29	0.28	0.28	0.28	0.28					

3rd Order (f=0.87MHz)																				
C (nF)	1.39					1.85					2.78					3.70				
R (Ω)	65.8	46.1	40.8	32.9	29.0	49.4	34.6	30.7	24.7	21.8	32.9	23.0	20.4	16.5	14.5	24.7	17.3	15.3	12.4	10.9
K1	0.71	0.75	0.78	0.82	0.84	0.64	0.68	0.69	0.73	0.75	0.61	0.65	0.67	0.70	0.72	0.56	0.62	0.64	0.69	0.71
K2	0.86	0.86	0.85	0.85	0.85	0.86	0.85	0.85	0.84	0.84	0.85	0.84	0.84	0.82	0.83	0.89	0.88	0.89	0.87	0.88
K3	1.17	1.18	1.18	1.18	1.19	1.22	1.23	1.23	1.23	1.24	1.30	1.31	1.31	1.31	1.32	1.35	1.37	1.37	1.38	1.38
K4	0.60	0.60	0.61	0.68	0.68	0.59	0.59	0.59	0.59	0.59	0.56	0.56	0.56	0.57	0.55	0.43	0.42	0.42	0.41	0.41
C (nF)	4.17					5.56					7.41					8.33				
R (Ω)	21.9	15.4	13.6	11.0	9.7	16.5	11.5	10.2	8.2	7.2	12.3	8.6	7.7	6.2	5.4	11.0	7.7	6.8	5.5	4.8
K1	0.53	0.58	0.61	0.65	0.68	0.48	0.52	0.55	0.58	0.61	0.45	0.47	0.47	0.48	0.49	0.50	0.52	0.53	0.55	0.55
K2	0.91	0.91	0.91	0.90	0.90	0.95	0.95	0.95	0.94	0.94	0.95	0.95	0.95	0.95	0.95	0.94	0.94	0.95	0.95	0.95
K3	1.38	1.39	1.40	1.40	1.41	1.45	1.46	1.47	1.47	1.48	1.51	1.53	1.53	1.54	1.54	1.54	1.56	1.56	1.56	1.57
K4	0.44	0.43	0.43	0.42	0.43	0.45	0.44	0.45	0.44	0.44	0.45	0.45	0.45	0.44	0.44	0.44	0.44	0.40	0.40	0.40
C (nF)	11.11					16.67					22.2									
R (Ω)	8.2	5.8	5.1	4.1	3.6	5.5	3.8	3.4	2.7	2.4	4.1	2.88	2.55	2.06	1.81					
K1	0.41	0.43	0.44	0.45	0.47	0.38	0.41	0.41	0.43	0.44	0.46	0.47	0.47	0.49	0.49					
K2	0.95	0.96	0.96	0.96	0.96	0.97	0.97	0.97	0.97	0.97	0.97	0.97	0.97	0.96	0.96					
K3	1.67	1.67	1.67	1.67	1.67	2.00	2.00	2.01	2.01	2.02	2.33	2.34	2.35	2.35	2.35					
K4	0.33	0.33	0.36	0.36	0.36	0.33	0.33	0.33	0.33	0.33	0.27	0.27	0.27	0.27	0.27					

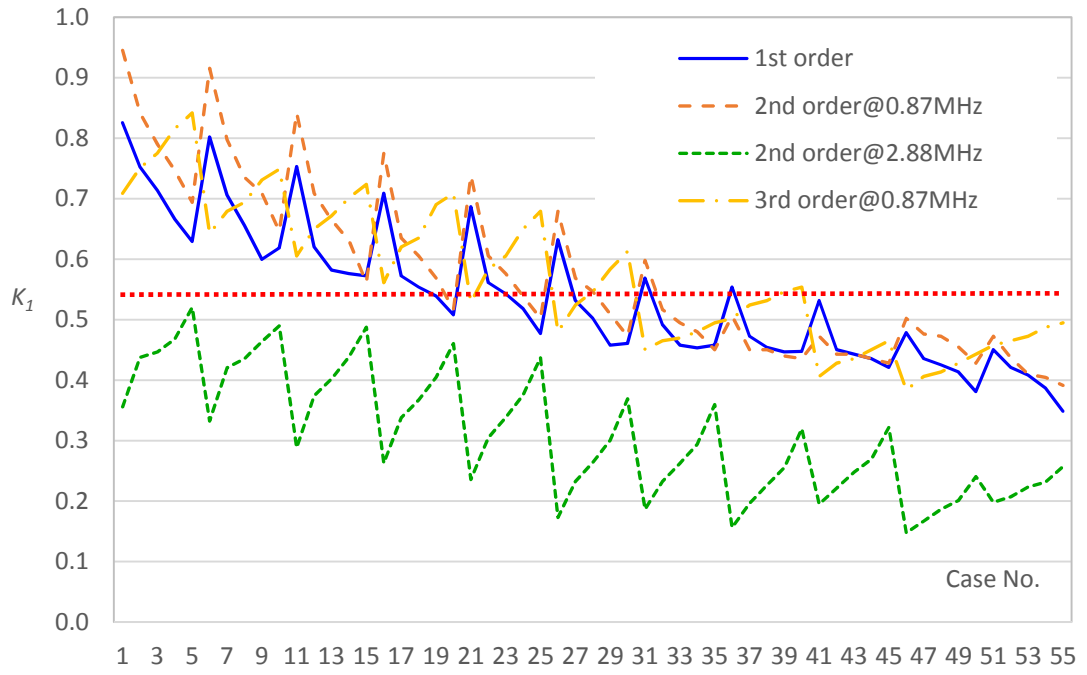


Fig. 4. 19 K_1 calculated for all cases in groups 1-4

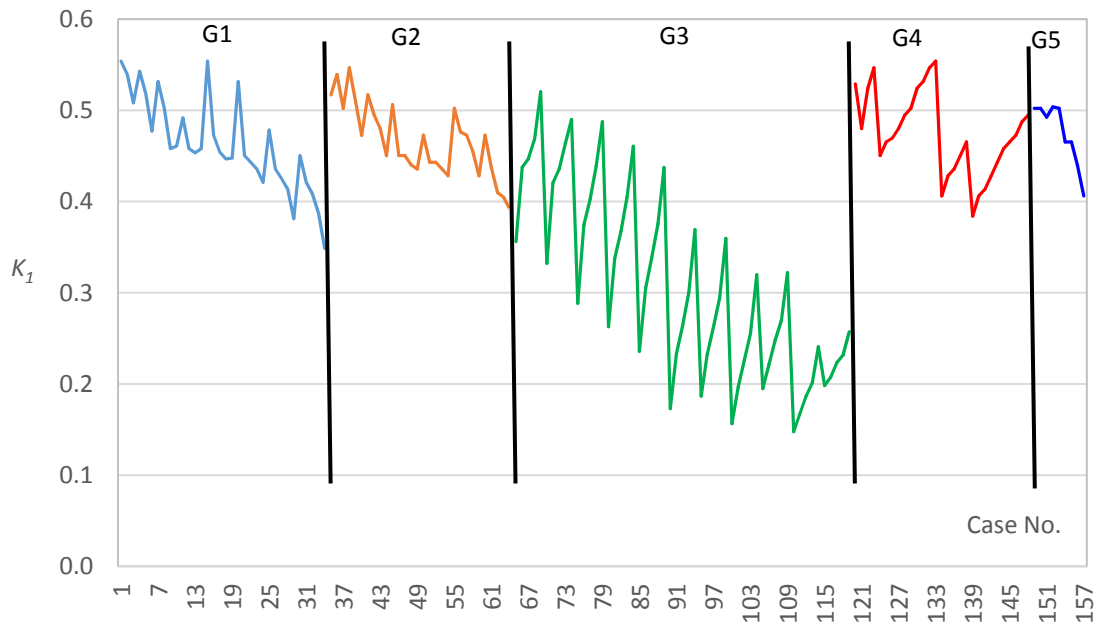


Fig. 4. 20 K_1 calculated for all remaining cases

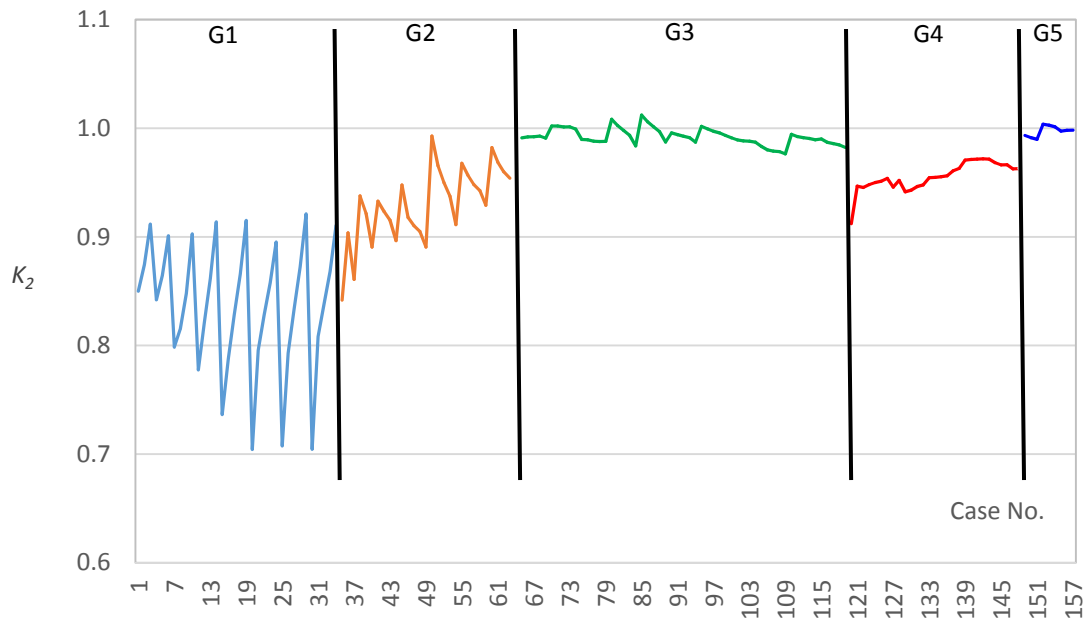


Fig. 4. 21 K_2 calculated for all remaining cases

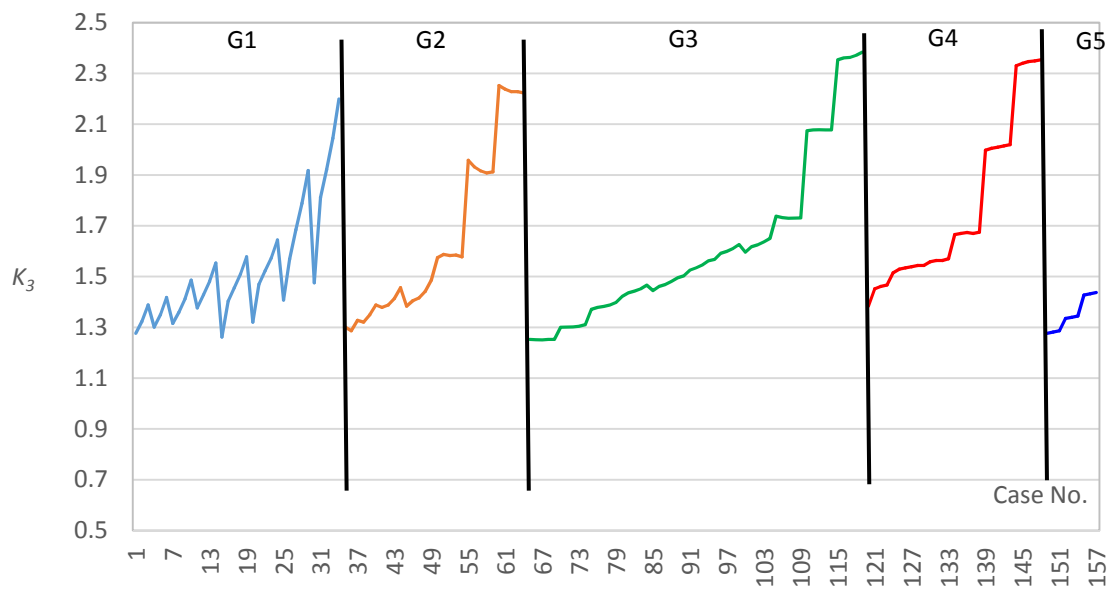


Fig. 4. 22 K_3 calculated for all remaining cases

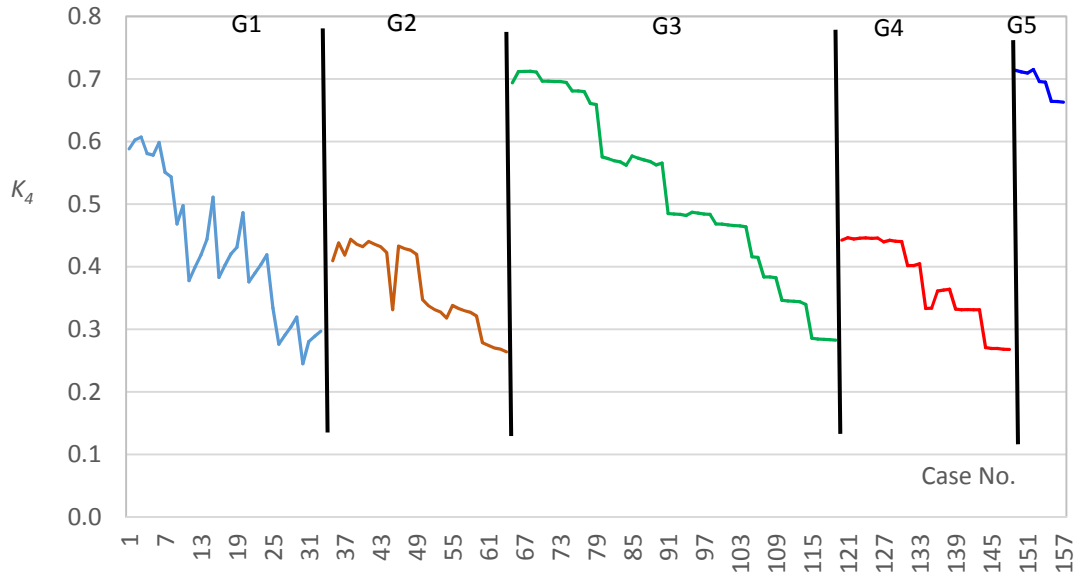


Fig. 4. 23 K_4 calculated for all remaining cases

As shown in Fig. 4. 21, the maximum amplitude of the VFTO doesn't experience a significant change in cases with suppressors tuned at 2.88MHz because the VFTO high frequency components around 2.88 MHz have small amplitudes in comparison with suppressors tuned at 0.87 MHz which can suppress VFTO peak voltage to 0.93-95%, while 1st order suppressors have the best performance by suppressing the VFTO peak voltage to about 84% as the average value. Fig. 4. 22 shows that maximum amplitude of VFTC increases by increasing the C size. In all groups, the VFTC peak value increases from about 1.5 p.u. to a value less than 2.5 at larger capacitors, therefore although increasing the capacitance has suppressing effects on some parameters such as peak values and steepness of VFTO, it is accompanied by the magnification of very fast transient currents at power transformer. Fig. 4. 23 shows the suppressing effect of increasing C size on front steepness of VFTO surge in each group. The Rate of Rise of VFTO can be suppressed to about 25% of its original value by adding a surge suppressor at the terminal of transformer. In this regard, suppressors tuned at 0.87 MHz have smaller average values of suppression factor; however the cases in group 1 with larger C have the smaller absolute values and more appropriate in terms of suppressing steepness of VFTO waveform. Fig. 4. 24 illustrates the effect of first order suppressor on VFTO peak value and amplitude of dominant frequencies in VFTO. It can be seen that both parameters reach their minimum value at larger C sizes. In cases with constant C size, both K_1 and K_2 decrease with reducing R and in cases with constant R , K_1 and K_2 decrease with increasing C , however this decrease is more remarkable in case with smaller R value while there is no significant reduction at larger R .

Fig. 4. 25 illustrates the results of calculation for the case with first order suppressor and maximum C size ($R=25 \Omega$, $C=22.2 \text{ nF}$). Fig. 4. 25a shows that there is 30% suppression level in VFTO peak voltage (from 1.92 p.u. to 1.35 p.u.). According to Fig. 4. 25b, the amplitude of dominant frequency at about 2.88 MHz has a

reduction of about 50%. Also from Fig. 4. 25a it is concluded that VFTO front steepness in the case with suppressor is considerably less than original case without suppressor. The VFTO peak in original case reached to a peak value of 1.92 p.u. within 0.48 μ s, while in the case with suppressor, VFTO reaches its peak (1.35 p.u.) within 1.38 μ s. This means that voltage surge maximum steepness is reduced from 4 p.u./ μ s to 0.98 p.u./ μ s (about 75% suppression).

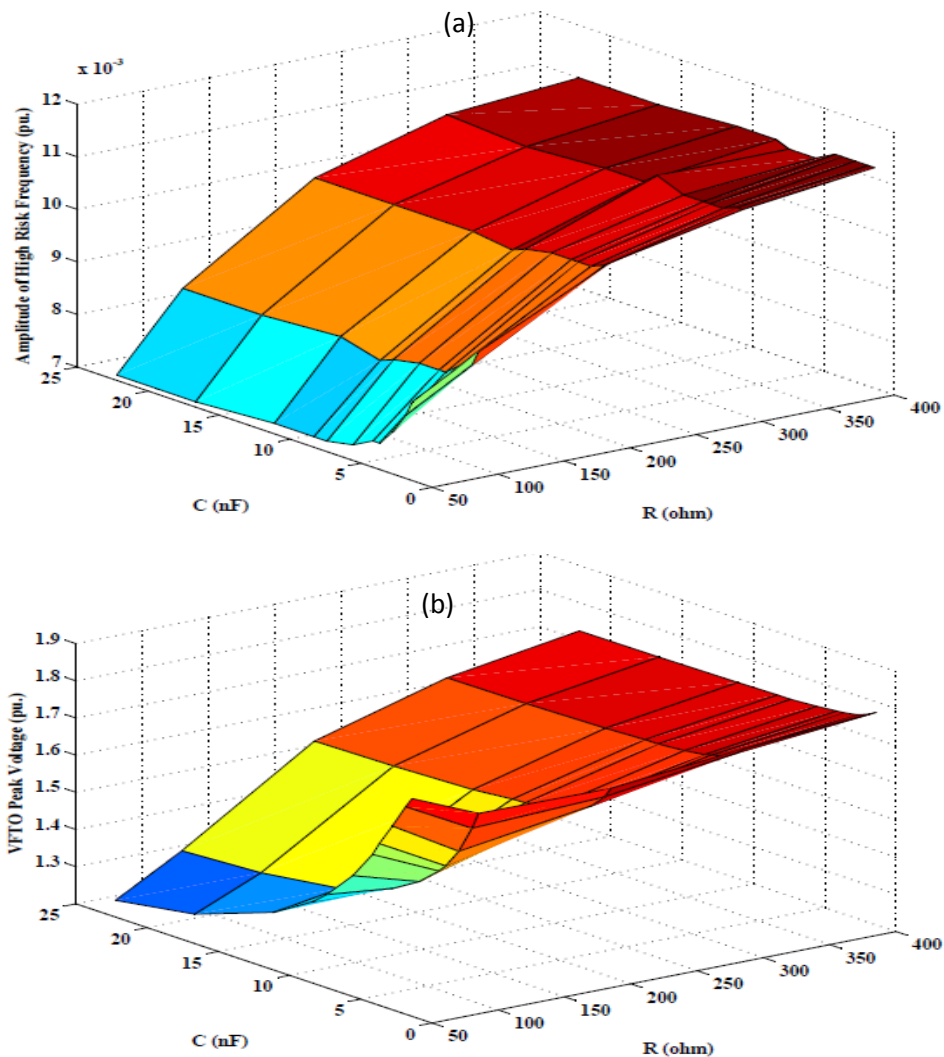


Fig. 4. 24 Effect of first order suppressor with different R & C values on: a) Maximum amplitude of VFTO b) Amplitude of high risk frequency

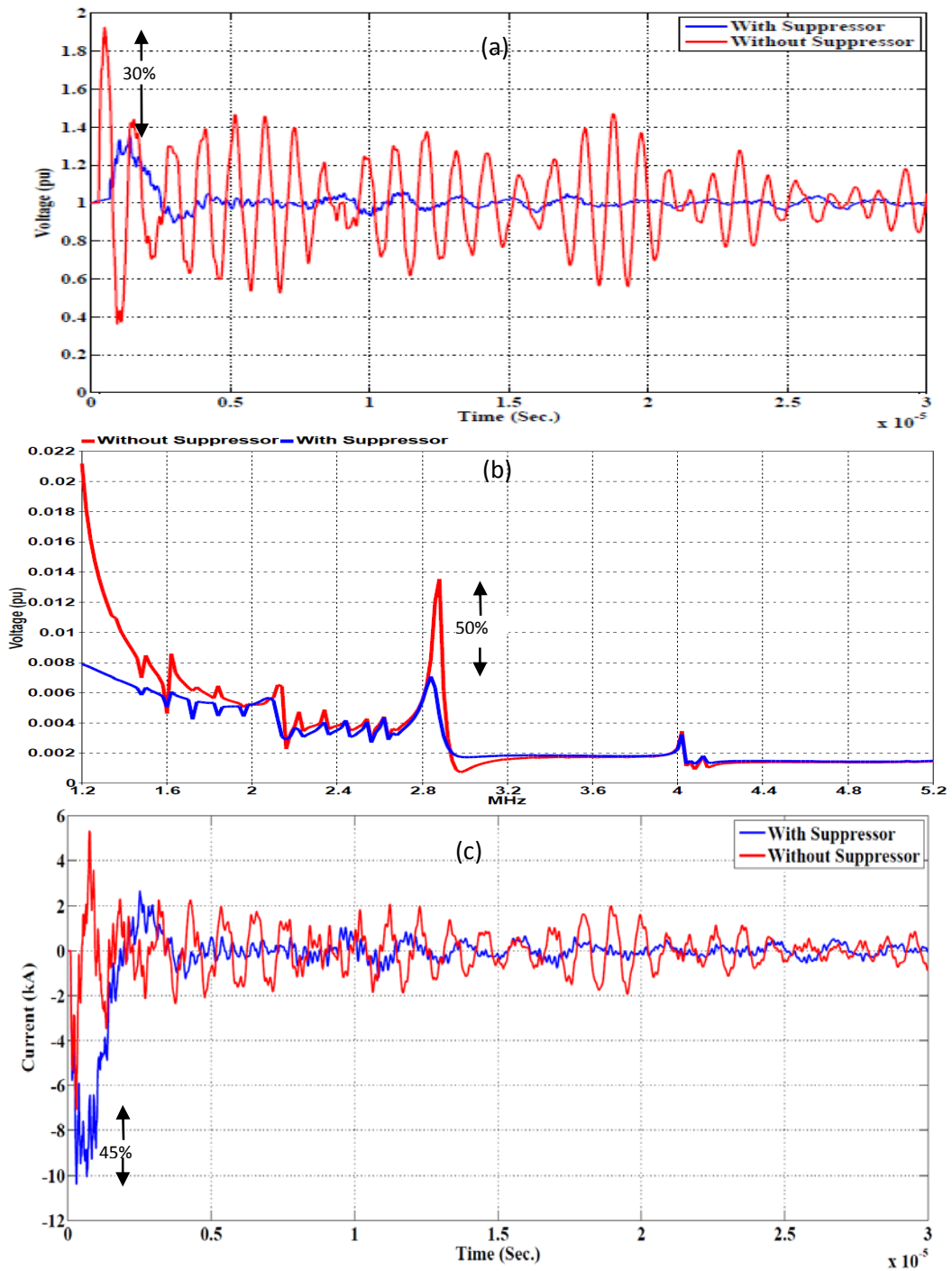


Fig. 4. 25 Suppression level with max C size on: a) Max amplitude of VFTO b) Amplitude of high risk frequency c) Max amplitude of VFTC

In order to find the best case among the 157 remaining cases, considering all introduced factors, a function which includes the performance of suppressors in suppressing VFTO high risk frequency, VFTO & VFTC peak values and VFTO maximum steepness is defined. Therefore the case with the best performance will have the minimum $K_t = K_1 + K_2 + K_3 + K_4$ which includes overall impact of all introduced factors. All indices are scaled from 0 to 1 to ease comparison procedure.

4.5 Cost analysis

For better comparison of all cases in terms of implementation cost, a cost index is present to quantify the estimated price. It has to be emphasized that for the purpose of comparing suppressors, it is enough to analyse the cases on their approximate price not the exact price. According to arrangement considered for surge suppressors, cost of each suppressor involves costs for capacitor bank, resistance and inductor values along with the costs for installation and Earthing Switch (ES) in cases with 2nd and 3rd order suppressors.

$$C = P_1 + P_2 + nP_3 \quad (4.16)$$

C: Total approximate cost

*P*₁: Fixed cost including insulation of capacitor bank, installation and resistor

*P*₂: Price of Earthing Switch in 2nd and 3rd order suppressors

*P*₃: Price of each capacitor unit

n: Number of capacitor units

It is worth mentioning that small value of inductance can be implemented in the form of bare aluminum conductors. Also the main costly component of resistor is its insulator rather than resistive element. Based on quotes received from some suppliers of high voltage post insulator such as PPC Insulators [72] and LAPP Insulators, each 400kV solid core post insulator is about A\$1200, and each 24 kV capacitor unit is about A\$500, therefore the approximate price of each capacitor arrangement can be obtained for comparing different arrangements. For third order suppressors, the cost of an additional capacitor bank must be included however the added capacitor can be considered with smallest size. Considering all above, a rough estimate of proposed surge suppressors can be obtained. For example, a typical 1st order surge suppressor with $C=4.17$ nF uses four sets of post insulators (costs $4 \times A\$1,200 = A\$4,800$), and 72 sets of capacitor units (costs $72 \times A\$500 = A\$36,000$), which results in total estimated cost of A\$41.8k. Fig. 4. 26 shows all the design cases sorted based on overall implementation cost. Price values are within the range A\$13k- A\$54k but normalized with respect to the highest cost to be visible and compared on the plot along with the value of K_i which is in the range of 0 to 1. All cases above case #80 with estimated price greater than A\$30k are eliminated because their basic price is more than half the maximum price and they are much more expensive than other cases without significant improvement except two cases; #91 and #95. Since all cheaper cases below #32 have acceptable performance, the optimum suppressor is selected among these cases. The optimum case is found to be #13 which has the minimum K_i . This case is corresponding to first order suppressor with $C=11.11$ nF and $R=50 \Omega$. In this case indices K_1, K_2, K_3, K_4 are 0.53, 0.70, 1.32, 0.48 respectively which means that the suppression level of VFTO high risk frequencies is 47%; magnitude of VFTO is 30% damped and surge steepness is almost half its original value while the magnitude of current is magnified by 32% which shall be accompanied by adopting careful measures for protecting control cables and low voltage equipment [18, 73].

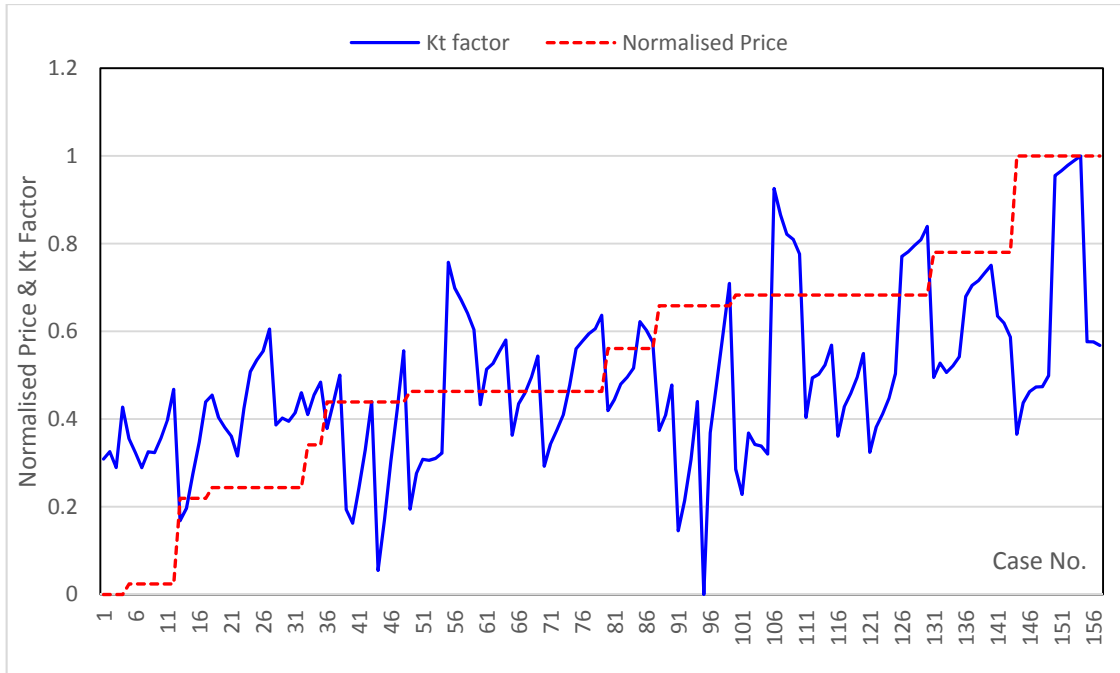


Fig. 4.26 Suppressors Kt factor in comparison with estimated price

4.6 Loss analysis

Since capacitive element is the dominant component in determining the impedance of all types of surge suppressors, those with lower values of C have higher impedance at fundamental frequency. The loss at fundamental frequency in first order suppressor is more than other types of RC surge suppressors because it has only one RC branch and all the current at fundamental frequency passes through R branch. By paralleling an inductance to R in second order suppressor, a low impedance branch is provided in parallel to R branch at fundamental frequency which makes the loss in second order less than first order. C_2 in series with R in third order suppressor makes impedance of R branch even higher than second order suppressor, therefore steady state loss in this case is less than both first and second order surge suppressors. It can be shown that if power frequency loss is a matter of extreme concern in network constraints, case #80 which is related to third order suppressor with $C=11.11\text{nF}$ & $R=10\ \Omega$ can be adopted. Despite the higher amount of loss in first order suppressors, small values of C in the range of few Nano Farads, this type of suppressor can still be used because power frequency loss is still fairly acceptable. It is obvious that there is relation between loss factor and price of surge suppressor. The lesser the loss at power frequency, the more expensive is the surge suppressor.

5 Comparison and Conclusion

5.1 Comparison with Existing Suppressing Methods

Despite all previous studies and experiments to address all aspects of VFTO suppression methods, they haven't documented the effectiveness of proposed suppression methods considering all parameters representing the VFTO severity as in this study. Resistor-Fitted Disconnectors are used in GIS for the purpose of accelerating the decay of very fast transients originating from the DS operation by paralleling a resistance to disconnector switch within the short duration of operation [74]. An appropriately designed resistor can absorb the transient energy produced by remaining charge on the main contact of DS. Reference [75] published test results applied to a 1100 kV gas insulated substation. According to the test results, if the resistance is 200 Ω , the VFTO maximum magnitude could be reduced from 2.88 p.u. to 1.5 p.u. By paralleling a 1 k Ω resistance, it could be suppressed to 1.25 p.u. equivalent to about 60% suppression. However, this method calls for some changes in construction of DS in GIS which makes it complicated and expensive, with low reliability [76].

Ferromagnetic Rings are mounted around GIS conductor to form a paralleled nonlinear resistance and inductance circuit connected in series with the main GIS conductor. It can increase the conductor equivalent inductance at high frequencies and suppress the VFTO effects. Several experimental researches verified suppressing effect of different magnetic rings. Reference [76] presents detailed description of experiment on two magnetic rings. It was concluded that VFTO magnitude could be reduced from 1.40 in case without ring to 1.22 in case with 20cm length ring and to 1.12 in case with 40 cm ring and VFTO steepness is reduced from 2.15 kV/ns in case without ring to 1.97kV/ns in case with 20cm length ring and to 1.56kV/ns in case with 40 cm ring. The major concern about the use of magnetic rings is that if they enter a condition of saturation, they don't have effect on VFT [77]. Results presented in [76] revealed that at higher voltage levels of performed test, magnetic rings have weaker suppressing effects due to magnetic saturation. High Frequency Resonator is an LC circuit mounted around GIS conductor and goes to resonance condition when its natural frequency matches with the dominant frequency of VFTO waveform [78]. L represents a cavity filled of SF₆ around GIS main conductor and C represents a SF₆ gap at the end of this cavity. Simulation and experimental study in [78] illustrated the ability of this method to reduce the energy of VFTO surge by about 27% and attenuating the dominant frequency by about 60%. While this method has good efficiency in damping high frequencies of VFTO, it can't damp the first peak of VFTO and also it is difficult to adjust the resonant frequencies by changing the dimensions of cavity and SF₆ gap [78].

Although several researches have investigated various techniques to mitigate the impact of VFT in gas insulated substations equipment, all of the proposed techniques involve a change in the design of GIS components and are difficult to implement or

very expensive approaches that mainly aimed at reducing the VFTO in all the GIS. These proposed approaches have to be considered at the design stage and implemented during manufacture stage of GIS. The method proposed in this study is a simple cost effective method which has no primary effect on the generated VFTO but it can suppress the VFTO on power transformer.

5.2 Conclusion

Based on an analytical formulation of VFTO waveform at the terminal of power transformer connected to GIS in a very simplified GIS-transformer arrangement, effect of shunt capacitance on suppressing dominant frequencies of VFTO surge was analysed. It was shown that suppressing these high frequencies of VFTO can avoid internal resonance of transformer resulted from coincidence of high risk frequencies with natural frequencies of transformer. Different topologies of RC surge suppressors were presented and the procedure for selecting best suppressor was performed according to a developed algorithm for assessing each suppressor in terms of defined performance and cost indices. It was found that first order suppressor with maximum C size and minimum R size can be an appropriate surge suppressor to suppress high risk frequencies of VFTO as well as VFTO peak voltage, front steepness however careful measures must be adopted to protect secondary equipment of substation against high amplitude VFTC. Other topologies can be used for situation with extreme concerns about loss at normal operation. In contrary with existing expensive VFTO mitigation techniques that call for the change in GIS design and construction, the proposed technique is easy to implement in any existing GIS without any change in the design at a very cost effective rate.

5.3 Future Work

Internal resonance of power transformer is an external effect of very fast transient overvoltage generated in GIS. Other effects of VFTO also can be investigated for future study in continuation of this work:

- 1) The malfunction of secondary equipment in GIS can be caused by voltages induced in these equipment generated by VFTO [18]. 3D simulation of real case GIS can be implemented to study the detailed distribution of the magnetic field around GIS and its effects on peripheral low voltage equipment such as cables, protection and measuring units.
- 2) GIS insulation aging can reduce the dielectric strength of SF₆ due to frequent operation of disconnecting switches and circuit breakers. According to section 3.1.4, changes in SF₆ dielectric characteristics can be reflected as minor shifts in VFTO dominant high frequency components. GIS asset management decisions based on monitoring the gas insulation condition by VFTO analysis can be concentrated in a separate study.

- 3) A part of VFTO arriving at SF₆-Air bushing is transmitted to GIS enclosure which is generally earthed. Occurrence of VFTO in GIS can result in very short time shocks to the personnel working in the station due to transient ground potential rise (TGPR). The impact of different earthing approaches to suppress this potential rise can be studied in another work.

References

- [1] CIGRE Working Group 33/13-09, "Very Fast Transient Phenomena Associated With Gas Insulated Substations," 1988.
- [2] IEC 60076-18, "Power Transformer, Part 18: Measurement of frequency response," ed, 2012.
- [3] Mehdi Babaei, Maziar Babaei, and M. Niasati, "Parametric Analysis of Over-voltages Caused by Back-flashover In Siah-bishe 400kV GIS Substation," presented at the 3rd International Conference on Electric Power and Energy Conversion Systems (EPECS 2013), Yildiz Technical University, Istanbul, Turkey, 2013.
- [4] "IEEE 100, The Authoritative Dictionary of IEEE Standards Term," Seventh ed: IEEE Express, 2000.
- [5] *ABB Switchgear Manual*, 12th ed.: ABB AG, 2012.
- [6] "Arrangement of GIS equipment," in *09D-A06-01-R5*, Hyosung, Ed., ed. South Korea, 2012.
- [7] H. P. S. Varga, "The Economics of GIS Application," in *Proceedings of International Symposium on Gas Insulated Substation: Technology and Practice*, Toronto, Canada, 1985.
- [8] *Power Engineering Guide: Transmission and Distribution*, 7th ed. Germany: SIEMENS, 2012.
- [9] "IEC 60071-4, Insulation Coordination," in *Part 4: Computational guide to insulation co-ordination and modelling of electrical networks*, ed: IEC, 2004.
- [10] "IEC 60071-1, Insulation Coordination," in *Part 1: Definitions, principles and rules*, ed: IEC, 2011.
- [11] J. A. Martinez, P. Chowdhuri, R. Iravani, A. Keri, and D. Povh, "Modeling and Analysis Guideline For Very Fast Transients," *IEEE Transactions on Power Delivery*, vol. 11, pp. 2028-2035, 1996.
- [12] "IEEE Std C37.122.1-1993: Guide for Gas-Insulated Substations," ed. NY: IEEE, 1994.
- [13] S. Singha and M. J. Thomas, "Toepler's Spark Law in a GIS with Compressed SF₆-N₂ Mixture," *IEEE Transactions on Dielectrics and Electrical Insulation*, vol. 10, p. 8, 2003.
- [14] S. Ogawa, E. Haginomori, S. Nishiwaki, T. Yoshida, and K. Terasaka, "Estimation of Restriking Transient Overvoltage on Disconnecting Switch for GIS," *IEEE Transactions on Power Systems*, vol. PWRD-1,, 1986.
- [15] S. A. Boggs, F. Y. Chu, and N. Fujimoto, "Disconnect Switch Induced Transients And Trapped Charge In Gas Insulated Substation," *IEEE Transactions on Power Apparatus and Systems*, vol. PAS-101, 1982.
- [16] J. D. McDonald, *Electric Power Substations Engineering*, 3rd ed.: CRC Press, 2012.
- [17] J. A. Martinez-Velasco, *Electric Power Engineering Handbook*, 2nd ed. NY: CRC Press, 2007.
- [18] M. M. Rao, M. J. Thomas, and B. P. Singh, "Transients Induced on Control Cables and Secondary Circuit of Instrument Transformers in a GIS During Switching Operations," *IEEE Transactions on Power Delivery*, vol. 22, pp. 1505-1513, 2007.

- [19] J. Meppelink, K. Diederich, K. Feser, and W. Pfaff, "Very Fast Transients in GIS," *IEEE Transaction on Power Delivery*, vol. 4, pp. 223-233, 1989.
- [20] M. J. T. M. Mohana Rao, and B. P. Singh, "Frequency Characteristics of Very Fast Transient Currents in a 245-kV GIS," *IEEE Transactions on Power Delivery*, vol. 20, pp. 2450-2457, 2005.
- [21] J. C. Das, *Transients in Electrical Systems: Analysis, Recognition, and Mitigation*, 1st ed.: McGrawHill, 2010.
- [22] J. D. Glover, M. S. Sarma, and T. J. Overbye, *Power System Analysis and Design*, Fifth ed.: Cengage Learning, 2011.
- [23] Y. Yang, Z. Wang, and C. Shao, "Determination of VFTO waveform in GIS according to simplified structure of GIS bus and circuit parameters," presented at the Power Systems Conference and Exposition, 2009. PSCE '09. IEEE/PES, Seattle, WA, 2009.
- [24] Y. Shibuya, S. Fujita, and T. Shimomura, "Effects of very fast transient overvoltages on transformer," *IEE Proceedings - Generation, Transmission and Distribution Transactions on Power Apparatus and Systems*, vol. 146, pp. 459 - 464 1999.
- [25] M. Szewczyk, W. Piasecki, M. Wroński, and K. Kutorasiński, "New Concept for VFTO Attenuation in GIS with Modified Disconnecter Contact System," *IEEE Transaction on Power Delivery*, vol. 30, pp. 2138-2145, 2015.
- [26] Y. Li, Y. Shang, L. Zhang, R. Shi, and W. Shi, "Analysis of Very Fast Transient Overvoltages (VFTO) from Onsite Measurements on 800 kV GIS," *IEEE Transactions on Dielectrics and Electrical Insulation*, vol. 19, pp. 2102-2110, 2012.
- [27] A. Tavakoli, A. Gholami, H. Nouri, and M. Negnevitsky, "Comparison Between Suppressing Approaches of Very Fast Transients in Gas-Insulated Substations (GIS)," *IEEE Transactions on Power Delivery*, vol. 28, pp. 303-310, 2013.
- [28] S. Haifeng, L. Guishu, Z. Xile, and C. Xiang, "Analysis of resonance in transformer windings under very fast transient overvoltages," in *2006 17th International Zurich Symposium on Electromagnetic Compatibility*, 2006, pp. 432-435.
- [29] A. Greenwood, *Electrical Transients in Power Systems*, 2nd ed.: Wiley 1991
- [30] Y. Shibuya, S. Fujita, and N. Hosokawa, "Analysis of very fast transient overvoltage in transformer winding," *IEE Proceedings - Generation, Transmission and Distribution Transactions on Power Apparatus and Systems*, vol. 144 pp. 461-468, 1997.
- [31] W. McNutt, T. Blalock, and R.A.Hinton, "Response of Transformer Windings to System Transient Voltages," *IEEE Transactions on Power Apparatus and Systems*, vol. PAS-93, , pp. 457-467, 1974.
- [32] N. Hashemnia, A. Abu-Siada, and S. Islam, "Improved power transformer winding fault detection using FRA diagnostics - part 1: axial displacement simulation," *IEEE Transactions on Dielectrics and Electrical Insulation*, vol. 22, pp. 556-563, 2015.
- [33] Y. S. Shigeto Fujita, and Masaru Ishii, "Influence of VFT on Shell-Type Transformer," *IEEE Transaction on Power Delivery*, vol. 22, pp. 217-222, 2007.
- [34] C.IGRE Working Group 33.02, "Guidelines for representation of networks elements when calculating transients," 1990.
- [35] P. Valsalal, S. Usa, and K. Udayakumar, "Modelling of metal oxide arrester for very fast transients," *IET Science, Measurement & Technology*, vol. 5, pp. 140-146, 2011.
- [36] P. Valsalal, S. Usa, and K. Udayakumar, "Response of metal oxide arrester in gas-insulated substation and methods to improve its dynamic characteristics," *IET Science, Measurement and Technology*, vol. 6, pp. 222-228, 2012.
- [37] J. G. Jie Chen, Aici Qiu, Kelun Li, Yan-Zhao Xie, Longyue Cui, Lei Wang, and Zhiqiang Chen, "Behavior Comparison of Metal Oxide Arrester Blocks When Excited by VFTO and Lightning," *IEEE Transactions on Electromagnetic Compability*, vol. 57, pp. 1608-1615, 2015.
- [38] A. Ardito, R. Iorio, G. Santagostino, and A. Porrino, "Accurate modeling of capacitively graded bushings for calculation of fast transient overvoltages in GIS," *IEEE Transactions on Power Delivery*, vol. 7, pp. 1316-1327, 1992.

- [39] A. M. Miri and Z. Stojkovic, "Transient Electromagnetic Phenomena in the Secondary Circuits of Voltage- and Current Transformers in GIS (Measurements and Calculations)," *IEEE Transaction on Power Delivery*, vol. 16, pp. 571-575, 2001.
- [40] J. Smajic, W. Halaus, J. Kostovic, and U. Riechert, "3D Full-Maxwell Simulations of Very Fast Transients in GIS," *IEEE Transactions on Magnetics*, vol. 47, pp. 1514-1517, 2011.
- [41] D. K. Cheng, *Field and Wave Electromagnetics*, 2nd ed.: Tsinghua University Press, 2006.
- [42] M. Szewczyk, K. Kutorasinski, M. Wronski, and M. Florkowski, "Full-Maxwell Simulations of Very Fast Transients in GIS: Case Study to Compare 3D and 2D-Axisymmetric Models of 1100 kV Test Set-Up," *IEEE Transactions on Power Delivery*, vol. PP, pp. 1-1, 2016.
- [43] "Ansoft Maxwell," vol. REV 6.0, ed. Canonsburg: ANSYS Inc, 2012.
- [44] R. Irawan, G. Scelsi, and G. Woolsey, "Continuous monitoring of SF₆ degradation in high voltage switchgear using Raman scattering," *IEEE Transactions on Dielectrics and Electrical Insulation*, vol. 12, pp. 815-820, 2005.
- [45] F. Y. Chu, "SF₆ Decomposition in Gas-Insulated Equipment," *IEEE Transactions on Electrical Insulation*, vol. EI-21, pp. 693-725, 1986.
- [46] L. Vial, A. M. Casanovas, J. Diaz, I. Coll, and J. Casanovas, "Decomposition of high-pressure (400 kPa) SF₆ and SF₆/N₂ (10:90) mixtures submitted to negative or 50 Hz ac corona discharges in the presence of water vapour and/or oxygen," *Journal of Physics D: Applied Physics*, vol. 34, p. 2037, 2001.
- [47] "IEEE Guide for Moisture Measurement and Control in SF₆ Gas-Insulated Equipment," *IEEE Std C37.122.5-2013 (Revision of IEEE Std 1125-1993)*, pp. 1-42, 2013.
- [48] "Specification of technical grade sulfur hexafluoride (SF₆) for use in electrical equipme," *IEC 60376*, pp. 1-23, 2005.
- [49] N. Hashemnia, A. Abu-Siada, and S. Islam, "Detection of power transformer bushing faults and oil degradation using frequency response analysis," *IEEE Transactions on Dielectrics and Electrical Insulation*, vol. 23, pp. 222-229, 2016.
- [50] E. J. Murphy and S. O. Morgan, "The dielectric properties of insulating materials, III alternating and direct current conductivity," *The Bell System Technical Journal*, vol. 18, pp. 502-537, 1939.
- [51] G. B. Gharehpetian, H. Mohseni, and K. Moller, "Hybrid modelling of inhomogeneous transformer winding for very fast transient overvoltage studies," *IEEE Transactions on Power Delivery*, vol. 13, pp. 157-163, 1998.
- [52] S. M. H. Hosseini, M. Vakilian, and G. B. Gharehpetian, "Comparison of Transformer Detailed Models for Fast and Very Fast Transient Studies," *IEEE Transactions on Power Delivery*, vol. 23, pp. 733-741, 2008.
- [53] A. Miki, T. Hosoya, and K. Okuyama, "A calculation method for impulse voltage distribution and transferred voltage in transformer windings," *IEEE Transactions on Power Apparatus and Systems*, vol. PAS-97 pp. 930-940, 1978.
- [54] H. S. Guishu Liang, Xile Zhang, and Xiang Cui, Senior Member, IEEE, "Modeling of Transformer Windings Under Very Fast Transient Overvoltages," *IEEE Transaction on Electromagnetic Compability*, vol. 48, pp. 621-627, November 2006 2006.
- [55] L. Rabins, "A New Approach to the Analysis of Impulse Voltages and Gradients in Transformer Windings," *Transactions of the American Institute of Electrical Engineers. Part III: Power Apparatus and Systems*, vol. 78, pp. 1784-1791, 1959.
- [56] J. L. Guardado and K. J. Cornick, "A computer model for calculating steep-fronted surge distribution in machine windings," *IEEE Transactions on Energy Conversion*, vol. 4, pp. 95-101, 1989.
- [57] Y. Shibuya, S. Fujita, and E. Tamaki, "Analysis of very fast transients in transformers," *IEE Proceedings - Generation, Transmission and Distribution Transactions on Power Apparatus and Systems*, vol. 148, pp. 377 - 383, 2001.

- [58] M. Popov, L. v. d. Sluis, G. C. Paap, and H. M. D. Herdt, "Computation of very fast transient overvoltages in transformer windings," *IEEE Transaction on Power Delivery*, vol. 18, pp. 1268–1274, 2003.
- [59] G. Liang, H. Sun, X. Zhang, and X. Cui, "Modeling of Transformer Windings Under Very Fast Transient Overvoltages," *IEEE Transactions on Electromagnetic Compatibility* vol. 48, pp. 621 - 627, 2006.
- [60] M. Popov, L. v. d. Sluis, R. P. Paul, and J. L. Roldan, "Analysis of Very Fast Transients in Layer-Type Transformer Windings," *IEEE Transactions on Power Delivery* vol. 22, pp. 238-247, 2007.
- [61] J. A. Martinez-Velasco, *Power System Transients-Parameter Determination*, Second ed.: CRC Press, 2010.
- [62] A. Shintemirov, W. H. Tang, and Q. H. Wu, "A Hybrid Winding Model of Disc-Type Power Transformers for Frequency Response Analysis," *IEEE Transactions on Power Delivery*, vol. 24, pp. 730 - 740 2009.
- [63] S. V. Kulkarni and S. A. Khaparde, *Transformer Engineering: Design and Practice*, Second ed. Boca Raton, FL: CRC Press, 2004.
- [64] Y. Wang, W. Chen, C. Wang, L. Du, and J. Hu, "A Hybrid Model of Transformer Windings for Very Fast Transient Analysis Based on Quasi-stationary Electromagnetic Fields," *Electric Power Components and Systems*, vol. 36, pp. 540-554, 2008/04/24 2008.
- [65] J. W. Arrillaga, N. R., *Power system harmonics* 2nd ed.. ed.: Hoboken, NJ : Wiley 2003.
- [66] J. C. Das, *Power System Harmonics and Passive Filter Designs*, 1st ed.: IEEE Press, John Wiley & Sons, Inc., 2015.
- [67] A. B. Nassif, W. Xu, and W. Freitas, "An Investigation on the Selection of Filter Topologies for Passive Filter Applications," *IEEE Transactions on Power Delivery*, vol. 24, pp. 1710-1718, 2009.
- [68] A. R. Hileman, *Insulation Coordination for Power Systems*. New York: CRC Press Taylor & Francis Group, 1999.
- [69] C. W. G. 33/13-09, "Disconnecter Operations in Gas Insulated Substations Overvoltages Studies and Tests Associated with 420kV Installation," 1988.
- [70] "Surge Suppressor Capacitors," in *Vishay Interactive Data Book*, ed. Germany: Vishay Electronic GmbH, 2008.
- [71] "Power Capacitors and Harmonic Filters Buyer's Guide," ABB, Ed., ed. Sweden: ABB, 2013.
- [72] "Solid Core Post Insulators," ed. Austria: PPC Insulators, 2016.
- [73] M. M. Rao, M. J. Thomas, and B. P. Singh, "Effect of Shielded Distribution Cable on Very Fast Transients," *IEEE Transactions on Power Delivery*, vol. 15, pp. 857-863, 2000.
- [74] J. Ozawa, T. Yamagiwa, M. Hosokawa, S. Takeuchi, and h. Kozawa, "Suppression of Fast Transient Overvoltage during Gas Disconnecter Switching in GIS," *IEEE Transactions on Power Delivery*, vol. 1, pp. 194-201, 1986.
- [75] Y. Yamagata, K. Tanaka, S. Nishiwaki, N. Takahashi, T. Kokumai, I. Miwa, *et al.*, "Suppression of VFT in 1100kV GIS By Adopting Resistor-fitted Disconnecter," *IEEE Transactions on Power Delivery*, vol. 11, pp. 872-880, 1996.
- [76] Y. Guan, G. Yue, W. Chen, Z. Li, and W. Liu, "Experimental Research on Suppressing VFTO in GIS by Magnetic Rings," *IEEE Transactions on Power Delivery*, vol. 28, pp. 2558 - 2565, 2013.
- [77] W. D. Liu, L. J. Jin, and J. L. Qian, "Simulation test of suppressing VFT in GIS by ferrite rings," in *Proceedings of 2001 International Symposium on Electrical Insulating Materials 2001*, Himeji, 2001, pp. 245 - 247.
- [78] J. Smajic, A. Shoory, S. Burow, W. Halaus, U. Riechert, and S. Tenbohlen, "Simulation-Based Design of HF Resonators for Damping Very Fast Transients in GIS," *IEEE Transactions on Power Delivery*, vol. 29, pp. 2528 - 2533, 2014.

Every reasonable effort has been made to acknowledge the owners of copyright material. I would be pleased to hear from any copyright owner who has been omitted or incorrectly acknowledged.

Signature: Mehdi Babaeilaktarashani

Date: 05/12/2016